Electrically conductive hydrogels with controlled drug release for cartilage tissue engineering

Filipe Alexandre Rodrigues Miguel

Thesis to obtain the Master of Science Degree in

Biotechnology

Supervisor: Dr. João Carlos Fernandes da Silva

Co-supervisor: Prof. Frederico Castelo Alves Ferreira

Examination committee

Chairperson: Prof. Luís Joaquim Pina da Fonseca

Supervisor: Dr. João Carlos Fernandes da Silva

Members of the committee: Dr. Paola Sanjuan-Alberte

December 2022

Declaration

I declare that this document is an original work of my own authorship and that it fulfills all the requirements of the Code of Conduct and Good Practices of the Universidade de Lisboa.

Preface

The work presented in this thesis was performed at the Stem Cell Engineering Research Group (SCERG) at the Institute for Biosciences and Bioengineering (iBB) of the Instituto Superior Técnico – Universidade de Lisboa (Portugal) during the period February-November 2022, under the supervision of Doctor João Carlos Silva and Professor Frederico Castelo Ferreira.

The literature research done in this thesis resulted in the publication of a first author review article entitled "Electrically Conductive Hydrogels for Articular Cartilage Tissue Engineering" in the journal *Gels* (IF: 4.432, https://doi.org/10.3390/gels8110710). The results of this thesis were submitted in an abstract entitled "Electrically conductive hydrogel loaded with PEDOT-Kartogenin nanoparticles for articular cartilage regeneration" for the conference "Tissue Engineering and Regenerative Medicine International Society (TERMIS) European Chapter Meeting 2023", which will be held in Manchester (United Kingdom) on the 28th to 31st March 2023.

Acknowledgements

Firstly, I would like to thank all the members of the Stem Cell Engineering Research Group (SCERG) that contributed to the realization of this Master's thesis, and for providing a very pleasant and fun work environment. I would like to acknowledge Professor Joaquim Cabral for giving me chance to join the SCERG research group to develop my master thesis project. Also, I would like to thank Professor Frederico Ferreira for all the insightful contributions to the project. A very special thanks to my supervisor, Dr. João Silva, for the constant support and guidance throughout the entire project, I learned more than I could hope for. Furthermore, I would like to thank Leonor Resina for teaching me how to produce and characterize nanoparticles, and for the help in the AFM and TEM analysis. Big thanks should be given to Dr. Teresa Esteves and Sofia Bettencourt for teaching me how to perform HPLC. Finally, I would like to thank Laura Sordini and Diana Marques for the help with the impedance measurements.

I would also like to thank for the funding received from the FCT project "InSilico4OCReg - In silico models guiding *in vitro* biophysical stimulation of biomimetic hierarchical scaffolds: a computational modelling approach towards functional osteochondral regeneration (PTDC/EME-SIS/0838/2021)".

Abstract

Articular cartilage is a highly specialized tissue, adapted to bear significant compressive loads in diarthrodial joints, being crucial for healthy articular motion. However, the absence of vascularization, low chondrocyte density and low proliferative potential inhibit an effective self-healing of the tissue after lesions or degeneration. Osteoarthritis, which results in the progressive degeneration of cartilage, is the most prevalent joint disorder, being a major cause of pain and disability worldwide. The most common treatment options for this condition are primarily focused on pain relief, failing to address tissue regeneration. Cartilage tissue engineering (CTE) focuses on the development of cartilage constructs through the combination of biomaterials with cells and bioactive factors (biochemical and physical). The potential of CTE to create engineered tissues with structural, mechanical, and functional properties similar to the native articular cartilage makes it a promising alternative to the current clinical approaches for cartilage repair. Hydrogels appeared as a suitable candidate for CTE due to their ability to recapitulate the biophysical properties of native cartilage. Moreover, hydrogels can be combined with conductive materials to mimic the natural electrochemical features of articular cartilage. Thus, in this work, electrically conductive hydrogels composed by hyaluronic acid-chondroitin sulfate and PEDOT nanoparticles were synthesized and characterized in terms of their structural, rheological and electrical properties. The nanoparticles were loaded with a chondro-inductive drug, kartogenin, and characterized in terms of morphology, size, surface charge, biocompatibility and drug release kinetics. Kartogenin release was shown to be tightly controlled by external electrical stimulation. Kartogenin-loaded PEDOT nanoparticles were incorporated in hydrogels together with human mesenchymal stem/stromal cells (MSCs) and exposed to electrical stimulation. Finally, the ability of the hydrogel system to promote the chondrogenic differentiation of MSCs was also assessed. Overall, the controlled release of the drug was demonstrated, and the proposed system exhibited promising results in promoting the proliferation and chondrogenic differentiation of MSCs, highlighting its potential for CTE applications.

Keywords: Cartilage tissue engineering, Drug delivery systems, Hydrogels, Kartogenin/PEDOT nanoparticles, Mesenchymal stem/stromal cells

Resumo

A cartilagem articular é um tecido altamente especializado adaptado para suportar cargas compressivas significativas nas articulações diartrodiais, sendo crucial para um movimento articular saudável. No entanto, a ausência de vascularização, baixa densidade de condrócitos e potencial proliferativo inibem uma autorregeneração eficaz do tecido após lesões ou degeneração. A osteoartrite resulta na degeneração progressiva da cartilagem, sendo a doença articular mais prevalecente e umas das principais causas de dor e incapacidade a nível mundial. As opções de tratamento mais comuns para este problema concentram-se principalmente no alívio da dor, falhando em abordar as lesões no tecido. A engenharia de tecido cartilaginoso (CTE) visa o desenvolvimento de tecidos artificiais de cartilagem, através da combinação de biomateriais, células e fatores bioativos (bioquímicos e físicos). O potencial de CTE para criar tecidos artificiais com propriedades estruturais, mecânicas e funcionais semelhantes à cartilagem articular nativa torna-o uma alternativa promissora às atuais abordagens clínicas para a reparação de cartilagem. Os hidrogéis são candidatos adequados para CTE devido á ao seu potencial para recapitular as propriedades biofísicas da cartilagem nativa. Adicionalmente, estes podem ser combinados com materiais condutores de modo a mimetizar as propriedades eletroquímicas do tecido nativo. Deste modo, para este trabalho, hidrogéis condutores de ácido hialurônico-sulfato de condroitina e nanopartículas de PEDOT foram sintetizados e caracterizados em termos das suas propriedades estruturais, reológicas e elétricas. As nanopartículas foram carregadas com uma droga condro-indutiva, kartogenina, e caracterizadas em termos da sua morfologia, tamanho, carga superficial, biocompatibilidade e cinética de libertação da droga. A libertação de kartogenina foi demonstrada sendo controlada através de estimulação elétrica. Nanopartículas de PEDOT carregadas com kartogenina foram incorporadas em hidrogéis juntamente com células estaminais humanas (MSCs) e expostas a estimulação elétrica, Em suma, a libertação controlada da droga foi demonstrada, e o sistema proposto exibiu resultados promissores no favorecimento da proliferação e diferenciação condrogénica das células presentes.

Keywords: Engenharia de tecido cartilaginoso, Sistemas de entrega de drogas, Hidrogéis, Nanoparticulas de kartogenina/PEDOT, Células mesenquimais estaminais

Table of contents

List of Figures

Glossary

ACI Autologous chondrocyte implantation

ADA Alginate

AuNPs Gold nanoparticles

BSA Bovine serum albumine

COL I Collagen type I

COL II Collagen type II

COL X Collagen type X

COX-2 Soluble phospholipase a2, cyclooxygenase 2

CS Chondroitin sulfate

CTE Cartilage Tissue engineering

DMEM Dubbeco's modified eagle medium

ESCs Embryonic stem cells

EtBr Ethidium bromide

FEG-SEM Field emission gun – scanning electron microscopy

GEL Gelatin

HA Hyaluronic acid

HPLC High performance liquid chromatography

IL-1β Interleukin-1 β

iNOS Inducible nitric oxide synthase

iPSCs Induced pluripotent stem cells

KTG Kartogenin

MACI Matrix assisted chondrocyte implantation

MMP-13 Matrix metalloproteinase-13

MMPs Matrix metalloproteinases

MSCs Mesenchymal stem cells

NPs Nanoparticles

PANa Sodium phytate

PEDOT Poly(3,4-ethylene dioxythiophene)

PLGA Poly(lactic-*co*-glycolic acid)

PVA Poly(vinyl alcohol)

QD Quantum dots

ROS Reactive oxygen species

RT Room temperature

TEM Transmission electron microscopy

TNF Tumor necrosis factor

UCNPs Upconverting nanoparticles

UCNT upconversion nanotransducer

WC Water content

1. Introduction

1.1 Problem and motivation

Articular cartilage is a load-bearing tissue present at the end of joint bones, being crucial for healthy articulation and movement. Osteoarthritis is a common joint disorder that leads to cartilage degeneration, being the major cause of pain and disability in adults. With an increasingly ageing and obese population, it is estimated that the prevalence of OA will also continue to increase over the next decades. Moreover, the lack of vascularization of articular cartilage severally limits its self-repair capacity. Current treatment options carry various limitations, failing to address the core problems that underlie cartilage degeneration. Thus, cartilage tissue engineering appeared as a promising alternative to the current treatments for cartilage defects, aiming to combine appropriate biomaterials with cells and bioactive factors to create cartilage substitutes that can promote tissue regeneration and restore function. However, the highly complex structure and biophysical environment of articular cartilage, from which it derives its functions and mechanical properties, remain a challenge to fully recapitulate. One of the aspects of articular cartilage that is often overlooked in tissue engineering strategies is the tissue's electrochemical properties, which are essential for its normal functioning.

1.2 Thesis objectives

The general aim of this thesis was the development of a system consisting of a biomimetic hydrogel scaffold with native-like functionalities, able to recapitulate the electrochemical environment of native tissue and potentially replace it. Additionally, the produced scaffold was designed to enable the controlled release of a nanoparticle-encapsulated drug upon an external trigger (electrical stimulation), which would induce the differentiation of seeded mesenchymal stem/stromal cells (MSCs), promoting tissue regeneration.

Specifically, in this project, kartogenin (KTG), a chondrogenic inducing small molecule, was loaded in PEDOT nanoparticles, which were then embedded in an electrically conductive hyaluronic acid-chondroitin sulfate hydrogel (HA-CS). The nanoparticles were characterized in terms of their size, stability, and electrochemical properties. The hydrogel scaffolds were characterized in terms of their morphological and biophysical/chemical (e.g., rheology, swelling, water uptake, electrical conductivity) properties. *In vitro* cell culture assays were performed to optimize both the concentration of KTG/PEDOT NPS to use and the electrical stimulation protocol for controlled KTG release. The potential of electrical stimuli-controlled KTG release in promoting the chondrogenic differentiation of MSCs was first assessed in 2D monolayer cultures. Finally, the conductive hydrogels were combined with MSCs, and their potential to induce chondrogenic differentiation by kartogenin release through external electrical stimulation was also assessed.

1.3 Thesis outline

This work is divided in 5 chapters. In the first, the motivation and objectives of this thesis can are described. Chapter 2 comprises the theoretical background of the work and the state-of-the-art. The materials and methods that were used in this work can be found in Chapter 3. Chapter 4 contains the results obtained in this work and their respective discussion. Chapter 5 was reserved for the conclusions drawn from this work. Finally, possible future perspectives of this project are discussed in the final Chapter 6.

2. Literature background

2.1 Articular cartilage composition and structure

Articular cartilage is a highly complex and specialized connective tissue present in diarthrodial joints, being paramount for healthy joint mobility (Figure 1). Articular cartilage iss able to provide a smooth and highly durable surface that facilitates the transmission of mechanical loads with a low friction index. It comprises a single cell type (chondrocytes), which are embedded in a dense matrix composed by collagen type II and proteoglycans[1]. Other types of collagen such as types V, VI, IX and XI can also be found in lower quantities, and although they are believed to modulate the structure of type II collagen, their exact function is not yet fully understood[2]. The native tissue's proteoglycans, which mainly consist of aggrecan, are comprised by a protein core with attached glycosaminoglycans (GAGs) as side chains[3]. Chondroitin sulfate is the most abundant sulfated GAG in the tissue, and the negative sulfate groups confer to aggrecan, and by extension the tissue's extracellular matrix, a net negative charge. Aggrecan is bound to single, long chains of hyaluronic acid (HA), forming large networks of aggregating proteoglycans[4]. However, in addition to articular cartilage general composition, various structural and compositional variations can be found along the tissue's multiple layers. Articular cartilage has a complex, multilayered structure, with each zone displaying different densities of chondrocytes, ECM composition and organization, water content and mechanical properties (Figure 1).

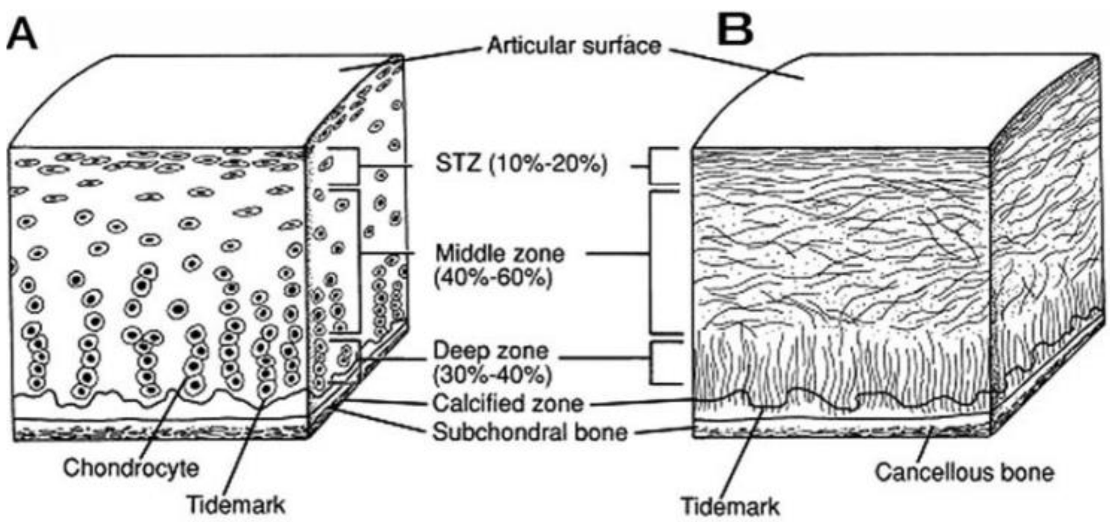

Figure 1 – Schematic representation of a cross-section cut of articular cartilage. A) Cellular profile of the different zones of articular cartilage. B) Collagen fibers distribution and orientation. Adapted from [5].

The superficial zone makes up to 10-20% of total articular cartilage thickness, with collagen fibers aligned parallel with the articular surface and a relative high number of flattened chondrocytes. Around 40 to 60% of the articular cartilage volume is represented by the middle zone, containing a lower density of spherical chondrocytes and collagen fibers organized obliquely, being the first layer tasked to resist compressive forces. The deep zone represents 30% of articular cartilage thickness and is the main responsible for providing resistance to mechanical loads, as it contains the highest diameter collagen fibers in a radial disposition and proteoglycan density, with the lowest number of chondrocytes[6]. The presence of ECM components like collagen, proteoglycans and glycoproteins leads to the swell of articular cartilage with water, which is retained within the matrix pores and intrafibrillar space. Water encompasses 60-85% of its weight, playing a fundamental role in lubricating the articulating surfaces of joints and in the transport of nutrients to chondrocytes and waste products out of the tissue. When the tissue experiences compression under mechanical stress, the intrafibrillar water is able to move through the ECM, despite experiencing a very high frictional resistance. The frictional drag forces during water flow dissipate the majority of energy conveyed into the tissue during compression, allowing articular cartilage to withstand such heavy loads[7]. Despite its importance, the hypocellular and avascular nature of this tissue severely limits its capacity for intrinsic repair required after trauma or degenerative conditions such as osteoarthritis (OA) or rheumatoid arthritis[8,9].

2.2 Impact and pathophysiology of osteoarthritis

Articular cartilage lesions present a high socioeconomic burden, with physical sequelae often manifesting in affected individuals. Trauma-related injuries are common, being one of the main contributors of lesions in the tissue[10]. These are associated with excessive or repetitive loads being applied to the tissue, which can lead to injury. In fact, articular cartilage lesions are highly prominent in high-impact sports athletes, as 36 to 38% have been reported to sustain these types of injury[11].

Another common cause of articular cartilage degeneration is OA. OA is the most common joint disorder, characterized by severe pain and loss of mobility as result of the progressive loss of articular cartilage, thickening of the subchondral plate and development of cysts in the subchondral bone[12] (Figure 2). Under normal conditions, articular chondrocytes maintain equilibrium between the synthesis and degradation of ECM components. However, in osteoarthritic states, this balance is disrupted, occurring a shift towards catabolism over anabolism, and eventually leading to the progressive loss of cartilaginous tissue. The early development and progression of OA heavily involves inflammation of the tissue, which is mediated through the secretion of inflammatory cytokines[13]. Among these, interleukin-1 β (IL-1β) and tumor necrosis factor (TNF)-α appear to be the main cytokines involved in OA. Both cytokines can be produced by chondrocytes, triggering the production of inflammatory and catabolic factors[14]. This is accompanied by an inhibition of chondrocyte anabolic activities, with studies showing chondrocytes treated with IL-1β or TNF-α exhibited decreased expression of major cartilage components like type II collagen and aggrecan[15,16]. These cytokines also promote the overproduction and release of various matrix metalloproteinases (MMPs) from chondrocytes[17,18]. These matrix-degrading enzymes are the main agents of cartilage degradation. IL-1β and TNF-α have also been shown to upregulate the expression of inducible nitric oxide synthase (iNOS), soluble phospholipase a2, and cyclooxygenase 2 (COX2) stimulating the production of reactive oxygen species (ROS) like nitric oxide and prostaglandin e2[19]. These ROS can accelerate cartilage loss by further inducing the production of MMPs and inhibiting anabolic macromolecules production. Apart from the effects on chondrocytes, these cytokines affect the immune system cells migrating for the inflammation site, inducing the excessive production of free radicals[20].

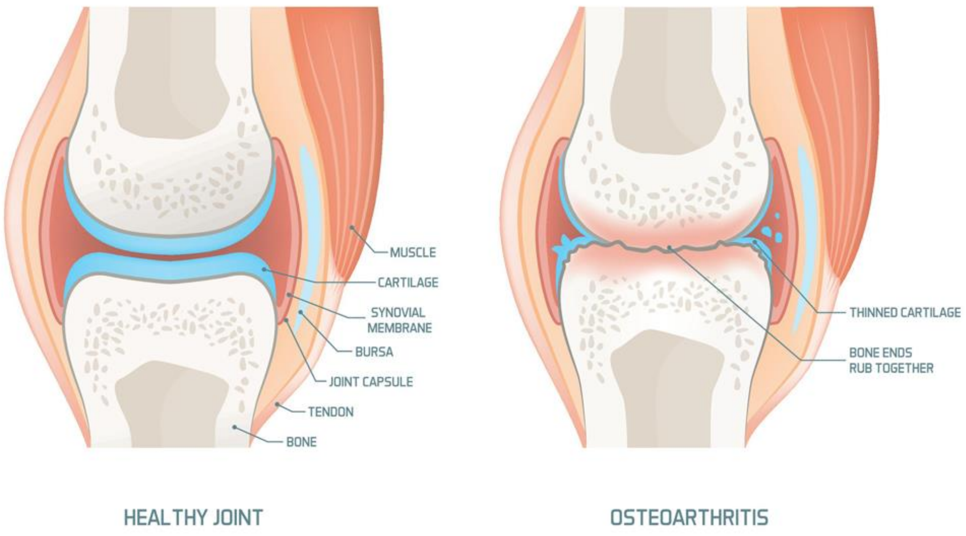

Figure 2 – Schematic representation of a healthy and osteoarthritic joint. Taken from[21].

Nowadays, it is estimated that 360 million people are currently affected by OA, with knee OA affecting approximately 10% of men and 13% of women over 60 years old, while hip OA affects 6,1% of men and 13% of women over 65 years[22–24]. When considering the various factors associated with the incidence of OA, age and sex are the major non-modifiable contributors and weight is the major modifiable contributor[25]. The incidence of this condition has seen a rise over the years; in the US alone, the number of adults suffering from OA increased from 21 million in 1995 to 27 million in 2005[26]. Additionally, as key predicators, the number of people affected by OA is estimated to keep increasing as a consequence of the obesity epidemic and population aging, with data suggesting an additional 26 thousand adults per 1 million will experience OA by 2032[27]. The impact of OA can also be felt economically, as its healthcare cost already exceeds 60 billion dollars per year in the US[28] and, given its prevalence and estimated growth, its burden will only continue increasing.

Despite its prevalence and socioeconomic impact, the pathogenesis of OA remains largely unknown, and the current non-arthroplasty treatments only offer short-term solutions, failing to rectify the core pathophysiological mechanisms that underlie the degeneration of cartilage. Pharmaceutical therapy is the most common option for OA treatment, and largely consists of acetaminophen, non-steroidal anti-inflammatory drugs, opioid analgesics and serotonin–norepinephrine re-uptake inhibitors. However, as previously stated, these treatment options are primarily focused on pain relief and anti-inflammation, being unable to repair cartilage damage[29]. Osteochondral autograft transplantation (mosaicplasty) is another regeneration technique, involving transfer of cartilage from non-load bearing sites to the damaged load-bearing sites. However, this method is only applicable to small defects and the transplanted cartilage is more prone to damage due to structural differences between the two cartilaginous regions[30]. In terms of cell-based approaches, autologous chondrocyte implantation (ACI) aims to repair articular cartilage lesions through the isolation of chondrocytes from a low weight-bearing area of the patient, followed by their expansion *in vitro*, and implantation into the damaged site. Matrix-assisted chondrocyte implantation (MACI) is a similar technique, where chondrocytes are seeded in a matrix scaffold, which is then glued to the articular cartilage defect with fibrin[31]. However, several problems emerge from these techniques, mainly the need for a two-surgery procedure, donor site morbidity and the dedifferentiation of chondrocytes during *in vitro* expansion[32,33].

2.3 Cartilage tissue engineering

Considering the unmet medical needs for the effective treatment of OA, regenerative medicine therapies have been a growing topic of research and discussion as promissory strategies to enhance cartilage repair and restore the quality of life of patients. From these types of therapies, cartilage tissue engineering (CTE) has emerged as a promising alternative to treat cartilage defects[34]. CTE basic principle employs the use of a biocompatible, biodegradable and biomimetic biomaterial scaffold that is combined with cells (chondrocytes or stem cells) and bioactive factors (e.g., growth factors, physical stimuli) to promote cell proliferation, differentiation and maturation, ultimately leading to tissue regeneration[35]. Over the years, a myriad of combinations of different cell types, bioactive factors and biomaterial scaffolds have been developed in other to produced viable cartilage substitutes with properties and function similar to the native tissue[36]. However, despite the recent advances in this field, a number of challenges still remain, like the multiphasic and gradient properties of articular cartilage. The different volumes, chondrocyte densities, extracellular matrix (ECM) composition, orientation and water content of the different layers confer them different compositions and mechanical properties[37]. In fact, when tissue engineering was firstly introduced, it was predicted that articular cartilage would be one of the first tissues to be successfully regenerated, due to its thin, and apparent simple structure, being avascular and composed by a single cell type. However, this would later be proved wrong as a result of not only its poor innate self-repair capabilities, but also of a better understanding of the highly complex structure of the tissue[38].

2.4 Cell-seeded hydrogels as scaffolds for CTE

One of the major challenges of CTE is the recreation of articular cartilage's complex structure and mechanical properties, from which it derives many of its functional properties. A biomimetic structure is fundamental for setting the correct environment for cells, and thus optimizing tissue regeneration. Scaffolds arise as a potential solution to this problem though their high customization. By choosing appropriate materials, pore precursors and manufacturing methods, the scaffold parameters can be optimized to provide a suitable, native-like environment for cells, aiding the tissue's regeneration[39,40].

Hydrogels are crosslinked hydrophilic polymer networks that typically contain 60-90% water, being highly absorbent with well-defined structures. Since investigations on biomedical applications of hydrogels started about 60 years ago, they have been successfully applied as drug carrier systems, devices used for diagnostic purposes and chemically modified implants for regenerative medicine[41]. One of the most enticing properties of hydrogels is their biocompatibility, although many factors can influence the immune system response to their presence. When designing hydrogels, various parameters can be controlled in order to modify their properties and function, which include composition, structure, mechanical properties, degradation profile, cell sources, controlled release of bioactive factors, and integration within the native tissue[42]. Their ability to enhance chondrocyte adhesion to levels similar to cartilage ECM is a key factor for CTE strategies. This property of hydrogels, alongside a native-like swelling, and a broad range of possible designs, has allowed their widespread use as scaffolds for CTE strategies[43]. In fact, as cell-seeded scaffolds, hydrogels have the potential to be designed as structurally and mechanically similar to cartilage, allowing the entrapment of cells like in native cartilage ECM[44]. Their viscoelasticity enables the effective transmission of mechanical loads to chondrocytes, which require these biophysical signals for their normal growth and function[45]. Furthermore, hydrogels are, initially, aqueous flowable solutions, that upon crosslinking start to gelate. This property makes hydrogel scaffolds easily injectable into an injured site without invasive surgeries, able to match any shape of damaged cartilage, with posterior polymerization. A variety of biomaterials, either synthetic or natural, have been utilized to successfully fabricate injectable polymeric hydrogels, including: gelatin[46], heparin[47], alginate[48], poly(ethylene glycol) (PEG)[49], poly(vinyl alcohol)[50], chondroitin sulfate[51], hyaluronic acid[52], and chitosan[53] (Table 1). When compared to natural polymers, synthetic polymers have the advantage of being highly stable and easily manipulated, able to be modulated to fit the biochemical and biomechanical requirements of native cartilage[54]. Natural polymers, despite having relatively inferior mechanical properties and being more subjected to batch-to-batch variability, are still tunable, and some can either be found in native cartilage tissue like hyaluronic acid and chondroitin sulfate or have similar monomers like chitosan and alginate. The similarity to the native tissue grants these types of polymers outstanding biocompatibility and advantageous cell-matrix interactions[55]. However, combining natural polymers or proteins with synthetic polymers might be the ideal way to create scaffolds for CTE, as it would combine the bioactivity and compatibility of natural materials with the good mechanical properties provided by synthetic materials[56].

Table 1 – Materials used to fabricate injectable hydrogels for CTE applications. Adapted from[57].

Injectable Hydrogel Material	Advantages	Disadvantages	References
Heparin	Naturally occurring negatively charged GAG able to interact with ECM proteins/growth factors and influence several cellular processes.	Poor mechanical properties	58
Collagen	High biocompatibility Biodegradable Promotes cell adhesion Non-immunogenic Biomimetic of native articular cartilage (collagen type II)	Poor mechanical stability Slow gelation Rapid degradation	59
Gelatin	Cost-effective High biocompatibility Biodegradable Promotes cell adhesion Non-immunogenic	Poor mechanical properties and stability Rapid degradation	60
Alginate	Fast gelation Cost-effective Non-immunogenic Non-toxic	Lack of strength to maintain structural shape of the tissue Poor cell attachment	60
Poly (ethylene glycol) (PEG)	Adjustable mechanical and structural properties Biocompatibility	Possible immunogenicity Non-biodegradable Poor cell adhesion and growth	61
Chondroitin sulfate	Easily available High biocompatibility Biodegradable Anti-inflammatory Biomimetic of native articular cartilage	Difficult processability Poor mechanical properties	62
Hyaluronic Acid	High biocompatibility Biodegradable Promotes cell growth and differentiation Non-immunogenic	Poor mechanical strength Rapid degradation	63
Chitosan	Biocompatibility Antibacterial and antifungal activity	Poor mechanical properties Poor structural control Extensive swelling in water	46

Over the years, a variety of cell types have been used for CTE purposes. As the only cell type present in native tissue, chondrocytes have been extensively explored *in vitro* to produce cartilage constructs[64]. However, a major problem arises when employing these cells that significantly inhibits their use. Chondrocytes are isolated from articular cartilage, but in order to obtain sufficient cell quantities, considerable amounts of healthy human cartilage from load-bearing sites would be required, which is challenging as it presents donors a high risk of joint injury[65]. The low proliferation capacity and dedifferentiation of chondrocytes *in vitro* also impairs their use in CTE strategies. Embryonic (ESCs) and induced pluripotent stem cells (iPSCs) have also been investigated for potential uses in CTE. Various approaches have been developed to induce the differentiation of these cells into chondrocytes, from co-culture with chondrocytes and preparation of embryoid bodies to differentiation towards chondrocytes through intermediate populations[66–68]. However, several problems have emerged with the application of these cells *in vivo*, namely the risk of teratoma and tumor formation[69]. Mesenchymal stem/stromal cells (MSCs) have become an object of interest in the scope of TE strategies, including for cartilage regeneration. These cells can be easily isolated from several tissues including bone marrow, umbilical cord blood and matrix, synovium and adipose tissue. MSCs are also highly proliferative and exhibit self-renewal and multilineage differentiation capacity[70]. Under specific chondrogenic factors (e.g., biochemical or physical), MSCs exhibit an outstanding chondrogenic potential, being able to differentiate into cartilage tissue. Additionally, during differentiation, MSCs are able to produce and secrete various ECM molecules like fibronectin, collagen, proteoglycans, GAGs and various growth factors and cytokines important for the regenerative process[71,72]. With these considerations, MSCs are great candidates to be combined with hydrogel scaffolds in order to construct cartilage substitutes.

The potential of hydrogels for CTE has been extensively explored, with many different types produced and yielding promising results. However, recapitulating the native tissue goes beyond the physical structure and properties of the scaffold. Articular cartilage has complex biophysical and biochemical properties that are essential for the correct functioning of the tissue, directly influencing the local cells. In order to successfully construct hydrogel scaffolds that can accurately mimic articular cartilage, acting as its substitute and allow an optimized differentiation of seeded MSCs, incorporating the beforementioned articular cartilage properties into these systems is key to their success. As such, there is now a need to find new ways to combine these scaffolds with relevant biophysical stimuli in order to more accurately replicate the native tissue's microenvironment for the seeded cells, which might lead to improved regenerative outcomes.

2.5 Electrical stimulation as a tool to enhance cartilage regeneration

Chondrocytes present in articular cartilage are responsible for producing the ECM, being crucial for this tissue's homeostasis and function. As previously discussed, the phenotype and maintenance of chondrocytes are dependent on various biophysical stimuli, like mechanical, electric, and magnetic, which were shown to promote the growth, differentiation, and maturation of the tissue[73,74]. Cartilage has natural electrochemical properties, which are derived from the flow of free electrolytes (Ca^{2+}, Na^{+}, K^{+}) through the fixed highly negative charges of GAGs in the side chains of proteoglycans[75]. Each negative charge associated with a proteoglycan requires a counter-ion, dissolved in the interstitial fluid, in order to maintain electro-neutrality in the interstitium[76]. However, this high counter-ion requirement creates an imbalance between this region and the external bath solution. The excess of mobile ions within the interstitium creates a swelling pressure, contributing for the hydrophilic nature of articular cartilage[77]. When the tissue is at equilibrium, the swelling pressure is balanced through the tensile forces generated by the solid matrix of articular cartilage. Interestingly, it is this balance that determines the dimensions of the cartilage[78]. Aside from the swelling pressure, an electrical potential and current can also be observed, which results from diffusion and streaming potentials. The diffusion potential results from the inhomogeneous distribution of the fixed negative charges along the cartilage ECM[79], while the streaming potential results from the fluid flow along the charged tissue[80]. The chondrocytes present in articular cartilage are in constant exposure to these electromagnetic signals, which in turn convert the physical stimuli into intracellular signals. In this particular case, the signal transduction is achieved through ion channels in the surface of the cell membrane, more specifically, voltage-gated calcium channels[81]. Electric signals lead to an influx of Ca^{2+} intracellularly, which in turn activates calmodulin, a cytoskeletal protein. This will lead to the production of the SOX9 transcription factor, triggering the production of typical cartilage ECM components collagen type II and aggrecan[82,83].

As the electrochemical properties of articular cartilage can direct the synthetic activities of chondrocytes, it was feasible to think that this effect could be replicated *in vitro* through external electrical stimulation. In fact, over the recent years, various works highlighted the chondrocyte's particular sensitivity to electrical stimulation. This stimulus has been shown to increase the proliferative capacity of the cells, the secretion of ECM molecules, and chondrogenesis induction, accelerating the repair of deep cartilage defects[84,85]. TGF-β1, TGF–β3 , BMP-2 and BMP-4 are key regulators of cartilage and bone morphogenesis, being expressed during chondrogenesis[86]. Utilizing electromagnetic fields (EMF), one study revealed a 31% increase in TGF-β1 protein and 411% increase in the number of chondrocytes when compared to the control, after 8 days of exposure[87]. The same group had previously reported an increase of aggrecan and type II collagen production in EMF-exposed chondrocytes[88]. In a different study using cartilage explants, chondrocytes exposed to electric fields were shown to have a 1.8-fold increase in proteoglycan production and 1.7-fold increase in collagen content when compared to non-stimulated cells[89].

Following the previously mentioned constraints in using chondrocytes for cartilage regeneration, the effects of electrical stimulation in MSCs chondrogenic differentiation have also been accessed by several research studies. Early works reported the positive effects of electrical stimulation in the proliferation and differentiation of MSCs towards osteogenic outcomes[90,91], but its chondrogenic inducing potentials remained elusive. However, a 2016 study from Kwon et al. revealed the high potential of electric stimulation in MSCs-based therapies for cartilage regeneration. Particularly, the obtained results show that, even in the absence of growth factors, MSCs under electric stimulation had an increase in the expression of chondrogenic markers type 2 collagen, aggrecan and SOX9 of 66-, 43- and 35-fold respectively, while GAGs expression was also enhanced. This was accompanied by the decrease of type 1 collagen expression, an indicator that the observed differentiation of MSCs was towards hyaline cartilaginous tissues[92]. More recently, a study evaluated the same effects of electric stimulation in MSCs seeded in hyaluronic acid-gelatin hydrogels[93]. Corroborating previous results, an increase in aggrecan and SOX9 expression could be observed after 21 days of stimulation, when compared to non-stimulated cells. The results also showed an increase in the production of GAGs and type II collagen. Furthermore, the levels of type II collagen normalized to total collagen where 2.43 times higher in stimulated cells[93]. Overall, previous results strongly suggest that electrical stimulation can promote MSCs chondrogenesis, making it a promising strategy for CTE strategies.

2.6 Electrically conductive hydrogels

Combining electrical stimulation with hydrogel scaffolds allows a better mimicking of the electrochemical properties of native cartilage while allowing the electrical stimulation of the seeded cells. These scaffolds should be electrically conductive to potentiate the effects of electrical stimulation. To attain conductivity, hydrogels can be combined with conductive materials during formulation. Over the years, various conductive nanocomposite hydrogels have been successfully formulated, produced and applied in diverse biomedical fields, with interesting properties that could potentially be applied in CTE (Table 2). The most common conductive materials combined with hydrogels can be divided in metallic/metal oxide nanoparticles, carbon-based materials and conductive polymers (CPs). Gold (Au), silver (Ag), and platinum (Pt) nanoparticles (NPs) have been combined with hydrogels for applications in drug delivery, cancer treatment and bioimaging, as these particles are highly stable and carry excellent optical signals. However, their main disadvantages come in the form of a high price and latent cytotoxicity, limiting their use for CTE purposes[94,95]. For carbons, graphene and carbon nanotubes (CNTs) have also been combined with hydrogel scaffolds for tissue engineering and cancer treatment. In the scope of CTE, these materials present very interesting characteristics as they are not only highly conductive, but have a very high mechanical strength. As such, combining these materials with hydrogels can potentially create conductive nanocomposites with similar mechanical properties to native articular cartilage. However, these materials have some level of cytotoxicity, and can also induce oxidative stress[96]. Conductive polymers are another class of conductive materials commonly combined with hydrogels. These are organic polymers with unique mechanical and optical properties, with characteristics similar to some inorganic semiconductors while maintaining polymer properties like flexibility and facilitated synthesis. Polyaniline (PANi), poly(3,4-ethylene dioxythiophene) (PEDOT), polythiophene (PT) and polypyrrole (PPy) have been incorporated into hydrogels for applications in tissue engineering, biosensors, drug delivery and cancer treatment[97]. Particularly, PEDOT has emerged as a highly promising conductive polymer for CTE. It was first reported in the year 1988, being chemically and thermally stable, while also being stable to air and moisture compared to the previously mentioned conductive polymers[98]. Furthermore, PEDOT carries a crucial advantage over the discussed metal NPs and carbons, as it is completely biocompatible[99]. This conductive polymer is also characterized by a high conductivity (up to 4500 S cm^{-1})[100] that arises from a combination of its conjugated backbone and dopant. The polymer backbone consists of alternating single and double bonds, which both contain localized σ-bond, while the latter also contains a less localized π-bond[101]. The series of π-bonds overlap each other and facilitate the delocalization of electrons. The doping process occurs during synthesis, usually through the introduction of a molecule that is placed with the monomer (creating small impurities), ultimately leading to the oxidation of the neutral polymer[102]. Interestingly, these dopants introduce charge carriers to the polymer, allowing its physical properties to be controlled with cycles of oxidation and reduction and forming the basis of the drug delivery applications of these CPs[103].

Table 2 – Properties and applications of conductive materials.

Conductive polymer	Advantages	Disadvantages	Applications	References
AuNPs	Low initial cytotoxicity High stability	Weak optical signal Long term cytotoxicity High price	Photodynamic therapy X-ray imaging Drug delivery Cancer treatment	104
AgNPs	High optical signal Anti-bacterial and fungal properties	Low stability Cytotoxicity High price	Cancer treatment Bone healing Drug delivery	105
PtNPs	High optical signal High stability	Oxidative stress Aggregation Possible cytotoxicity	Bioimaging Drug delivery Cancer treatment	106
Graphene	High mechanical strength Easily synthesized High conductivity	Oxidative stress Aggregation Possible cytotoxicity	Drug delivery Cancer treatment Tissue engineering Bioimaging	96
CNTs	High mechanical strength High conductivity	Oxidative stress Possible cytotoxicity	Tissue engineering Biosensors Drug delivery	107
Polyaniline (PANi)	High stability High conductivity	Low cell adhesion and growth	Antimicrobial therapy Drug delivery Tissue engineering	108
Poly(3,4-ethylene dioxythiophene) (PEDOT)	High stability High conductivity Biocompatibility	Low mechanical Strength	Drug delivery Tissue engineering	109
Polythiophene (PT)	Good optical properties Biocompatibility	Low conductivity Low stability	Biosensors Tissue engineering	110

2.7 Applications of electrically conductive hydrogels in CTE strategies

Although a there is wide variety of electrically conductive hydrogels successfully produced and applied to diverse biomedical fields, their latent potential for CTE remains largely untapped, with literature on this topic being scarce. However, the existing studies that applied these types of scaffolds for CTE purposes exhibited promising results (Table 3)

Distler et. al produced a 3D-printable PPY:polystyrenesulfonate (PPY:PSS) alginate-gelatin (ADA-GEL) nanocomposite hydrogel, that exhibited enhanced conductivity when compared to pristine ADA-GEL[111]. In fact, the addition of 0.1M of PPY lead to a conductivity increase from 0.5 to 1.4 S m^{-1} at 100 Hz, which is close to range found in native cartilage. The mechanical properties of the hydrogel were also suitable for a potential cartilage substitute, with tensile strengths in the order of native cartilage at 1-1.5 MPa. Additionally, the conductive scaffold offered cytocompatibility and cell-material interactions similar to the control ADA-GEL, with only a slightly reduced cell attachment, which was likely due to the higher stiffness of the PPY:PSS functionalized hydrogel. In a different study, Zhang and colleagues produced a poly(vinyl alcohol) (PVA) with sodium phytate (PANa), which exhibited excellent mechanical properties[112]. The scaffold was able to resist strains of 600% before breaking with a tensile strength of 7 MPa. It also presented a high elastic resilience, with cyclic loading tests in 0-50% strain ranges showing negligible changes in tensile strength through the loops. Additionally, its conductivity was close to native cartilage ranges at 1.65 S m^{-1}. Another interesting property of the hydrogel was its anti-swelling properties. If a hydrogel scaffold absorbs too much water, it can diminish its stiffness and compromise its mechanical integrity. This study's scaffold only exhibited a 50% swelling after 7 days, with no significant changes in the next 18 days.

Table 3 - Summary of research studies on electrically conductive hydrogels for articular cartilage tissue engineering. Adapted from [57].

Hydrogel	Conductive Filler	Main Outcomes	References
Poly(vinyl alcohol) (PVA)	Sodium phytate (PANa)	Easy to produce and cost-effective PVA-PANa hydrogel. Excellent mechanical strength with a fracture stress of over 7 MPa and stable in different solutions for over 20 days. Ionic conductivity of 1.65 S m−1. Hydrogel features are close to the properties of native articular cartilage.	112
Poly-D,L-lactic acid/polyethylene glycol (PDLLA)	Graphene Oxide (GO)	Biodegradable PDLLA-GO nanocomposite hydrogel that promotes hBMSCs chondrogenic differentiation even in the absence of chondroinductive factors. The addition of GO also improved the mechanical properties of the hydrogel.	113
Oxidized alginate–gelatin (ADA-GEL)	Polypyrrole: polystyrenesulfonate (PPy:PSS)	Cytocompatible, 3D-printable and electroactive oxidized alginate–gelatin PPy hydrogel that allow improved cell-material interactions.	114

		Both the tensile strength (≈1.2 MPa) and conductivity (≈1.0–1.4 S m−1) of this hydrogels are within the range of values found in native articular cartilage.	
Chitosan- β-glycerophosphate (CS-BGP)	Oligopyyrole (OPy)	Biodegradable and cytocompatible CS-BGP-OPy hydrogel. The addition of OPy significantly increased the conductivity of the scaffold to 1.9 S m−1, which is relatively close to the value reported for native cartilage.	112

2.8 Small molecules for the induction of MSCs chondrogenesis

The involvement of growth, differentiation, and transcriptional factors in the development of cartilage and regulation of chondrogenesis has been extensively studied[115,116]. In order for MSCs to differentiate into mature chondrocytes, a precise combination of these factors is required. Due to their importance for chondrogenesis, growth factors were assumed to be a promising way to induce differentiation of MSCs into chondrocytes, promoting cartilage repair. In fact, many studies have demonstrated the efficacy of these factors in stimulating cartilage formation both *in vitro* and *in vivo*. TGF-β3 was shown to induce a dose-dependent effect on the production of chondrogenic markers by MSCs[117], while mice implanted with hydrogels containing chondrocytes and TGF-β3 had substantial increase in GAGs and collagen content, when compared to controls[118]. Another study revealed that the growth factor IGF-1 can also induce the proliferation and expression of chondrogenic markers in MSCs[119]. However, despite the great number of studies reporting the potential of these and other growth factors to induce chondrogenesis, others works have concurrently uncovered their limitations. These come in the form of a short half-life *in vivo*, instability, and immunogenicity. For example, TGF-β comes with an *in vivo* half-life of few days to hours, making it unable to perform its function for the necessary time, as a 3-month period is usually required for repairing cartilage defects[120]. As such, to reach a significant regenerative processs, high dosages of TGF-β would be needed, but intra-articular injections of high-dosages of this growth factor have been associated with synovitis, synovial fibrosis, joint swelling, and osteophyte formation[121,122]. Additionally, TGF-β and other growth factors, as exogenous proteins, easily denature during storage, which can eventually lead to immunogenicity *in vivo*. With these limitations, utilizing exogenous growth factors for cartilage regeneration might not be optimal, which made the search for other bioactive factors that share their potential but have fewer drawbacks highly valuable.

Recently, small molecules are emerging as a promising alternative to growth factors for the modulation of cell differentiation, including MSCs chondrogenesis. They exhibit various advantages over growth factors, which highlight their use for CTE strategies. Firstly, they are easier to obtain; their simple structure allows their sufficient production and easy modifications through various methods of synthetic chemistry. Hence, small molecules can be produced for a substantially lower cost than growth factors.

Secondly, the small size also allows them to bypass the immune system, being unlikely to trigger an immune response[123]. Finally, small molecules are able to induce cell differentiation in a rapid and accurate manner[124].

In 2012, a study conducted by Johnson *et al.* screened 22 thousand structurally diverse, heterocyclic, drug-like small molecules for effects in MSCs chondrogenesis. It was through this screening that kartogenin (KTG) was firstly reported as a hydrophobic, non-protein small molecule that can act as a chondrogenic agent[125]. The results highlighted its potential to notably induce the differentiation of MSCs into chondrocytes, in a dose dependent manner, without any associated toxicity. Additionally, its stability allows for storage and transportation at room temperature. It was revealed that KTG induces chondrogenesis by disrupting the interaction between core-binding factor β (CBFβ) and actin-binding protein filamin A (FLNA). Consequently, CBFβ is translocated to the nucleus of the cells, binding to RUNX1 transcription factor, which in turn will activate genes that mediate chondrogenesis[125]. Since its discovery, several studies have supported its potential for CTE strategies[126,127]. Despite this, it was found that directly injecting KTG might not be optimal since the molecule may be quickly cleaned *in vivo* and overstimulate growth of normal tissue in untargeted sites[128]. Furthermore, due to its hydrophobic nature, KTG exhibits a low solubility in water, which turns the accurate control and administration of the dose harder[129]. In response to this, various studies have coupled KTG with drug delivery systems, which have shown to be a promising way to offset these problems. Particularly, loading KTG into NPs can enhance the drug's pharmacokinetics in the body, increasing its aqueous solubility and permeability[130]. More importantly, this type of conjugation can also allow for a more controlled and sustained release profile of the drug, improving its desired effects[131] (Table 4)

Many of the works conjugating KTG with hydrogels or loading it in NPs have achieved a level of sustained KTG delivery, but usually only through its passive release. However, designing a system that permits the encapsulation of this drug, and its release dependent on a specific trigger, allows the full control of its delivery. In fact, PEDOT NPs have been successfully utilized to encapsulate drugs, with electrical stimulation employed to control their release[132,133]. In one study, curcumin, an anti-cancer highly hydrophobic drug (similar to kartogenin) was loaded in PEDOT NPs, where its non-stimulated release was found to be almost null. However, the authors identified a pulse-dependent release of the drug, where even 1 pulse of the selected voltage led to 8% of total loaded curcumin to be released. On this basis, loading kartogenin in PEDOT nanoparticles and conjugating them with a hydrogel can be an extremely promising system for cartilage repair. These nanoparticles could provide a dual effect, as they would allow the controlled release of KTG upon electrical stimulation, while providing conductivity to the hydrogel scaffold, recreating a more native-like environment for the seeded cells.

Table 4 - Summary of reported nanoparticle formulations containing kartogenin.

Nanoparticle composition	KGN loaded or conjugated	Size (nm)	KGN release properties	Properties affecting release	Reference

KGN-chitosan self-assembled nano-/micro-particles	Conjugated	150 ± 39 1840 ± 540	Passive: 30% release over 50 days for nanoparticles and 50% release over 50 days for microparticles	Size	134
KGN-loaded PLGA in HA hydrogels	Loaded	270	Passive: 60% over 60 days with hydrogel and 85% over 60 days without hydrogel	Cross-linking and hydrophilicity of polymer matrix	135
PN-KGN	Conjugated	25	Passive: 20% over 30 days	Covalent attachment of KGN	136
QD with KGN loaded βCD	Loaded	5	Passive	Hydrophilic RGD peptide, hydrophobic βCD	137
UCNPs with KGN conjugated to surface	Conjugated	20	Triggered: 60% over 4 h with NIR activation	NIR-triggered	138
UCNT with KGN-loaded βCD conjugated at surface	Loaded	59 ± 5	Triggered: 60% over 3 days	NIR-triggered	139

With the previous considerations, this project focused on the creation of an electrically conductive hydrogel based on natural polymers found in articular cartilage (HA and CS), and able to recreate some of its native properties. The hydrogels were embedded with KTG-loaded PEDOT nanoparticles and electrical stimulation was employed achieve a controllable drug release, with KTG promoting the chondrogenic differentiation of hydrogel-embedded MSCs, leading to tissue regeneration.

3. Materials and methods

3.1 Nanoparticles

3.1.1 PEDOT and KTG/PEDOT nanoparticles fabrication

PEDOT and KTG-loaded PEDOT NPs were produced through in situ emulsion polymerization. A detergent, sodium dodecyl benzenesulfonate (DBSA, Sigma Aldrich), was added to miliQ water at 9.3 mM and magnetically stirred (750 rpm) at 40ºC in a hot plate (RCT Classic; IKA) for 1 hour in order to form micelles. 3,4-Ethylenedioxythiophene (EDOT) (Sigma Aldrich) was added to the solution to a final concentration of 32.2 mM and, in the case of KTG-loaded NPs, a 4mg/ml KTG in DMSO solution was also added to the mixture for a final concentration of 0.4 mg/ml, which was then magnetically stirred (750 rpm) at 40ºC for 1 hour. Finally, a 182,4 mg/ml ammonium persulfate solution (in miliQ water) was added to the mixture for a final concentration of 18,24 mg/ml and magnetically stirred (750 rpm) at 40ºC for 17 hours, in order to start the polymerization reaction.

After 17 hours, the produced NPs followed various washing steps. The reaction mixture was centrifuged at 11000 rpm for 40 min at 4ºC, with the supernatant retrieved and stored for drug-loading efficiency analysis in the case of KTG-loaded PEDOT NPs. MiliQ water was newly added, and the pellet was thoroughly resuspended by 5 min vortex and 15 min ultrasonication (Ultrasonic Cleaner; VWR). These centrifugation-resuspension cycles were repeated 2 more times, and after the final centrifugation the supernatant was retrieved and the nanoparticles were dried in an oven for 3 days in order to completely remove the solvent.

3.1.2 Nanoparticles characterization

After drying for 3 days, the NPs were thoroughly resuspended with miliQ water in 5 and 1 mg/ml suspensions for further characterization.

3.1.2.1 Scanning electron microscopy and Transmission electron microscopy.

The structural characterization of the NPs was performed using a field emission gun scanning electron microscopy (FEG-SEM) (Model JSM-7001F; JEOL) and transmission electron microscopy (TEM). For FEG-SEM, prior to imaging, the samples were mounted on a holder using carbon tape and were coated with a 30 nm gold/palladium (60:40) layer (Model E5100 Sputter Coater; Polaron/Quorum Technologies). Using an average accelerating voltage of 15 kV, the samples were imaged at several magnifications. TEM was performed in a JEOL 2010F microscope equipped with a field emission electron source and operated at an accelerating voltage of 200 kV. The point-to-point resolution was 0.19 nm, and the resolution between lines was 0.14 nm. Samples were dispersed in an aqueous suspension using an ultrasonic bath, and a drop of the suspension was placed over a grid with holey-carbon film.

3.1.2.2 Dynamic light scattering

The size and zeta potential of PEDOT and KTG-loaded NPs resuspended in miliQ water at 1 mg/ml were assessed trough dynamic light scattering (DLS) in a Zetasizer (Malvern Panalytical). The refractive index of the suspension was water, as in accordance with Bocca et.all[140].

3.1.2.3 Atomic force microscopy

Images from the nanoparticles were obtained using a Dimension 3100 Nanoman atomic force microscope (AFM) (Veeco Instruments Inc.), with a fitted NanoScope V controller (Veeco Instruments Inc.), under ambient conditions in tapping mode, with a silicon TAP 150-G probe (Budget Sensors) with a frequency of 150 kHz and a force constant of 5 N/m. For sample preparation, 20 µL of 1 mg/mL PEDOT and KTG/PEDOT NPs suspensions were deposited onto glass slides and left at room temperature (RT) until solvent dryness. AFM measurements were performed on various parts of the deposited NPs, which produced reproducible images as the ones displayed in this work. The scan window size was set to 5×5 µm^2 to 20 x 20 µm^2. Data was analyzed using the NanoScope Analysis software (Version 1.50, Bruker Corporation).

3.1.2.4 Cyclic voltammetry

In order to study the electrochemical properties of the produced NPs, cyclic voltammetry (CV) was employed. A 5 mg/ml suspension of NPs was put in a screen-printed electrode (Metrohm DropSens), which was submerged in a de-aerated 0.05% Tween 20 (Sigma Aldrich) solution prepared in phosphate buffered saline (PBS, Sigma Aldrich). The setup was combined with a Bipotentiostat µStat 300 (Metrohm DropSens). The assay was performed with a potential range of -0.8V to 1V and a sensitivity of 1×10^{-4} A/V, with scan rates of 0.01; 0.02; 0.04; 0.08; 0.1; 0.2 and 0.3 V/s.

3.1.2.5 Tween 20 concentration optimization

As KTG is a highly hydrophobic drug, electrically stimulating its release to aqueous media can be challenging. As such, it was hypothesized that utilizing a detergent to increase its affinity to the medium would allow for a more efficient release upon triggering it through electrical stimulation. As such, a setup similar to the one used for the cyclic voltammetry tests was employed, were 5 mg/mL of KTG/PEDOT NPs were adsorbed in an electrode, and electrically stimulated at a constant 0.6 V (coincident with a KTG oxidation peak) for 3 x 3 min (30 seconds rest). However, for this assay, an electrolyte medium with increasing concentrations of Tween 20 (0, 0.001%, 0.005%, 0.05% Tween 20) was utilized. The solutions used were then analyzed in a plate reader at 274nm in order to quantify the release of KTG.

3.1.2.6 High performance liquid chromatography

The encapsulation efficiency (EE%) and drug loading (DL) of KTG in the produced PEDOT NPs was determined by analyzing the supernatant obtained after centrifuging the reaction mixture through reverse-phase high performance liquid chromatography (HPLC), using a Luna C-18 column (Phenomex). The mobile phase was acetonitrile(ACN):0.01% trifluoroacetic acid (TFA in water, Fisher Scientific) starting at a 90:10 ratio. This ratio steadily changed to 0:100 in the first 10 min of each run, and maintained for 3 min, which then steadily returned to a 90:10 ratio ACN:0.01% TFA in the next 9 min. The flow rate of the samples was 1 ml/min and they were analyzed at a wavelength of 274 nm. The concentration of the samples was calculated through a calibration curve (Figure S1), where samples with 1, 5, 10, 25 ,50, 100, 150, 400 ug/mL were analyzed, while also allowing to infer the retention time of drug. EE% and DL were calculated using the following formulas:

$$EE\% = \frac{Initial\ KTG\ mass\ \ - free\ KTG\ mass\ in\ supernatant}{Initial\ KTG\ mass}$$

$$DL = \frac{Initial\ KTG\ mass\ (mg) - free\ KTG\ in\ supernatant}{final\ nanoparticle\ mass}$$

The controlled release of KTG from the KTG/PEDOT NPs with electrical stimulation was also assessed through HPLC. A PBS solution with 15 ug/mL of NPs and 0.003% Tween 20 was electrically stimulated for 3 min, then left to rest for 30 sec and this was repeat until a total of 9 min stimulation was achieved , between -3 and 3 V at a frequency of 500 mHZ using a AFG1022 potentiostat (TEKTRONIX) and a custom made 12-well plate lid with parallel titanium electrodes (0.8 cm apart). The solution was the retrieved and analyzed by HPLC in the previously described conditions.

3.1.2.7 Fourier-transform infrared analysis

The presence of KTG in the KTG/PEDOT NPs was confirmed through Fourier-transform infrared (FTIR). FTIR spectra were recorded on a FTIR Jasco 4100 spectrophotometer equipped with an attenuated total reflection (ATR) accessory (Top-plate) and a diamond crystal (Specac model MKII Golden Gate Heated Single Reflection Diamond ATR). For each sample, 32 scans were recorded between 4000 and 600 cm^{-1} with a resolution of 4 cm^{-1}. The obtained spectra were analyzed using the Jasco Spectra Manager software.

3.2 Hydrogels

3.2.1 Hydrogel fabrication

For the characterization assays, hydrogels were fabricated using HyStem® hydrogel kit (Advanced Biomatrix), following the producer's instructions. This kit comes with a thiol modified hyaluronan (Glycosil) and a thiol-reactive crosslinker (Extralink). Glycosil and Extralink were reconstituted with 1 and 0.5 ml of degassed water respectively, vortexed immediately, and placed on a rocker platform for 1 hour until the components were fully dissolved. This was followed by the production of three distinct hydrogels: HyStem-CS, HyStem-CS-PEDOT:PSS, HyStem-CS-PEDOT NPs. For fabrication, glycosil was supplemented with CS (Sigma) to a final concentration of 1% v/v, and Clevios™ PH1000 PEDOT:PSS (Heraeus Epurio) or PEDOT NPs were added to a final concentration 10% v/v or 0.2 mg/ml, respectively. Finally, Extralink was added to the different glycosil mixtures in a 1:4 v/v ratio in order to start the cross-linking process.

The hydrogels for human bone marrow-derived MSCs (hBMSCs) culture were prepared as previously described, but PEDOT NPs were replaced by KTG/PEDOT NPs added to a final concentration of 14 μg/ml prior to addition of the cross-linker.

3.2.2 Hydrogel characterization

Following fabrication, the hydrogels were characterized in terms of their water content, swelling, conductivity, and rheological properties.

3.2.2.1 Morphology

The structure and morphology of the fabricated air-dried hydrogels was assessed through FEG-SEM. The samples were mounted on a holder using carbon tape and were coated with a 30 nm gold/palladium (60:40) layer. The scaffolds were then imaged using an average accelerating voltage of 15 kV.

3.2.2.2 Water content and swelling ratio

To assess water content (WC), the newly formed hydrogels were left in eppendorfs at RT for 7 days until they were completely dry. In the case of swelling ratio (Q), newly formed hydrogels were left at RT for 1 day, and then hydrated in excess PBS at RT. The weight of the hydrating hydrogels was measured at timed intervals, after excess water was removed by gentle blotting. Four (n=4) independent hydrogels were used in the analysis. The water content and swelling ratios were calculated as follows:

$$WC = \frac{Initial\ gel\ weight\ \ - Dry\ gel\ weight}{Initial\ gel\ weight} \times\ 100$$

$$Q = \frac{Hidrated\ gel\ weight\ (mg) - Initial\ gel\ weight\ (mg)}{Ininitial\ gel\ weight\ (mg)} \times 100$$

3.2.2.3 Electrochemical impedance spectroscopy

The impedance of newly formed hydrogels was analyzed through electrochemical impedance spectroscopy (EIS) using a PalmSens4 potentiostate and the PSTrace5 software (PalmSens). The samples were put between 2 stainless steel cylindrical electrodes that measured the voltage. In order to maintain the contact area with the electrode's surfaces the same across the different gel samples, these were produced in identical 3D printed molds. To keep the same distance between the electrodes across the different sample measurements, a circular mold was put between the electrodes (without directly contacting them), which prevented them to come closer after contact with the hydrogel surfaces. The assay was performed at a fixed potential of 0.01 V, with a frequency range of 0.01 to 100000 Hz. To calculate the resistance of hydrogels formulated with nanoparticles, an equivalent circuit was utilized. A Randles circuit, consisting of an active electrolyte resistance in series with a parallel combination of the double-layer capacitance and the impedance of a faradaic reaction (given by the Warburg element) was used as an equivalent circuit (Figure 3).

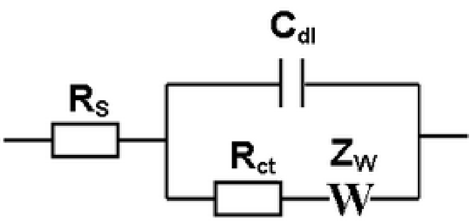

Figure 3 – Randle's equivalent circuit schematic.

As for the HA-CS hydrogel, a simplified Randles circuit with the absence of the Warburg element was utilized (Figure 4):

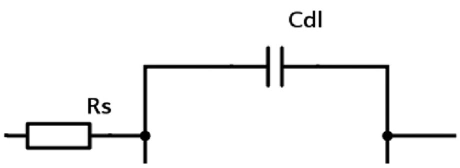

Figure 4 -Simplified Randles circuit schematic.

Furthermore, the frequency-dependent conductivity of the hydrogels was calculated as follows:

$$\sigma_{ac} = \left(\frac{Z'}{Z'^2 + Z''^2}\right)\frac{d}{A}$$

where Z' is the real measured impedance, Z'' the imaginary measured impedance, *d* the height of the hydrogel and *A* its cross-sectional area.

3.2.2.4 Rheology

The rheological properties of the produced hydrogels were assessed using an MCR 92 modular compact rheometer (Anton Paar). The measurement was made using a cone-plate geometry with a cone diameter of 50 mm, and a constant measurement gap of 0.1 mm, with a sample volume of 0.5 ml. The elastic behavior of the gels was studied through an oscillating time sweep test, were the time dependent storage modulus (G') and loss modulus (G'') were recorded, with a frequency of 1 Hz at 25ºC for 90 min. An amplitude sweep test was also performed at a frequency of 1 Hz at 25ºC until a maximum strain of 200% was reached.

3.3 *In vitro* cell culture studies

Various cytocompatibility assays were performed with hBMSCs in order to optimize the biological performance and ensure a biocompatible environment before combining the various elements of the final system. After this criteria was met, the chondrogenic potential of KTG released from nanoparticles via electrical stimulation was accessed with hBMSCs seeded in 2D-culture plates or embedded in 3D hydrogels.

3.3.1 hBMSC culture

The human hBMSCs used in this thesis were part of the cell bank available at the Stem Cell Engineering Research Group, Institute for Bioengineering and Biosciences (iBB) at Instituto Superior Técnico. MSC were previously isolated according to protocols previously established at iBB-IST. Samples were obtained from Instituto Português de Oncologia Francisco Gentil, Lisboa, and Centro Clínico da GNR, Lisboa, under collaboration agreements with iBB-IST. All human samples were obtained from healthy donors after written informed consent according to Directive 2004/23/EC of the European Parliament and of the Council of March 31, 2004, on setting standards of quality and safety for the donation, procurement, testing, processing, preservation, storage, and distribution of human tissues and cells (Portuguese Law 22/2007, June 29), with the approval of the Ethics Committee of the respective clinical institution. Isolated cells were kept frozen in liquid/vapor nitrogen tanks until further use. Vials with cryopreserved hBMSCs (Donor: Male 46 years) were thawed at 37ºC in a water bath. Afterwards, the cells were diluted in cell culture medium (1:6, v/v) - low glucose Dulbecco's Modified Eagle Medium (DMEM; Gibco Thermo Fisher Scientific) supplemented with 10% v/v fetal bovine serum (FBS; Gibco, Thermo Fisher Scientific) and 1% v/v antibiotic-antimycotic solution (Anti-Anti Solution; Gibco, Thermo Fisher Scientific) - and centrifuged for 7 minutes at 1250 rpm. Afterwards, the supernatant was removed, and the cells were resuspended in fresh culture medium, counted using the trypan blue (Trypan blue solution 0.4%; Gibco, Thermo Fisher Scientific) exclusion method, and plated on a T-flask at a cell density of 3000 cells/cm^2 that was kept at 37ºC and 5% CO2 in an incubator. Culture media was fully renewed every 3-4 days. Cell passaging was performed when hBMSCs reached 90% confluence. For that, cells were washed with PBS, incubated with a trypsin solution (0.05%, v/v) (Trypsin; Gibco, Thermo Fisher Scientific) for 7 minutes at 37ºC and 5% CO2 in order for the cells to detach, and afterwards centrifuged and counted. The cells were then distributed in the appropriate number of cell culture flasks at a density of 3000 cells/cm^2. All experimental assays were performed using hBMSCs between passage 3 and 5.

3.3.2 Materials and device sterilization

The NPs used in cell culture studies with hBMSCs were sterilized under UV light for 1 hour. In the case of the electric stimulation lid device, these were cleaned with ethanol 70% (v/v) and left under UV light exposure for 3 hour after each use. Besides the stimulation period performed inside the incubator, the devices were kept inside a sterile laminar flow hood during all the experiment. Prior to cell culture, the hydrogels prepared with sterile materials were further sterilized though washing with a 2% Anti-Anti solution in PBS for 3 h (3 washes, 1 h each).

3.3.3 Cytotoxicity assays

In order to confirm the biocompatibility of the various elements in the proposed hydrogel system, several cytotoxicity assays were performed.

3.3.3.1 Nanoparticles cytotoxicity assay

For this cytocompatibility assay, 10^4 hBMSCs/cm^2 were seeded in a 96-well plate (Falcon BD), and cell culture media with 2; 5 or 10 ug/ml PEDOT or KTG-PEDOT NPs was added to the respective wells. The cell metabolic activity was monitored on days 1, 3 and 7 using AlamarBlue assay (AlamarBlue Cell Viability Reagent; Thermo Fisher Scientific). After washing the wells with PBS, a 10% (v/v) AlamarBlue solution diluted in culture media was added and left for incubation for 3h at 37ºC and 5% CO_2. The fluorescence intensity of the resultant solutions was then measured in a plate reader (Infinite

200 Pro, Tecan) at an excitation/emission wavelength of 560/590nm. A well without cells was used as blank control. Furthermore, on day 7, cells were stained with calcein AM 2 μM (Thermo Fisher Scientific) in PBS and incubated for 30 min at room temperature, washed with PBS, and visualized in a fluorescence microscope (LEICA DMI300B, Leica Microsystems) equipped with a digital camera (NIKON DXM1200F, Nikon Instruments Inc.).

3.3.3.2 Tween 20 cytotoxicity assay

To understand the biocompatibility threshold for the concentration of Tween 20, 10^4 hBMSCs/cm^2 were seeded in a 96-well plate, and cell culture media (DMEM + 10% FBS + 1% Anti-Anti) with 0.005; 0.003 and 0.001% v/v Tween 20 was added to the respective wells. The cytocompatibility of the different Tween 20 concentrations after 7 days of culture was confirmed by staining the cultures with calcein AM 2 μM (v/v) , which were imaged under fluorescence microscopy.

3.3.3.3 Electrical stimulation cytotoxicity assay

In order to confirm the cytocompatibility of the electric potential required for the release of KTG from the NPs, 10^4 hBMSCs/cm^2 were seeded in a 12-well plate and cultured with DMEM + 10% FBS + 1% Anti-Anti media for 2 days. The cell cultures were then electrically stimulated for 3 minutes (with 30 second pauses) for 9 min total with 1, 2 and 3 V at 500 mHz. Non-stimulated hBMSCs were used as control. Cell viability was assessed with a LIVE/DEAD assay kit (Thermo Fisher Scientific), where cells were stained with a 2 μM (v/v) calcein AM and 4 μM (v/v) ethidium homodimer-1 in PBS and imaged under fluorescence microscopy.

3.3.4 Evaluation of the chondrogenic inducting potential of different concentrations of non-stimulated KTG/PEDOT NPs

The effects of non-stimulated KTG/PEDOT NPs in the chondrogenic differentiation of hBMSCs was assessed by seeding 3.2×10^3 cells/cm^2 in a 96 well-plate, and supplementing with incomplete chondrogenic media - DMEM high glucose with 100nM dexamethasone (Sigma-Aldrich), 50 ug/ml ascorbic acid (Sigma-Aldrich), 40 ug/ml L-proline (Sigma-Aldrich), 1% v/v ITS + supplement (Corning), 1 mM sodium pyruvate and 1% v/v Anti-Anti solution – with increasing concentrations of KTG/PEDOT NPs (2, 5, 10 and 50 ug/mL) for 14 days. As a positive control, complete chondrogenic media was used with TGF-β3, and a negative control with incomplete chondrogenic media with 50 ug/mL PEDOT NPs. Four replicates (N=4) were used in this analysis. The cell metabolic activity was monitored on days 7 and 14. Additionally, after 14 days of culture, the cells of each conditions were stained with 1% (w/v) Alcian blue, a compound that stains glycosaminoglycans.

3.3.5 Assessment of the chondrogenic inducing potential of KTG/PEDOT NPs and HA-CS-KTG/PEDOT NPs hydrogels with and without electrical stimulation

To understand the effects of KTG-loaded nanoparticles in the chondrogenic differentiation of hBMSCs, $2.6x10^4$ hBMSCs/cm^2 were seeded in a 12-well plate and supplemented with incomplete chondrogenic media - DMEM high glucose with 100nM dexamethasone (Sigma-Aldrich), 50 ug/ml ascorbic acid (Sigma-Aldrich), 40 ug/ml L-proline (Sigma-Aldrich), 1% v/v ITS + supplement (Corning), 1 mM sodium pyruvate and 1% v/v Anti-Anti solution – supplemented with 2 ug/ml of KTG/PEDOT NPs or PEDOT NPs. The differentiation was carried through 21 days, with media being exchanged every 3 to 4 days. With every media exchange, the wells were thoroughly washed with PBS to retrieve the remaining NPs, and new NPs at 2 ug/mL were added. With each exchange, the cells were electrically stimulated for 3 x 3 min (30 second rest between each stimulation) between -3 and 3 V at a frequency of 500 mHZ. Cells seeded in the absence of NPs and non-stimulated correspondent groups were used as controls.

In the case of the hydrogels, the assay was performed similarly, where $2.22x10^5$ hBMSCs/mL hydrogel were encapsulated in a HA-CS hydrogel together with 14 ug/mL KTG/PEDOT NPs or PEDOT NPs, but no new NPs were added with each media exchange. hBMSCs encapsulated in HA-CS hydrogel and non-stimulated correspondent groups were used as controls.

3.3.5.1 Cell viability and metabolic activity assays

The metabolic activity of hBMSCs (2D cultures in plates or 3D hydrogel cultures) was measured on days 3, 7, 14 and 21 of the culture using the Alamar Blue assay as previously described in subsection 3.3.3.1. Three independent hydrogels were considered for each condition (n=3). To account for possible hydrogel autofluorescence, acellular hydrogels were used as blank controls. For the case of hydrogels, cell viability was assessed after 21 days of culture through a LIVE/DEAD assay as previously described, and observed under fluorescence microscopy.

3.3.5.2 Sulfated GAGs quantification

After 21 days of culture the cells in 2D cultures were harvested, centrifuged, and the obtained cell pellets were frozen and stored at -80ºC until further use. In the case of the hydrogels, these were digested with 40 mM N-acetyl cysteine and the cells were collected and centrifuged, which yielded a cell pellet with some hydrogel remainants.

The measurement of sulfated GAG levels was carried out using a 1,9-Dimethylmethylene Blue (DMMB, Sigma-Aldrich) assay. A DMMB dilution buffer pH 6.5 (50 mM sodium phosphate (Sigma-Aldrich), 2 mM N-acetyl cysteine (Sigma-Aldrich) and 2 mM EDTA (Merck) in ultrapure miliQ water) was prepared. DMMB stock solution (pH 3) was prepared by adding a 3.2 mg/mL DMMB in absolute EtOH solution (Sigma-Aldrich) to a solution of 2.73 g NaCL and 3.04 gL glycine in ultrapure MiliQ water, with a total volume of 1L. The previously obtained pellets were digested with a 0.1 mg/mL papain (from papaya latex, Sigma-Aldrich) in DMMB dilution buffer solution for 16 hours at 60ºC. Afterwards, DMMB stock solution was mixed with the digested pellets in 96-well plates. The mixtures were incubated for 5 min at RT, and the fluorescence was read at 525 nm in a plate reader. The amounts of sGAG for each condition were calculated by recurring to a calibration curve (Figure S2) using chondroitin sulfate (sodium salt from bovine cartilage, Sigma-Aldrich) standards. The sGAG amounts were then normalized to the metabolic activity of the cells at day 21 of differentiation.

3.3.5.3 Quantitative Real Time-Polymerase Chain Reaction (qRT-PCR) Analysis

After 21 days of culture (both 2D cultures in plates or 3D hydrogel, with and without electrical stimulation), the expression levels of *Sox9*, *COL I*, *COL II*, *COL X* and *MMP-13* were quantified by qRT-PCR analysis. Total RNA was extracted from the pellets using a RNeasy Mini Kit (QIAGEN) following the manufacturer's guidelines. RNA concentration and quality was evaluated using a Nanodrop (NanoVue Plus, GE Healthcare). cDNA was synthesized from the extracted RNA using a High-Capacity cDNA Reverse Transcription kit (Applied Biosystems) according to the manufacturer's protocol. The reaction mixtures were incubated in a T100^{TM} thermal cycler (Bio-rad) with the following temperature protocol: 5 min at 25°C, 30 min at 42°C and 5 min at 85°C, and then were maintained at 4°C. The qRT-PCR analysis was performed using NZYSpeedy qPCR Green Master Mix (2x), ROX plus (NZYTech) and StepOnePlus real-time PCR system (Applied Biosystems). All reactions were carried out at 95°C for 10 min (denaturation step), followed by 40 cycles of 95°C for 15 sec and 60°C for 1 min. The expression of target genes was normalized to the housekeeping gene glyceraldehyde 3-phosphate dehydrogenase (*GAPDH*) and then expressed as fold-change relative to the baseline expression of hBMSCs at day 0 prior to cell seeding. The primer sequences used in the qRT-PCR analysis are summarized in Table 5.

Table 5 – Primer sequences used for quantitative real time PCR analysis.

Gene	Fwd primer sequence	Rev primer sequence
GAPDH	5'-GGTCACCAGGGCTGCTTTTA -3'	5'-CCTGGAAGATGGTGATGGGA-3'
COL I	5'-CATCTCCCCTTCGTTTTTGA-3'	5'-CCAAATCCGATGTTTCTGCT-3'
COL II	5'-GGAATTCCTGGAGCCAAAGG-3'	5'-AGGACCAGTTCTTGAG-3'
Sox9	5'-TACGACTACACCGACCACCA-3'	5'-TTAGCATCATCTCGGCCATC-3'
COL X	5'-CCAGGTCTCGATGGTCCTAA-3'	5'-GTCCTCCAACTCCAGGATCA-3'
MMP13	5'-TCCTCTTCTTGAGCTGGACTCATT-3'	5'-CGCTCTGCAAACTGGAGGTC-3'

3.3.5.4 Immunofluorescence analysis

The presence and distribution of collagen type II, one of the major components of native articular cartilage was analyzed in seeded hBMSCs (2D cultures) after 21 days of chondrogenic differentiation. The cells were washed with PBS, fixed with 4% PFA for 20 min at RT and kept in PBS at 4ºC until the staining procedure. Afterwards, the cells were washed with 1% bovine serum albumin (BSA, Sigma-Aldrich) in PBS for 5 min, and incubated for 45 min with a blocking solution composed by 1% BSA, 10% FBS and 0.3% Triton X-100 in PBS to block and permeabilize cells. A primary antibody mouse anti-human collagen II (Invitrogen, dilution 1:50 in 1% BSA, 10% FBS and 0.3% Triton X-100) solution was added and left for incubation overnight at 4ºC. After washing with 1% BSA in PBS, goat anti-mouse IgG Alexa Fluor 546 (Thermo Fisher Scientific, dilution 1:100 in 1% BSA solution (in PBS)) were utilized as secondary antibodies and incubated in 1 h at room temperature protected from light. Finally, the cell nuclei were counterstained with DAPI (Thermo Fisher Scientific, 1.5 µg/ml) for 5 min and washed with PBS. The cells where then visualized through fluorescence microscopy (LEICA DMI300B, Leica Microsystems) equipped with a digital camera (NIKON DXM1200F, Nikon Instruments Inc.).

3.4 Statistical analysis

Results are presented as mean ±SD. Statistical analysis of the obtained results was performed through one-way ANOVA in Excel. Results were considered statistically significant when p-values obtained were lower than 0.05 (95% confidence intervals, *$p<0{,}05$).

4. Results and discussion

4.1 Nanoparticle formulation and characterization

Both PEDOT and KTG/PEDOT nanoparticles were formed using an EDOT monomer, with DBSA acting simultaneously as a surfactant and doping agent, and APS providing the free radicals for polymerization. Due to the high hydrophobicity of kartogenin, the drug remained in the core of the micelles formed by the surfactant, being loaded in the PEDOT NPs through in situ emulsion polymerization.

4.1.1 Nanoparticle morphology

Following production, the morphology of both PEDOT and KTG/PEDOT nanoparticles was assessed through SEM (Figure 5) and TEM (Figure 6) analysis. For the SEM analysis, a picture of the aluminum foil without NPs is also present in order to more clearly identify the NPs in the other pictures. These microscopy techniques have been successfully utilized to measure nanoparticle sizes[141,142], however this is not feasible for these NPs, as images acquired with both techniques show particle aggregation. As such, singular particles become indistinguishable and their size unable to be accurately measured through these techniques.

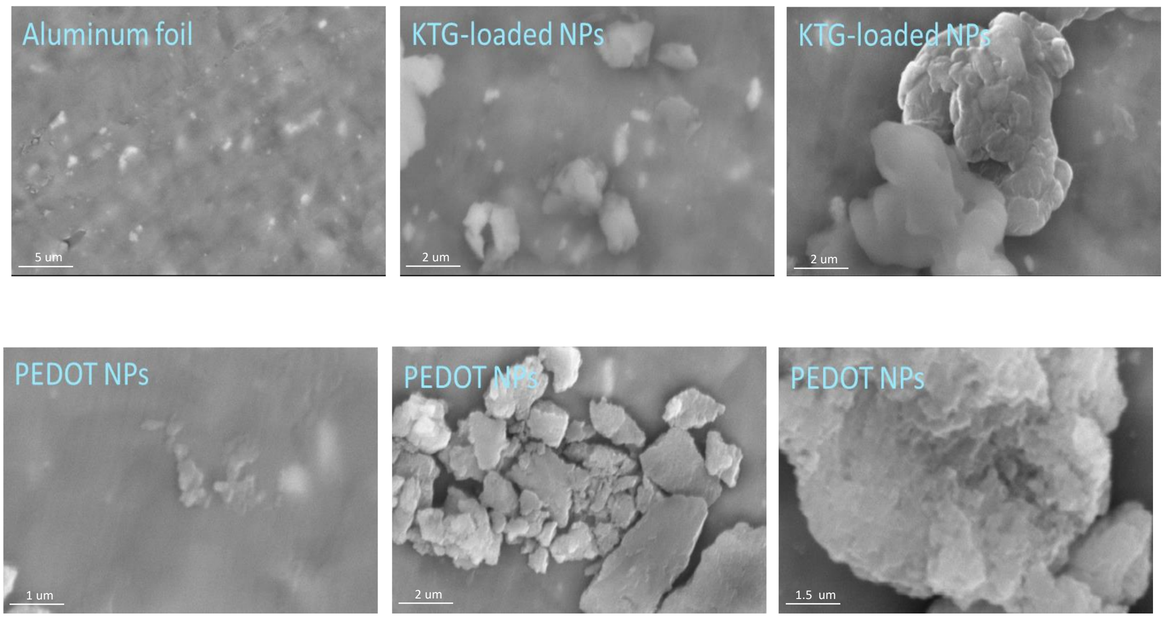

Figure 5 - SEM images of KTG/PEDOT and PEDOT nanoparticles. Scale bars are depicted in the images.

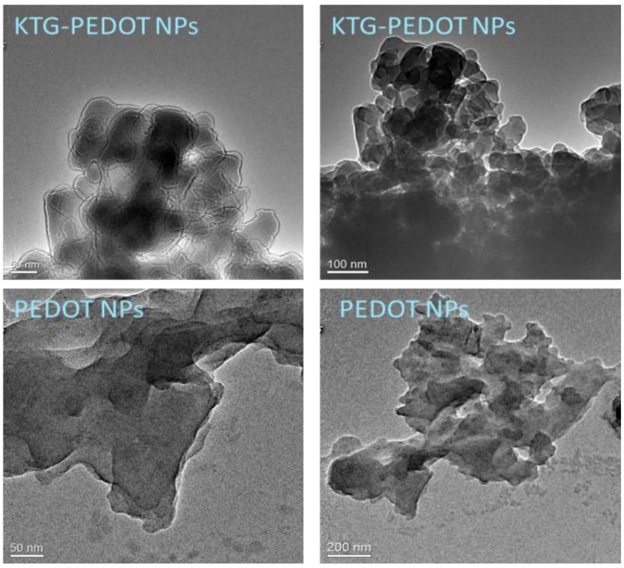

Figure 6 -TEM images of PEDOT and KTG/PEDOT NPs. Scale bars are depicted in the images.

4.1.2 Nanoparticle size and stability

The size of the PEDOT and KTG-loaded PEDOT NPs was determined through DLS, with effective diameters of 99 ± 71 and 172 ± 90 nm respectively (Figure 7, A). The size distribution of the particles is represented by the polydispersity index (PdI), which ranges from 0 to 1, with 0 being a homogenous nanoparticle population and 1 being a highly heterogeneous one. Despite both being somewhat heterogeneous, PEDOT NPs (PdI = 0.245) were significantly less heterogeneous than the KTG-loaded NPs (PdI = 0.490), which can also be seen through the lower size standard deviation. The dispersity among the NP populations can be explained by the lack of full control during the synthesis process, and the chemical reactions during NP development not being homogenous processes, which often introduces intra and inter-batch heterogeneity[143]. In fact, this might explain the higher PdI of KTG-loaded PEDOT NPs, as the introduction of an additional molecule to the formulation (when compared to PEDOT NPs) introduces further complexity to the chemical synthesis, elevating heterogeneities. The size of the nanoparticles was also determined through AFM, with PEDOT NPs exhibiting a size of 31.7 nm and KTG/PEDOT a size of 91.5 nm (Figure 8). Despite in both assays KTG/PEDOT NPs exhibiting larger diameters than PEDOT NPs, the absolute values varied significantly. However, inter-technique differences for NP measurement are common[144].

DLS was also utilized to measure the ζ-potential of the NPs, which came at -71 ± 10.3 mV for PEDOT and -75 ± 5.8 mV for KTG-loaded NPs (Figure 7, B). The ζ-potential can give insight on the stability and electrokinetic potential of an NP colloidal dispersion, being the potential difference between the dispersion medium and the stationary layer surrounding the NP. Because the particle surface has a charge, it creates a surrounding bound layer with the correspondent counter-ions, traveling with the nanoparticle as it diffuses through the dispersion. Hence, the magnitude of the ζ-potential indicates the degree of electrostatic repulsion between particles with the same charge, were higher values (either positive or negative) indicate a higher repulsion, and thus a resistance to NP aggregation and flocculation. The produced NPs have absolute ζ-potentials above 61 mV, which is the threshold were particles are considered highly stable. In fact, these nanosuspensions were able to maintain stability for over 2 months without significant sedimentation due to particle aggregation.

Nanoparticles are able to enter cells through endocytosis, depending on their surface chemistry, size and shape. Several studies have identified particles with diameters of 100 nm to be optimally internalized by cells[145,146]. However, particles with diameters upwards of 240 nm have been shown to able to be internalized at lower rates[147]. Particle surface charge is another critical factor influencing the cellular uptake of nanoparticles. As the cell membrane is negatively charged, nanoparticles with a positive surface charge have improved electrostatic interactions and adhesion than neutral or negatively charged NPs[148]. However, unlike negatively charged NPs, the uptake of cationic NPs can disrupt the cell membrane, leading to increased toxicity and even cell death[149,150]. Hence, as the produced PEDOT and KTG-loaded PEDOT NPs have respective diameters of 99 and 172 nm and are negatively charged, they should be internalized by the MSCs without cytotoxicity. As Johnson et al, was able to demonstrate the chondrogenic inducing effects of KTG even when the drug was supplemented in the cell media, an intracellular delivery of the drug through combination with nanoparticles might optimize its effects upon release[151].

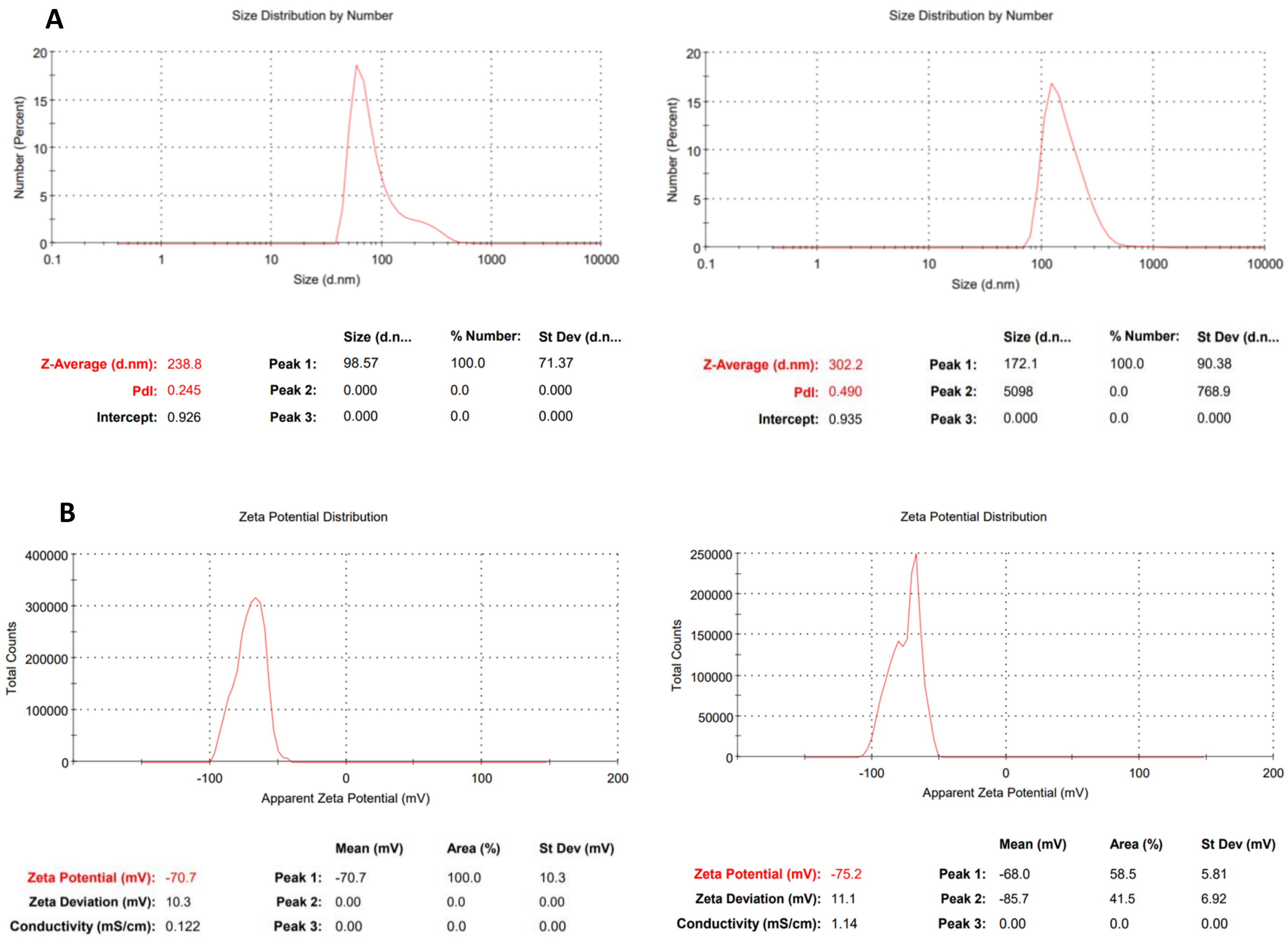

Figure 7 – Dynamic light scattering assessment of size (A) and (B) zeta potential of PEDOT (left) and KTG/PEDOT (right) nanoparticles resuspended in miliQ water, at a concentration of 1 mg/ml. PEDOT NPs exhibited a size of 98.57 nm, with a zeta potential of -70.7 mV. The size of KTG/PEDOT NPs was 172.1 nm while the zeta potential was -75.2 mV.

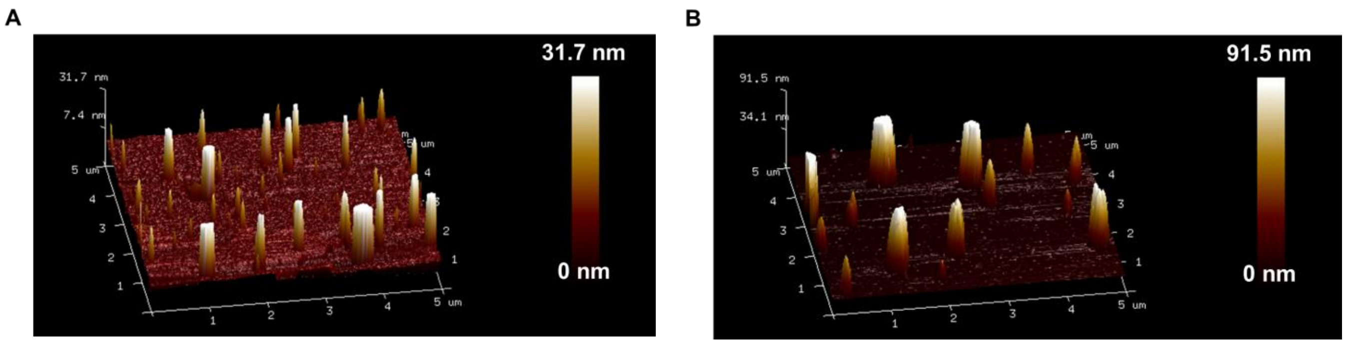

Figure 8 – Atomic force microscopy of A) PEDOT and B) KTG/PEDOT nanoparticles. PEDOT NP size was 31.7 nm while KTG/PEDOT NP was 91.5 nm.

4.1.3 Electrochemical properties

The electrochemical response of the produced nanoparticles, adsorbed to the electrode surface, was assessed through CV, which registered oxidation-reduction cycles within a potential range of -0.8 and 1 V at different scan rates (Figure 9). PEDOT NPs demonstrated a typical anodic peak at around 0 V, and a cathodic peak at around -0.2 V which is close to what has been previously describe[152]. As kartogenin is a compound that also experiences redox behavior, the KTG/PEDOT NPs voltammograms can get partially "masked" by KTG. This is evident by the appearance of a "shoulder" to the right of the previously mentioned oxidation peak at 0 V, meaning the drug has an irreversible oxidation peak at 0.2 – 0.3 V, depending on the scan rate. However, another irreversible oxidation peak at 0.6-0.7 V, depending on the scan rate, can also be observed. The current densities of the scans are given by a superposition of a capacitive current (double layer at electrode-electrolyte interface) and a faradaic current (mass transfer in redox electrochemical reactions at the electrode) responsible for the oxidation/reduction peaks[153]. In the voltammograms of both nanoparticle types, as the scan rates increase, it is possible to observe a concomitant increase in current density. In terms of the capacitive current, this is explained by its linear dependence with the scan rate. Furthermore, there is also an increase in the faradaic current, as faster voltage cycling leads to a more rapid conversion of a species to its oxidized/reduced forms[154]. As current is defined by the rate of electron flow per unit of time, faster conversion leads to higher currents. Through the voltammograms, it is also possible to confirm the adsorption of the species to the electrode and that the reaction rate is not limited by the diffusion of the species to the electrode's surface. In the case of adsorbed species, plotting the peak current densities against the scan rate should result on a linear dependence[154,155]. In fact, this linearity can be observed by plotting the latter KTG oxidation peak intensities against the scan rates (Figure S4), with an R^2 of 0.9998. Overall, these results show the existence of an electrochemical response by the fabricated NPs and loaded drug upon applied voltages. This response will be the key for the proposed electrically triggered-drug release mechanism, that will be latter explained.

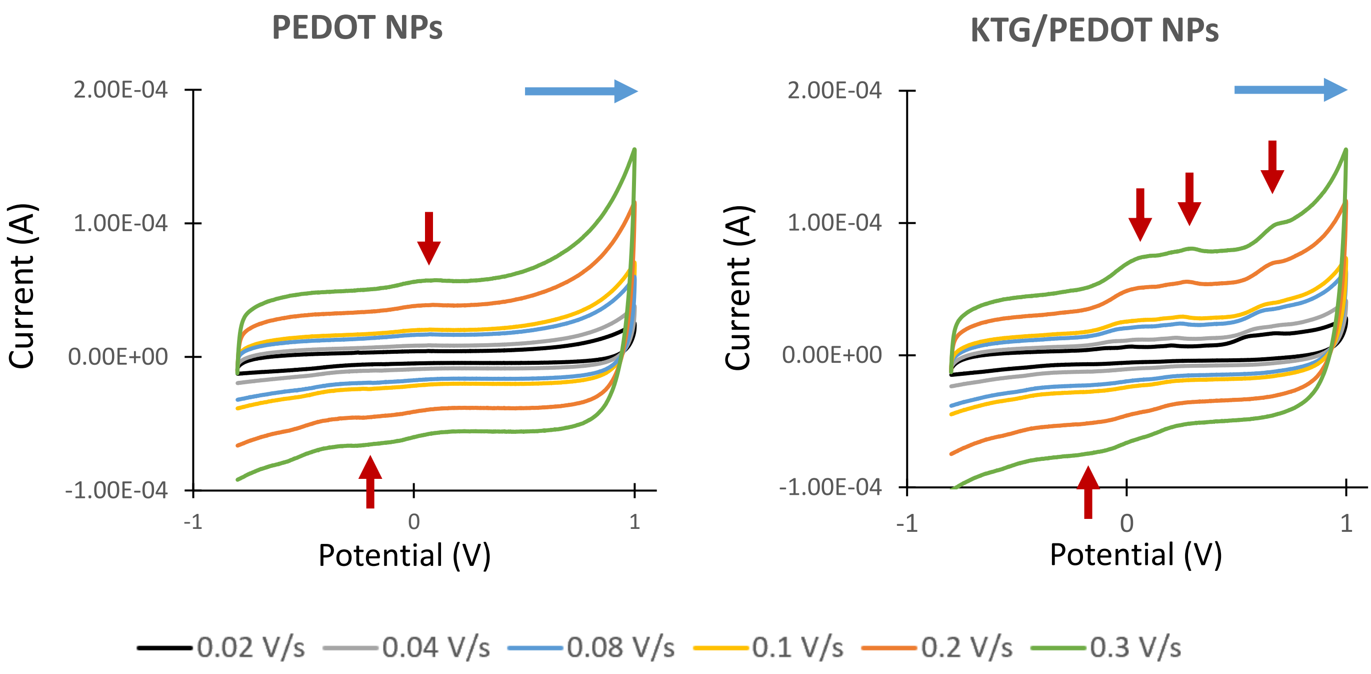

Figure 9 – Voltammograms of PEDOT and KTG/PEDOT nanoparticles obtained by cyclic voltammetry with PBS and 0.05% Tween 20 as an electrolyte. The voltage range was -0.8 to 1 V, and the assay was performed at various scan rates (0.02, 0.04, 0.08, 0.1, 0.2 and 0.3 V/s) for both nanoparticle formulations (n=3). Red arrows point to oxidation and reduction peaks, and blue arrow to the direction of the scan.

4.1.4 Drug loading into PEDOT nanoparticles

In order to assess the mass of KTG that was successfully loaded in the PEDOT NPs, the supernatant acquired after their production and centrifugation (containing the leftovers of the chemical processes and the unloaded KTG) were analyzed through HPLC (Figure 10). Through the area of the absorption peak at the KTG retention time, the drug loading efficiency was calculated to be 60%, and a drug loading of 0.3 mg KTG / mg NPs. Usually, nanoparticle drug delivery systems have very low drug loading efficiencies, with most systems reporting values lower than 5%[156,157]. However, the drug loading efficiency achieved by this system can likely be explained by the high hydrophobicity of KTG, since other works using these types of molecules reported similar results[158,159]. As the drug was loaded through *in situ* emulsion polymerization, it remained inside the micelles generated by the surfactant, instead of interacting with the aqueous medium. As such, a large proportion of KTG was present during polymerization of the NPs. Furthermore, it is favorable for the hydrophobic drug to be loaded inside the PEDOT NPs, as these provide a hydrophobic core for KTG, shielding it from the surrounding medium[160]. With the goal of confirming that the drug was successfully loaded, Fourier transform infrared spectrometry (FTIR) of KTG, PEDOT NPs and KTG/PEDOT NPs was employed (Figure 11). This technique utilizes infrared light that, depending on its energy (wavelength) can trigger the vibration of specific molecular bonds after absorption, leading to stretching or bending[161]. As such, drops in transmission signify absorption peaks of identifiable functional groups, and the comparison of these peaks across the measured samples can confirm the presence of KTG in the PEDOT NPs[162]. In the

KTG spectra a peak at wavenumber 3300 cm^{-1} indicates the presence of a N-H bond from the secondary amine. At wavenumber 3050 cm^{-1}, we can see the O-H bond from the drug's carboxylic acid. A C=O bond from the same carboxylic acid responsible for the peak at wavenumber 1710 cm^{-1}. From the aromatic amine, a C-N bond can be observed at wavenumber 1260 cm^{-1}. The drug loading can be confirmed through the comparison of several peaks among the analyzed samples. At wavenumber 3050 cm^{-1}, the O-H bond stretch characteristic of KTG is slightly represented in the KTG/PEDOT NPs spectra, but totally lacking in PEDOT NPs. The same can be seen in the wavenumber region between 2350 and 2175 cm^{-1}, where a slight absorbance in KTG is also represented exclusively in KTG/PEDOT. At wavelength 1050 cm^{-1}, there is an absorbance peak in both PEDOT and KTG PEDOT NPs, however, the latter is comparatively higher, which can be due the contribution of KTG, also having a peak in that wavenumber. At 1000 and 783 cm^{-1}, KTG/PEDOT exhibits some slightly higher peaks than PEDOT correspondent to KTG absorption peaks. Despite visible and able to confirm drug loading, the KTG absorption peaks in KTG/PEDOT spectra are notably slight, which is likely due to a low concentration of NPs in the sample used for the assay. In addition, drug loading was calculated to be 0.3 mg KTG / mg NPs, meaning that the absorption contribution of KTG in the KTG/PEDOT spectra might be lighter.

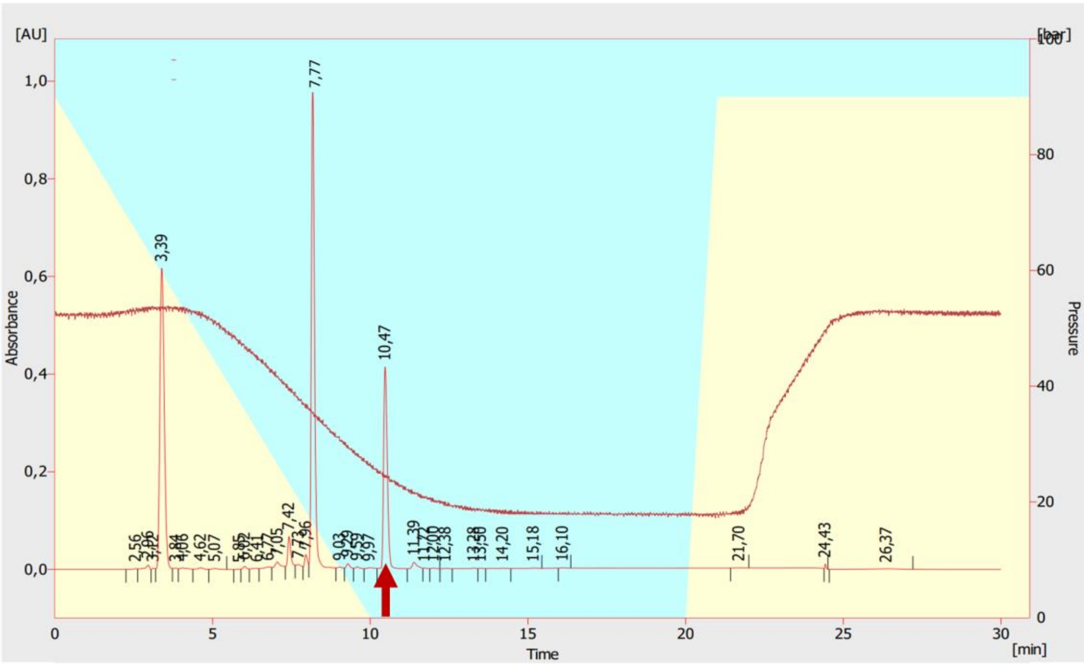

Figure 10 – HPCL chromatogram of the KTG/PEDOT NPs supernatant retrieved after fabrication. KTG retention time is at 10,47 min. The amount of unloaded KTG was calculated using a prepared calibration curve. Red arrow points to KTG retention time.

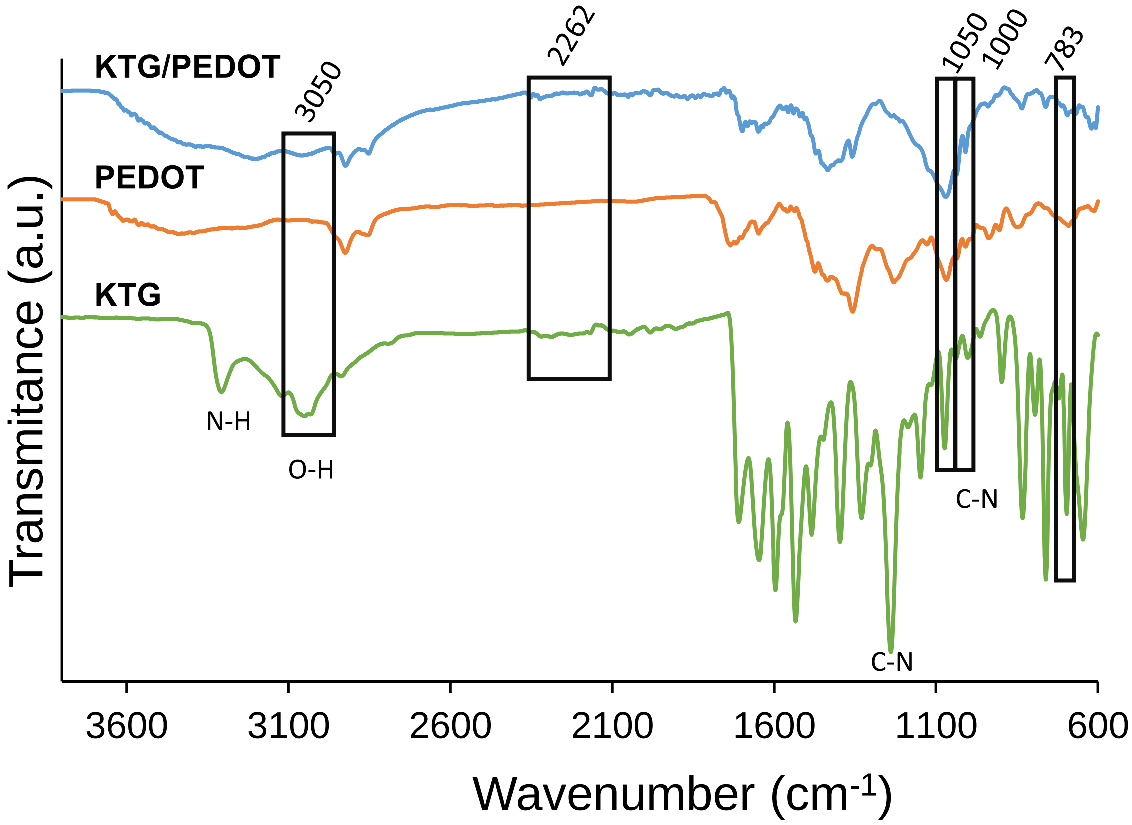

Figure 11 – FTIR analysis of KTG drug, PEDOT NPs and KTG/PEDOT NPs. 5 KTG peaks that can confirm its presence in the nanoparticles were identified at wavenumbers 3050, 2262, 1050, 1000 and 783 cm^{-1}. Some of the covalent bonds responsible for the absorption peaks can also be seen bellow their respective peaks.

4.1.5 Controlled KTG release with electrical stimulation

After positive confirmation that KTG was encapsulated inside PEDOT nanoparticles, the next step was to control its release through electrical stimulation. As KTG is a very hydrophobic drug, it was hypothesized that triggering its release in a heavily aqueous media, even with the right voltages, would be difficult. As such, an assay was performed in other to understand if the electrically triggered release of the drug would improve if with an electrolyte medium consisting of PBS with increasing concentrations of Tween 20 (no Tween, 0.001%, 0.005%, 0.05% v/v). An assay with a similar set up to cyclic voltammetry, were KTG/PEDOT NPs were adsorbed to the electrode surface, was performed, but instead of cycling through voltages, a fixed voltage of 0.6 V (coincident with the second KTG oxidation peak) was applied every 3 min, with 30 seconds rest between for a total of 9 min of stimulation. The release medium was measured in a plate reader at 320 nm (Figure 12), and the release percentage of KTG was calculated with the aid of a calibration curve (Figure S3). As theorized, increasing the affinity of the release media for the drug greatly improves drug release upon electrical stimulation. In the absence of Tween 20, only 3% of the loaded drug was released, while in the presence of 0.05% Tween this value reached a staggering 50 ± 5%. However, as a powerful detergent, the implementation of Tween 20 with cells requires careful management of its concentration, as it can disrupt the cell membranes after a certain concentration threshold.

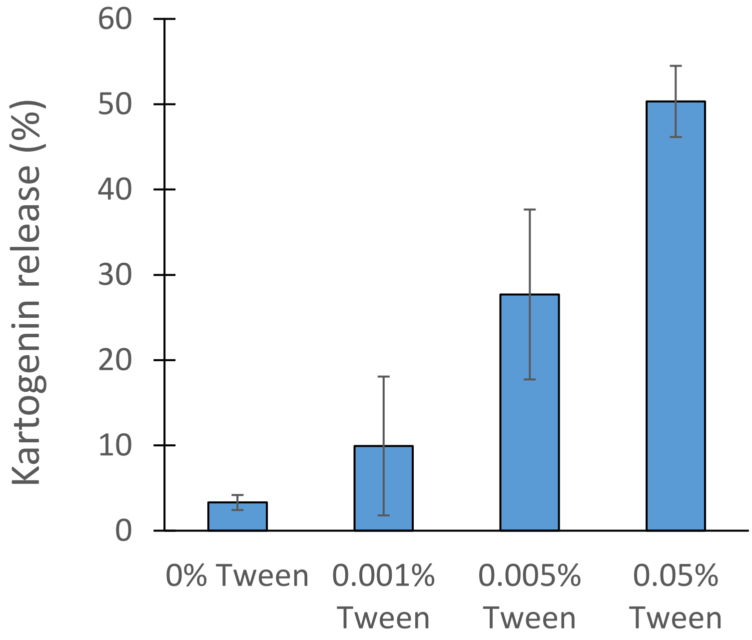

Figure 12 – KTG release assay under electrical stimulation with increasing concentrations of Tween 20. KTG/PEDOT NPs adsorbed to an electrode were stimulated at 0.6V for 3 x 3 min with 30 second rest. The electrolyte medium was composed by PBS with 0, 0.001, 0.005 and 0.05% v/v Tween 20 (n=2).

Despite the positive results showing the control of KTG release with electrical stimulation, and its dependence on the affinity to the release medium, the experimental conditions of the previous release assay are fundamentally different from the ones required for the stimulation of NPs when these are to be combined with cells and hydrogels. In this case, the stimulation will occur through direct coupling, where a plate lid with two parallel electrodes will be placed in direct contact with the cell culture media reservoir, with applied voltages creating an electric field[163]. In this setup, the nanoparticles would no longer be adsorbed onto the electrode (but instead either in suspension or entrapped in a hydrogel). Because electric field strength is distance dependent[164], the potential “felt” by the nanoparticles would be significantly less than the applied potential, as the particles are at different distances from the electrodes. As such, applying the potential used for the previous assay would likely not result in drug release, as the actual potential that reached the NPs would be very low. Consequently, a different electrical stimulation protocol was required. For this protocol, instead of a fixed potential (direct current), an alternating current was employed, with potentials being cycled between -3 and 3 V at a frequency of 500 mHz for 3 min. In Figure 13 the HPLC chromatograms of the media (PBS with 0.003% Tween 20) where 15 µg/mL KTG/PEDOT NPs were stimulated once or twice using the abovementioned protocol can be observed. It is possible to see that the KTG/PEDOT NPs sample without stimulation did not exhibit any drug release, evidenced by the lack of a peak at a retention time of 10.67, correspondent to the KTG retention time. However, the sample that was stimulated once showed a peak at the KTG retention time with an area of 24 mAU.s, the same peak having an area of 49 mAU.s in the KTG/PEDOT NPs samples that were stimulated twice. Through a previously prepared calibration curve, it was estimated that there was a 5 and 10.5% KTG release from NPs stimulated once or twice, respectively. This result indicates that KTG can be released from KTG/PEDOT NPs in a controlled manner upon electrical stimulation without significant passive release.

When kartogenin was first identified as a chondro-inductive drug, it was determined that its effective median concentration to induce the chondrogenic differentiation of hBMSCs was 100 nM[125]. However, higher values of KTG still exhibited slightly improved effects without added toxicity. As such, the theoretical concentration of nanoparticles required for the release of 100 nM of KTG post electrical stimulation (assuming the 5% release of the loaded drug with the previously described protocol) was calculated according to the following formula:

$$NP\ concentration\ = \frac{Required\ KTG\ concentration\ \times KTG\ MM}{DL\ \times Drug\ release}$$

where KTG is kartogenin, MM its molecular mass an DL its drug loading in the KTG/PEDOT NPs. It was estimated the minimum KTG/PEDOT concentration to achieve the desired KTG release would be 2 µg/ml.

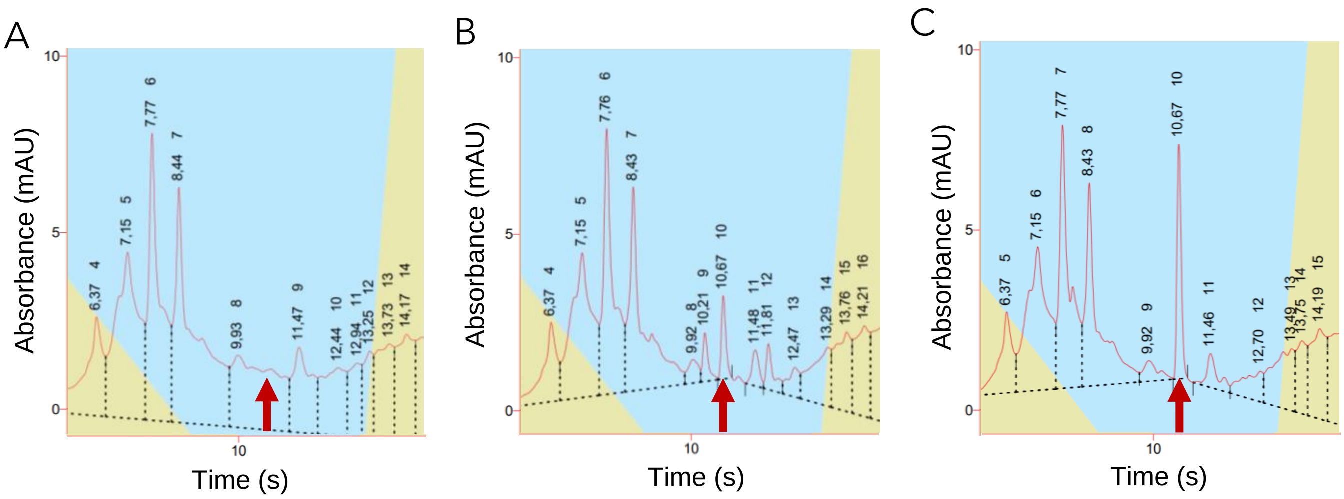

Figure 13 – HPLC chromatograms of (A) non-stimulated KTG/PEDOT NPs, (B) KTG/PEDOT NPs stimulated 1 time with the referred stimulation protocol and (C) KTG/PEDOT NPs stimulated 2 times. Red arrows point to the retention time of KTG.

The proposed release mechanism of the drug is a combination of changes in the electrostatic interaction between the drug and conductive polymer and an actuation response of the latter. By cycling through voltages, the electroactive PEDOT NPs and the loaded drug will experience oxidation/reduction cycles. In an oxidation cycle, both polymer and drug will become oxidized, increasing the positive charge within the NPs. This will create repulsive interactions between the two species, driving the release of the drug[165,166]. This effect is further amplified by PEDOT actuation. When reducing PEDOT NPs, electrons are injected into the polymer chains, compensating the positive charges acquired in the oxidation cycle. To maintain overall electroneutrality, negatively charged counter ions are expelled to the media, inducing the contraction of the particles[167]. This event produces a hydrodynamic pressure inside the particle that causes expulsion of the drug. Furthermore, actuation creates cracks and holes in the polymer, which can aid the release of the drug[109]. As such, by using alternating current, oxidation and reduction cycles can be applied to the nanoparticles, altering electrostatic interactions, and producing cycles of actuation that cause frequency dependent contractions and cracks.

4.2 Cytocompatibility assays

The designed strategy for cartilage regeneration encompassed a variety of elements that need to interact with hBMSCs, namely KTG-loaded PEDOT NPs, Tween-20, electrical current, and hydrogels. In order to ensure the biological viability of these interactions, the cytocompatibility of each individual element was assessed.

To assess the cytocompatibility of the NPs, increasing concentrations (2, 5 and 10 ug/mL) of PEDOT and KTG/PEDOT supplemented in culture media were combined with hBMSCs 2D cultures for 7 days. Culture media without NPs was used as a positive control and media supplemented with Tween 20 0.05% v/v was used as a negative control. Figure 14A shows live cells stained with calcein after 7 days. It is possible to see that the cells maintained their viability across all the concentrations of both PEDOT and KTG/PEDOT NPs, exhibiting their characteristic elongated spindle-like morphology. Especially at higher concentrations, the presence of the NPs can be seen in the form of amorph black shapes sitting on top of cells, which correspond to aggregates of nanoparticles blocking the fluorescence of the cells. In some conditions like PEDOT NPs at 10 ug/mL or 5 ug/mL KTG/PEDOT NPs, a closer inspection reveals intensely fluorescent green dots that appeared to be within the marked cells that contain very small black dots in their centers. These appear to be nanoparticles that were internalized by the hBMSCs, which, as previously discussed, would likely happen considering the size and surface charge of the produced NPs. However, future assays need to be performed in order to confirm NP internalization, possibly through confocal microscopy or by analyzes with flow-cytometry using fluorescent labeled NPs[168]. The metabolic activity of the cells at days 1,3 and 7 was also studied in order to ensure the biocompatibility of the NPs (Figure 14B). As it can be observed, hBMSCs proliferated well during the studied time frame for all NPs samples. Overall, the confirmation of the compatibility of both types of NPs was expected, as PEDOT has been described as having excellent biocompatibility in multiple studies[169,170].

A

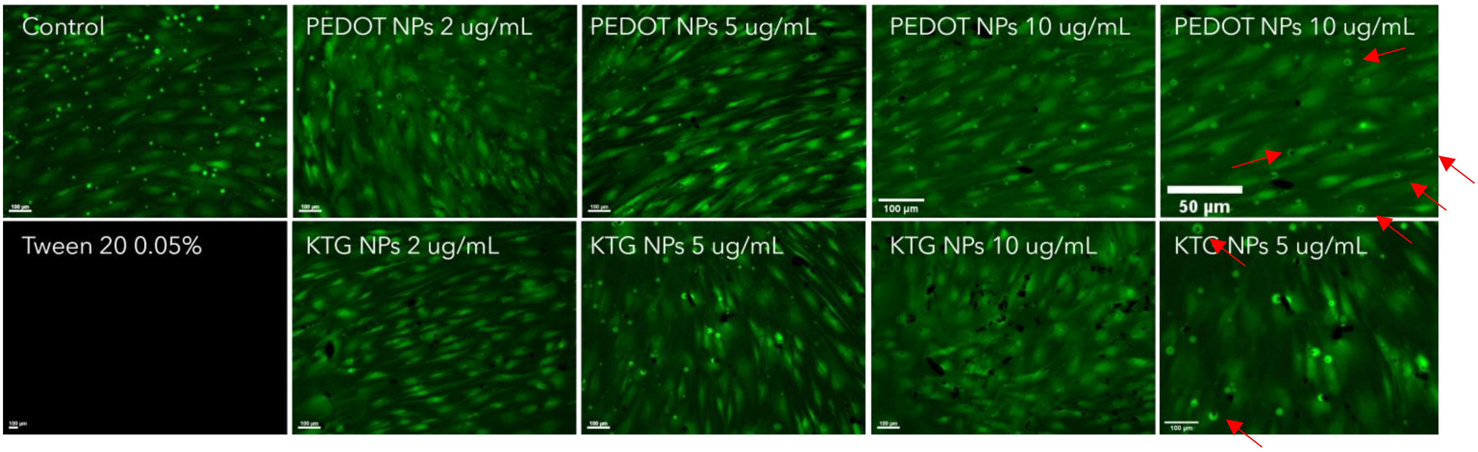

B

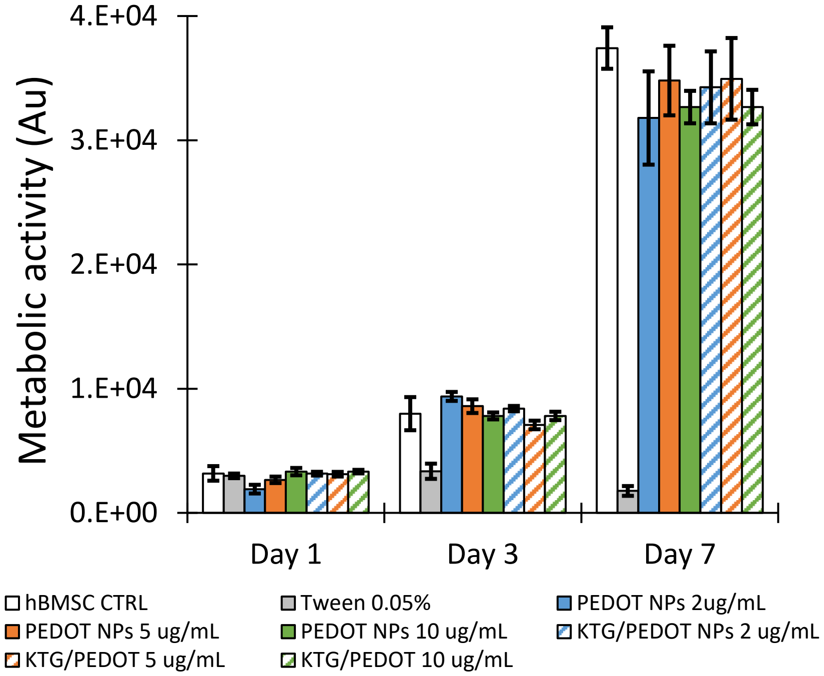

Figure 14 – Calcein staining (A) and metabolic activity assay (B) of hBMSCs cultured with 2, 5 and 10 ug/ml of PEDOT or KTG/PEDOT NPs for 7 days. Culture media without NPs was used positive cytocompatibility control and media with Tween 20 0.05% v/v as a negative control. Live cells stained in green. Scale bars are present in the figures.

As previously discussed, kartogenin is a highly hydrophobic drug, and while this greatly improved its loading in the nanoparticles, it constitutes a hindrance for drug release in aqueous mediums. Tween 20, a surfactant, was used to increase the affinity and dissolution of the drug to the media. However, Tween 20 can also disrupt the cell membrane at certain concentrations by breaking up its lipids, causing cell death. As such, in order to successfully implement Tween 20 in the final system, it is important to find a concentration that can simultaneously improve the release of KTG upon electrical stimulation while not harming the cells. It was previously shown that this compound causes the lysis of mammalian cells at concentration higher than 0.005% v/v[171]. Accordingly, the cytocompatibility of this compound was assessed by exposing hBMSCs to culture media supplemented with 0.001, 0.003 and 0.005% (v/v) Tween 20 for 7 days. Culture media with no Tween 20 was used as a positive control and media with Tween 20 0.05% as a negative control. After the 7 days, live cells where stained with calcein (Figure 15). As expected, it is possible to observe the viability of the cells when cultured with the 3 different Tween 20 concentrations, exhibiting a normal morphology. For the subsequent assays employing the detergent Tween 20, a concentration of 0.003% v/v was utilized, since it exhibited compatibility, and as previously shown, and could also improve the release of KTG. Furthermore, as it is not in the limit concentration that causes cells lysis, this choice accounted for potential preparation errors, as mistakes leading to over supplementation of Tween 20 could damage the cells in further assays.

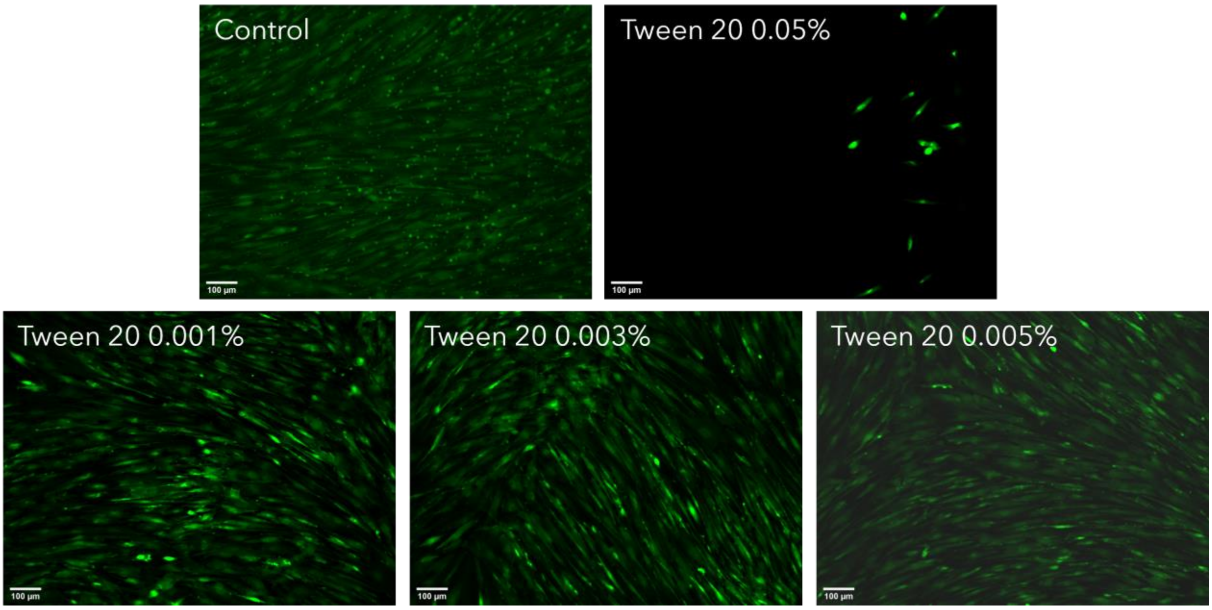

Figure 15 – Calcein staining of hBMSCs cultured in media with increasing concentrations of Tween 20 (0.001, 0.003, 0.005% v/v) over a period of 7 days. Culture media without NPs was used positive cytocompatible control and media with Tween 20 0.05% v/v as a negative control. Scale bar: 100 µm.

In order to study the effects of applied potentials in the viability of cultured cells, biocompatibility assays were performed with cells electrically stimulated with different potentials. As such, hBMSCs were platted in 12-well plates and stimulated the next day with 1, 2 and 3 V for 3x3 min at a frequency of 500 mHz, with 30 seconds rest between each stimulation. Following stimulation, live cells were stained in green with calcein and dead cells stained in red with EtBr (Figure 16). Cells that received no stimulation were used as controls. In stimulating conditions, it can be observed that the cells maintained a high degree of viability, with very few dead cells. Since stimulation with 3 V for 3x3 min at 500 mHz was shown to trigger the release of KTG from the PEDOT NPs, and exhibited no significant negative effects on cell viability, this potential was chosen to be used in the subsequent assays that employed electrical stimulation.

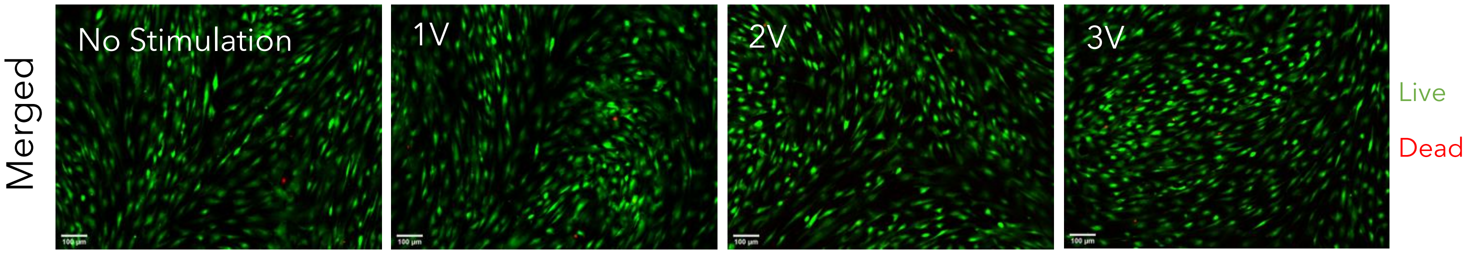

Figure 16 – LIVE/DEAD assay with calcein and ethidium bromide staining of hBMSCs after being electrically stimulated with alternating current between -3 and 3 V at 500 mHz. Cells that receive no stimulation were used as a positive control for cytocompatibility. Scale bar: 100 µm.

4.3 Hydrogel development and characterization

In order to successfully construct a system applying hydrogels as cartilage substitutes and promote tissue regeneration, the properties of the scaffolds should be similar to the ones of native tissue. As previously stated, hydrogels possess many parameters that can be modified and fine-tuned, being highly customizable. As such, various properties of three different hydrogels fabricated for this work (HA-CS; HA-CS-PEDOT:PSS and HA-CS-PEDOT NPs) were studied.

4.3.1 Hydrogel morphology

In order to visualize the morphology of the three hydrogel formulations, dry samples of the scaffolds were seen through SEM (Figure 17).

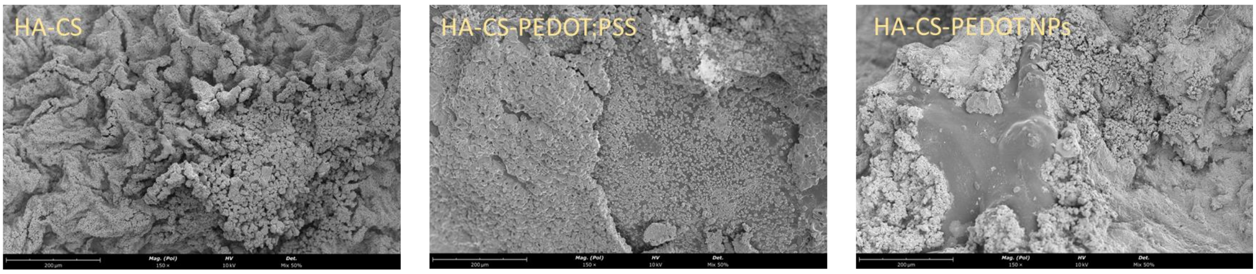

Figure 17 – SEM images of dried HA-CS, HA-CS-PEDOT:PSS and HA-CS-PEDOT NPs hydrogels. Scale bar: 200 µm.

4.3.2 Water content and swelling ratio

As articular cartilage is heavily encompassed by water, one of the crucial properties of hydrogels would be their high water content, which is critical to support integrity and diffusion of substances[172]. Furthermore, besides the innate amount of water they carry upon fabrication, the capacity of the scaffold to absorb surrounding water is also an important property, as it can have a profound impact on its mechanical properties[173]. The water content of three types of hydrogels (HA-CS; HA-CS-PEDOT:PSS and HA-CS-PEDOT NPs) was calculated by subtracting the weight of completely dry scaffolds to the wet weight post-fabrication. Every hydrogel formulation exhibited a very similar high water contents, of around 97% (Table 6). To assess swelling ratio, newly formed hydrogels were left incubating at RT in order for the unbound superficial water to evaporate. They were afterwards immersed in excess PBS and their weight was followed for 7 days (Figure 18). Significant differences between the different hydrogel formulations were observed. HA-CS hydrogels exhibited a constant increase in swelling ratio for the first 108 h, followed by no significant changes in swelling. Both HA-CS-PEDOT:PSS and HA-CS-PEDOT NPs hydrogels showed limited swelling, with a maximum of 13.87% for HA-CS-PEDOT:PSS and 6.04% for HA-CS-PEDOT NPs. Interestingly, in the first 40 hours, the swelling rates of both formulations appeared nearly identical. One of the reasons for the lower water absorption capacity of these formulations could be the apparent lower porosity observed through SEM[174]. Introduction of PEDOT:PSS and PEDOT NPs could act as cross-linking points for the polymer, resulting in stronger interactions between polymer chains, tightening the gel structure and creating stiffer scafolds[175]. Consequently, the mobility of polymers chains is hindered, minimizing water absorption. Lower swelling rates in hydrogels with embedded nanoparticles have been observed in previous studies[176,177]. As articular cartilage is a water rich tissue, swelling-resistant hydrogels for CTE applications are invaluable. This property allows hydrogels to be injected into a damage site, without absorbing the surrounding body fluid, preserving its mechanical properties, and not damaging surrounding tissues[178]. Furthermore, hydrogel swelling can lead to loss of adhesive properties, which are essential cartilage substitute scaffolds[179]. Overall, these results showed that introducing PEDOT NPs to HA-CS hydrogels improves the scaffold's swelling-resisting properties, without compromising its water content.

Table 6 – Water content of HA-CS, HA-CS-PEDOT:PSS and HA-CS-PEDOT NPs.

Gel	Average WC	STDV
HA-CS	96.8%	0.4%
HA-CS-PEDOT:PSS	97.2%	0.1%
HA-CS-PEDOT NPs	97.2%	0.3%

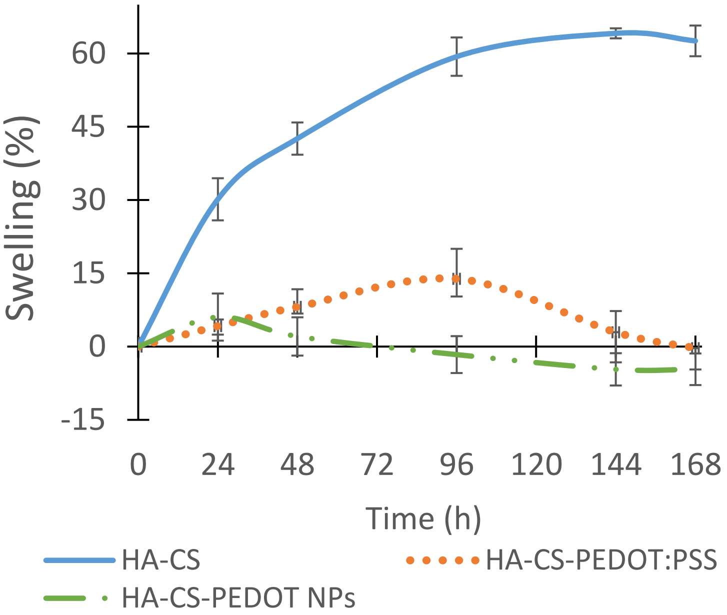

Figure 18 – Swelling rate of HA-CS, HA-CS-PEDOT:PSS and HA-CS-PEDOT NPs over the course of 7 days. Results are presented as mean ± SD of 4 independent (n=4) hydrogel samples for each condition.

4.3.3 Rheological analysis

After assessing the water content and swelling capacities of the hydrogels, its rheological properties were evaluated. Rheology allows the study of a material's response to externals forces (stress), being normally quantified in terms of its deformation rate (strain)[180]. As cartilage is a load bearing tissue, understanding how potential cartilage substitute scaffolds respond to mechanical stress is essential for a successful implementation. Hydrogels developed from ECM-based proteins are viscoelastic, with a mechanical behavior combining elements from both elastic and viscous responses[181]. Elastic materials respond instantaneously to deformation while the response of viscous materials depends on the rate of deformation. In rheological assays, the elastic response is given by the storage modulus (G') and the viscous response by the loss modulus (G'').

4.3.3.1 Hydrogels gelation kinetics

In order to analyze the gelation kinetics of the hydrogels, an oscillating time sweep assay was performed. The different formulations of hydrogels were prepared, and after addition of the cross-linker, the assay was swiftly initiated, with the storage and loss modulus being recorded (Figure 19). Since hydrogels are initially aqueous flowable solutions, it is expected G'' to be, initially higher than G', as the hydrogel will mainly act as a viscous liquid. However, when cross-linking occurs and the hydrogel experiences a sol-gel transition, the material should exhibit a more elastic response, with G' > G''. As such, the crossover of G' and G'' splits the hydrogel gelation process in two stages, primarily viscous when G' < G'' and primarily elastic when G' > G'', being a measure of gelation time[182]. For the HA-CS hydrogel, it can be observed that the crossover time was right in the beginning of the measurement, meaning that gelation started occurring as soon as the cross-linker was added. However, this was unexpected, as the producers of the Hystem hydrogel kit state gelation occurs after 20 min. This could be both due to differences in definitions of gelation time, as the manufacturer do not state the method used for this determination (many times a visual tube inversion test is used to infer gelation[183]), or due to the addition of CS to the formulation. Despite a different hydrogel formulation and experimental setup, another work measuring gelation of a HA-CS hydrogel through a rheological time-sweep also reported an instant gelation after addition of the cross-linker[184]. In the case of HA-CS-PEDOT NPs, an initial viscous response can be observed after the addition of the cross-linker until crossover at 22.5 min. It appears that the cross-linking in this hydrogel had a slight delay, starting a very low G' value that had a sudden increase at 8 min. For HA-CS-PEDOT NPs hydrogel, a definite crossover can be detected at 29 min, although it is difficult to claim a definite gelation time due to high fluctuations of G' and G'' for the first 18 min. These fluctuations are likely caused by a setup error, as G' will be dependent on the cross-linking state of the hydrogel, which is irreversible[185] and thus should not fluctuate. Overall, both HA-CS-PEDOT:PSS and HA-CS-PEDOT NPs hydrogels exhibited gelation times close to the Hystem kit fabricator's stated time at, 22.5 and 29 min respectively. The longer gelation times can actually be beneficial or even crucial for CTE strategies employing injectable hydrogels, as the scaffolds can more easily fit surgical requirements by staying in a sol state for a longer period of time after addition of the cross-linker. In this sol state, hydrogels can be more easily manipulated and injected into a damaged cartilage site, having enough time to match the defect and only then transition to a gel phase and start adhering.

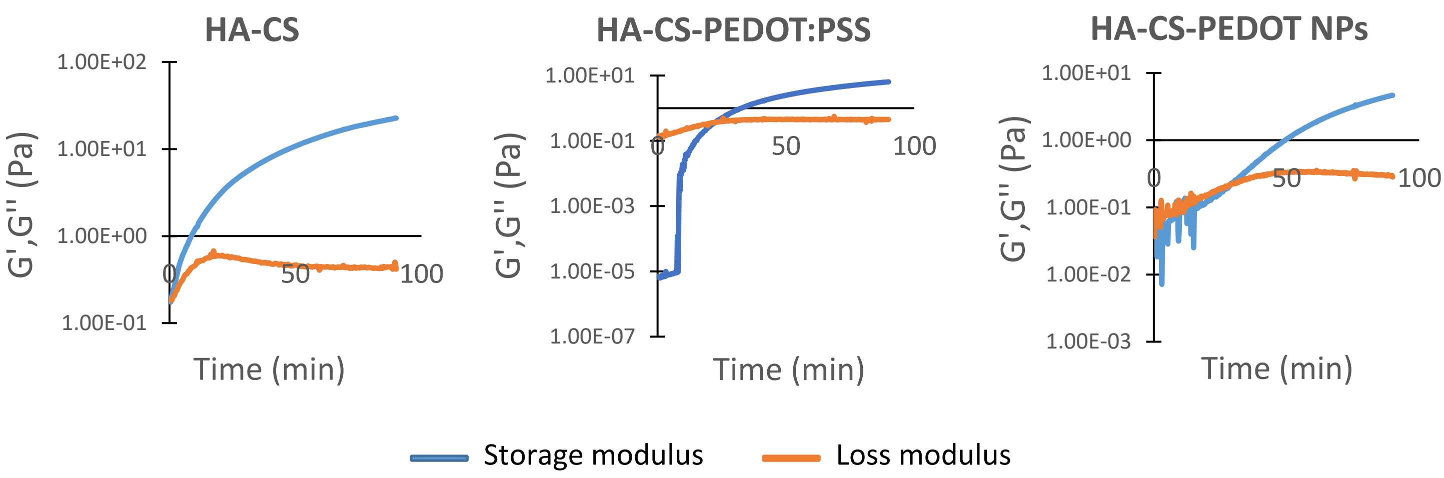

Figure 19 – Oscillating time sweep showing the gelation kinetics through storage (G') and loss modulus (G'') of HA-CS, HA-CS-PEDOT:PSS and HA-CS-PEDOT NPs. G' and G'' crossover indicates gelation time (n=1).

4.3.3.2 Hydrogel response to mechanical stress

Understanding the gelation kinetics of the hydrogels can give precious insight on their potential to be used as injectable scaffolds. However, it is equally important to understand how they would perform against mechanical stress post-gelation. As such, the three types of hydrogels post sol-gel transition were put through an amplitude sweep rheology assay (Figure 20). Here, a shear stress is applied to the hydrogels that exhibit a response in the form of shear strain. From plots obtained through this technique, various important parameters like Young's modulus, yield strength and fracture strain can be acquired[186]. The response of materials under stress usually exhibits various stages (although this heavily depends on the material type, as some stages might not be present). The first stage is the linear elastic region, where the stress is proportional to the strain and the slope of the curve being Young's modulus. Until the final point of this stage, defined as the yield strength, the material exclusively experiences a reversible elastic deformation. When this point is crossed, the materials start to experience irreversible plastic deformation until it eventually fractures[187]. In the case of the HA-CS hydrogel, these regions are well visible. There is a near linear proportionality between stress and strain until an 88% strain is reached, where a yield stress of 84 Pa was recorded. The hydrogel eventually fractured at a 185% strain. The HA-CS-PEDOT:PSS and HA-CS-PEDOT NPs hydrogels exhibited very different stress-strain curves compared to HA-CS gel. Lower shear stresses lead to much higher strains, and fracture wasn't observed in the analyzed strain window. Because an elastic region cannot be properly identified, the yield stress cannot be acquired. The behavior observed for these gels is likely due to an error while performing the assay. After adding the cross-linker, the same amount of time was waited for the three types of hydrogels before staring the measurements. However, as previously seen, gelation of the HA-CS hydrogel started occurring immediately after the addition of the crosslinker, while the other formulations took longer than 20 min to gelate. As such, it appears that the PEDOT-based hydrogels had not fully initiated gelation when the amplitude sweep was started, being mainly in their sol phase. This would explain why the low stresses (comparatively to the HA-CS hydrogel) led to such high deformation of the gels, since, as seen in the kinetics assay, the hydrogels have a very low G' and G'' modulus pre-gelation. This would also explain the lack of total linearity in the elastic region of HA-CS (achieved after a complete gelation), with instead a very slight exponential curve. The gelation kinetic curves show that, even after crossover, G' still significantly increases over time, meaning that HA-CS was still acquiring some mechanical strength during the amplitude sweep, which lead to small exponential increases in the elastic region.

Despite being difficult to take conclusions on the PEDOT-based hydrogels response to mechanical loads, as gelation had not fully occurred, some insight can still be obtained through analysis of the HA-CS hydrogel, since it is the basis of all the formulations. Previously, it was discussed how the addition of PEDOT:PSS and PEDOT NPs can increase the tightness of the hydrogel structure by creating cross-linking points. The stronger interactions between polymer chains would very likely confer improved mechanical strength to the gel, enabling it to sustain higher mechanical loads and strains without fracture. In fact, various studies have shown that increasing nanoparticle concentration in hydrogels improved its mechanical properties, especially in the elastic region where higher reversible strains were achieved[188,189]. As such, it is feasible to assume that HA-CS-PEDOT:PSS and HA-CS PEDOT NPs hydrogels would exhibit superior mechanical properties when compared to HA-CS hydrogel in a correctly performed assay.

When studying the response of hydrogels to mechanical loads, the most important region to be analyzed is the elastic region. As potential cartilage substitutes, these hydrogels would need to be able to provide mechanical stability and support to the tissue under constant cyclic loads. Since trespassing the yield strength leads to permanent deformation of the gels and eventual compromise of structural integrity due to fracture, it is paramount that the scaffolds mechanical strength is close to articular cartilage within their elastic region. This can be measured through Young's module, which is the relation between the deformation of a material and the power needed to deform it within the elastic region[190]. Through the slope of the elastic region, the Young's module of HA-CS hydrogel was calculated to be 121 Pa. Despite the PEDOT hydrogels likely having a higher value, the Young's modulus of native cartilage is in the order of MPa, magnitudes higher than the one observed in the HA-CS hydrogels[191]. The lack of mechanical strength severely hinders the application of these scaffolds as cartilage substitutes, as they would not withstand the high cyclic loads experienced in the tissue. However, a vast amount of strategies have successfully been employed in order to optimize the mechanical strength of HA hydrogels without compromising its biologic properties[192–194].

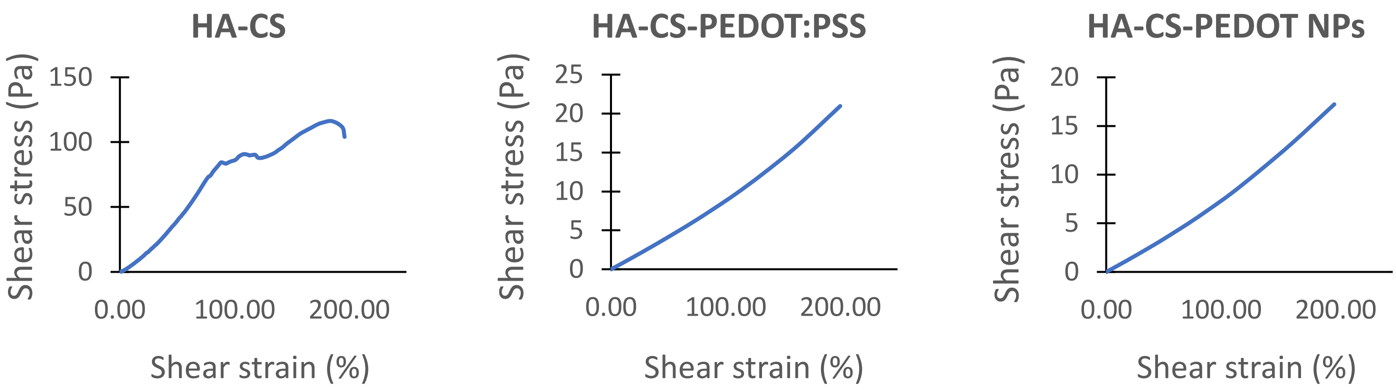

Figure 20 – Amplitude sweep of HA-CS, HA-CS-PEDOT:PSS and HA-CS-PEDOT NPs. The assay was performed at a frequency of 1Hz at 25ºC until a strain of 200% was reached (n=1).

4.3.4 Hydrogel impedance

In this work, the impedance (and consequently conductivity) of the hydrogels is a key parameter, as it is important not only for the correct mimicking of the native tissue electrochemical properties, but also for the effective trigger of drug release through electrical stimulation. Conductive hydrogels can allow a more effective transmission of electric signals to the seeded cells and the embedded nanoparticles without the use of high potentials[195]. Frequency dependent impedance of the three hydrogel formulations was measured through electrochemical impedance spectroscopy (Figure 21A), and the frequency dependent conductivity calculated (Figure 21B). In this technique, a sinusoidal potential is applied to an electrochemical system (in this case the various hydrogels) and measures the sinusoidal potential out of the system. The frequency dependent impedance (Z) is given by the ratio between the applied voltage and the measured current. From the impedance curves, it is possible to observe that all hydrogels exhibited low impedance, at high frequency values. However, at lower frequencies, like the ones found in electroactive tissues (1Hz)[196], resistive currents dominate, with higher impedances for all hydrogel formulations being observed. However, it is clearly visible that the addition of PEDOT:PSS or PEDOT NPs notably increases the conductivity of the hydrogels across the entire frequency range. Various other works have highlighted the potential to modulate hydrogel conductivity with the addition of conductive polymers[195,197–199]. The dependence of hydrogel conductivity with the presence of PEDOT:PSS or PEDOT nanoparticles constitutes a powerful tool to fine-tune the electrical properties of the scaffolds for cartilage regeneration. For the system of this particular work, the concentration of KTG/PEDOT embedded in the hydrogels, to serve as scaffolds for hBMSCs, can be modified in order to confer different degrees of conductivity. This effect might be crucial and important to optimize in order to ensure that the applied electrical stimulation is enough to trigger the controlled release of KTG from the nanoparticles.

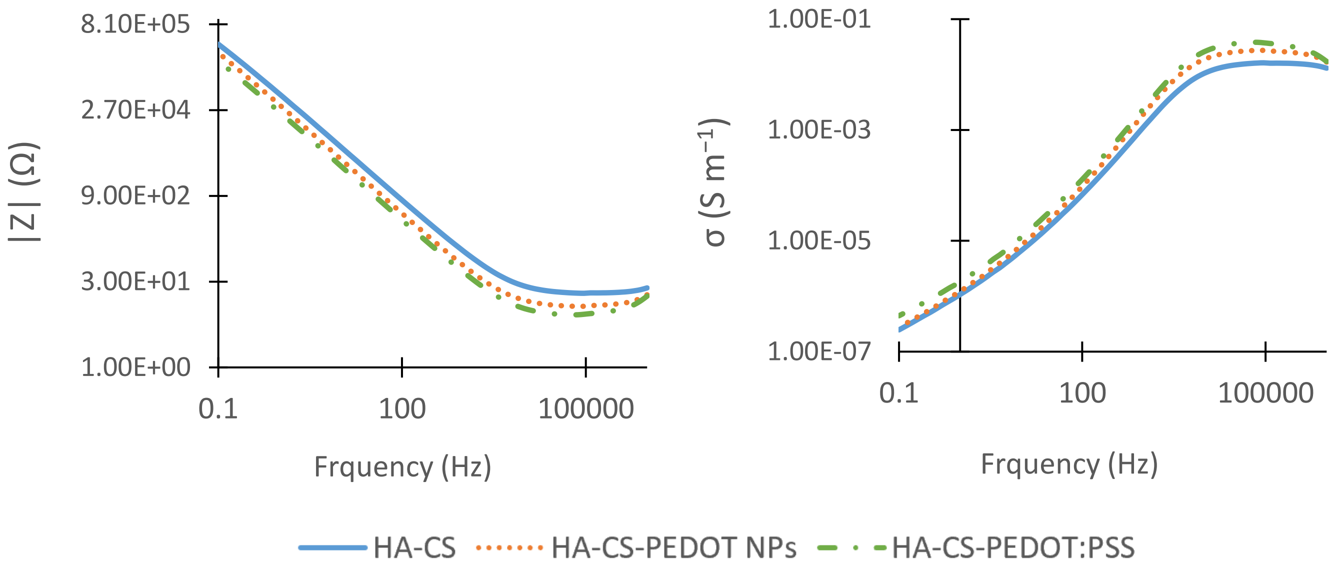

Figure 21 – Electrochemical impedance spectroscopy results of HA-CS (control), HA-CS-PEDOT:PSS (PSS) and HA-CS-PEDOT NPs (NPs), with plots of impedance over frequency (A) and calculated the frequency dependent conductivity (B) (n=1).

4.3.5 Effects of non-stimulated KTG/PEDOT NPs in chondrogenic differentiation of seeded hBMSCs

To assess if non-stimulated KTG/PEDOT NPs would have an effect in the chondrogenic differentiation of hBMSCS, these cells were cultured for 14 days in an incomplete chondrogenic media with increasing concentrations of KTG/PEDOT NPs (Figure 22). As it can be observed, as a powerful chondrogenic inducer, cells culture in chondrogenic media with TGF-β3 demonstrated an increased sulfated GAG production when compared to cells cultured in incomplete media, highlighting the enhanced chondrogenic differentiation. However, cells cultured with increase concentrations of NPs did not exhibit an increase in GAG production when compared to the INC condition, which indicates that the NPs do not have a direct effect of hBMSC chondrogenic differentiation. Since electrical stimulation was not employed in this assay, it was expected that conditions with KTG/PEDOT NPs would not show an increased chondrogenic differentiation when compared to empty PEDOT NPs, which was corroborated by the obtained results. This further suggests that there is not a significant passive release of KTG from the nanoparticles in the absence of electrical stimulation. The GAGs present in each condition were stained with Alcian blue, and can be seen in figure S5.

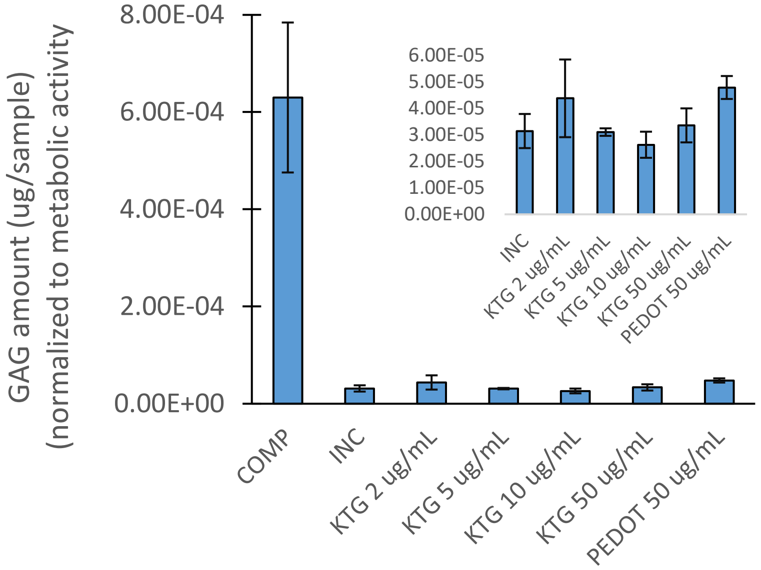

Figure 22 – Sulfated GAGs content of each sample after 14 days of chondrogenic differentiation in incomplete chondrogenic media (INC). Complete chondrogenic media (COMP) was used as a positive control and incomplete media with 50 ug/mL PEDOT NPs as a negative control. GAG levels were normalized to the metabolic activity of hBMSCs on day 14 of the assay (n=4).

4.3.6 Effects of KTG/PEDOT NPs in the chondrogenic differentiation of hBMSCs with electrical stimulation

As previous assays confirmed that KTG release from KTG/PEDOT NPs could be controlled through electrical stimulation, the chondro-inductive effects of this release were assessed. A high density of hBMSCs (2,6x10^4 cells/well) were seeded in 12-well plates, and cultured in incomplete chondrogenic media with 2 ug/mL of KTG/PEDOT NPs, while non-stimulated cells cultured in incomplete chondrogenic media with 2 ug/mL PEDOT NPs or without NPs were used as controls. With every media exchange, new NPs at the same concentration were added and the cells where electrically stimulated with the before-mentioned protocol. The metabolic activity of the cells was measured on day 3, 7, 14 and 21 (Figure 23A). It can be seen that hBMSCs in all conditions maintained their metabolic activity along de 21 days of differentiation, with a slight drop on day 21. This is also illustrated by the fold increase calculated between day 3 and 21 of culture (Figure 23B), where all the conditions exhibited a fold increase of approximately 0.92. A possible explanation for the observed results was the high hBMSC seeding density, as the cells were already confluent on day 3, which likely inhibited proliferation. Due to this inhibition, possible effects of electrical stimulation or KTG release in the proliferation of hBMSCs could not be accounted through this assay. Although it is heavily dependent on the parameters of electrical stimulation (e.g., potential and frequency), short electrical stimulation exposure times have been seen to increase the proliferation rate of MSCs cultured in monolayer with chondrogenic medium[200].

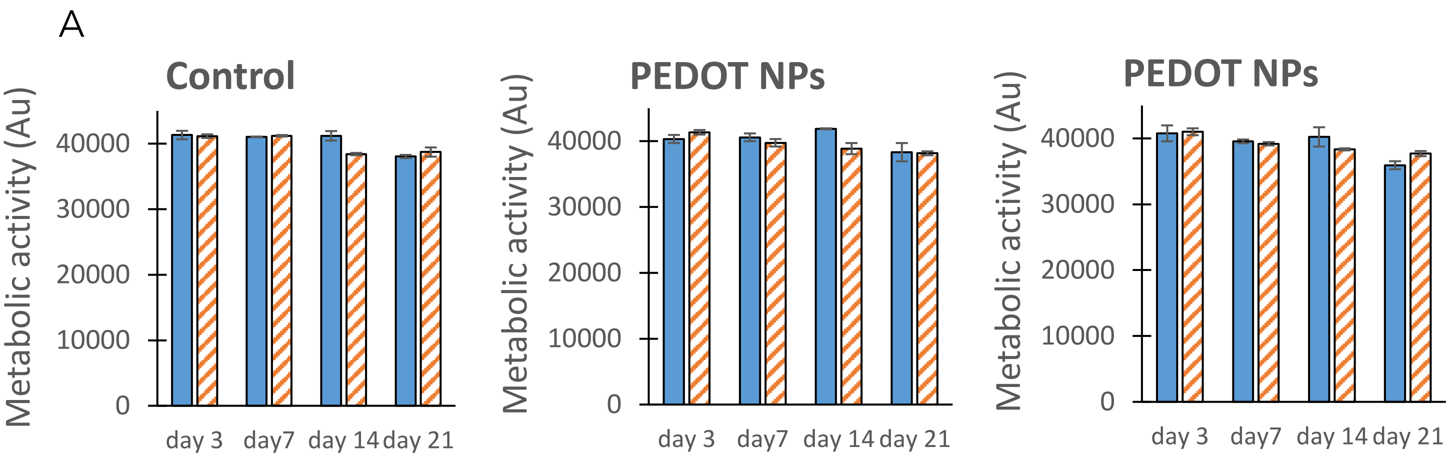

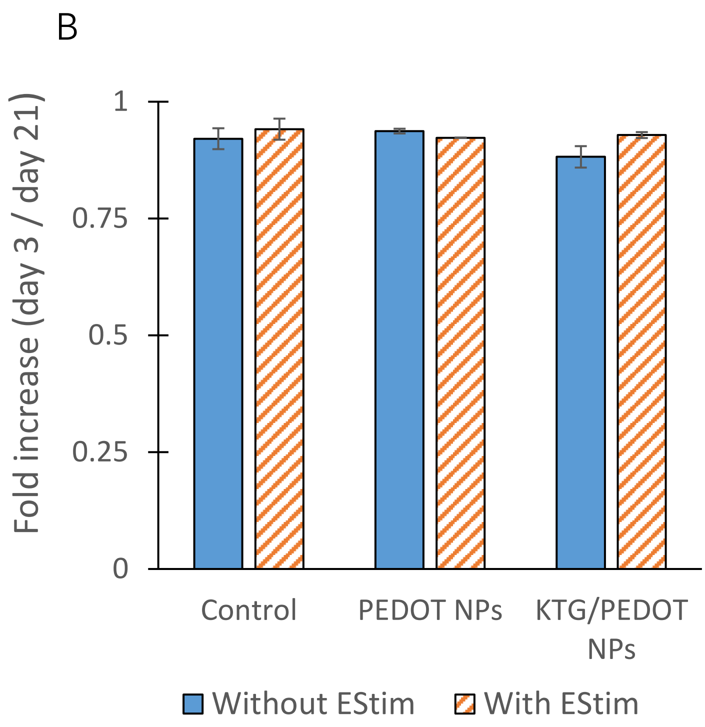

Figure 23 – (A) Metabolic activity of hBMSCs across the 21 days of culture with PEDOT or KTG/PEDOT NPs in incomplete chondrogenic media with or without electrical stimulation. (B) Fold increase after 21 days of culture in relation to day 3. Non-stimulated hBMSCs cultured in standard expansion media without NPs were used as controls (n=3).

As previously stated, GAGs are a very prominent component of native articular cartilage, and an important marker of chondrogenic differentiation[201,202]. As such, the amount of GAGs present in each sample after 21 days of chondrogenic differentiation was evaluated (Figure 24). It is possible to see that all in all the conditions (except KTG/PEDOT NPs with electrical stimulation) presented nearly same amount of GAGs, which suggests a similar level of chondrogenic differentiation. The close amount of GAG levels between electrically stimulated or non-stimulated samples (control and PEDOT NPs) indicates that the stimulation did not have direct effects on hBMSCs chondrogenesis. However, in the case of KTG/PEDOT NPs, the samples that received electrical stimulation exhibited a significantly increase of GAG levels when compared to non-stimulated samples. Despite this particular electrical stimulation protocol not showing direct effects on cell chondrogenesis, it is capable to trigger the release of KTG loaded in the NPs. These results not only further confirm the controllable drug release, but also show the effectiveness of KTG in enhancing the chondrogenesis of hBMSCs.

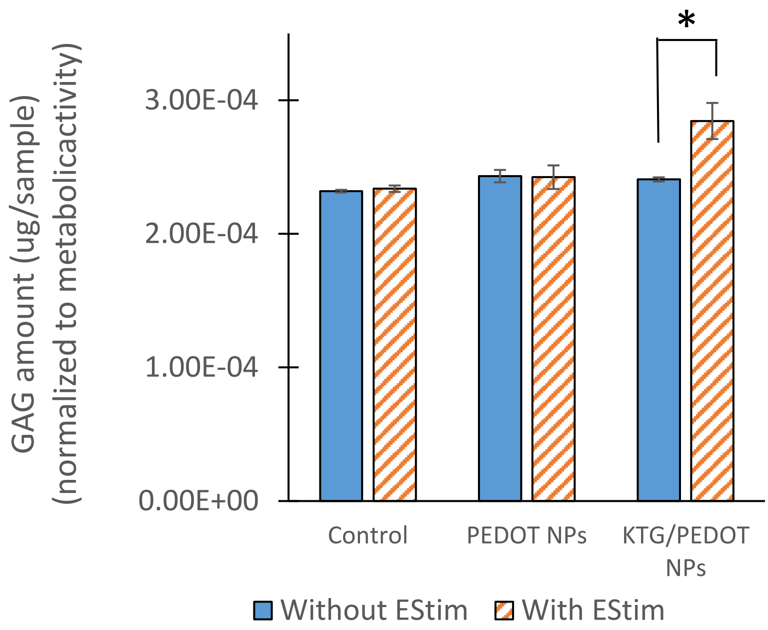

Figure 24 – Sulfated GAGs content of each sample after 21 days of chondrogenic differentiation. GAG levels were normalized to the metabolic activity of hBMSCs on day 21 of the assay. Non-stimulated hBMSCs cultured in standard expansion media without NPs were used as controls (3 technical replicates from a single biological replicate (1 donor)).

After 21 days of chondrogenic differentiation, hBMSCs were also analyzed through immunocytochemistry analysis (Figure 25). Collagen type II, one of the main components of articular cartilage ECM, was expressed in all conditions, either with or without electrical stimulation. In conditions with either PEDOT or KTG/PEDOT NPs, aggregates of each NP type can be observed in the form of amorph black shapes. Interestingly, a higher cell density can be seen surrounding the NP aggregates, illustrated by a higher number of DAPI stained nuclei in their surroundings. The higher hBMSC density is also accompanied by a denser collagen type II expression, which might suggest a higher production of this compound around NP aggregates.

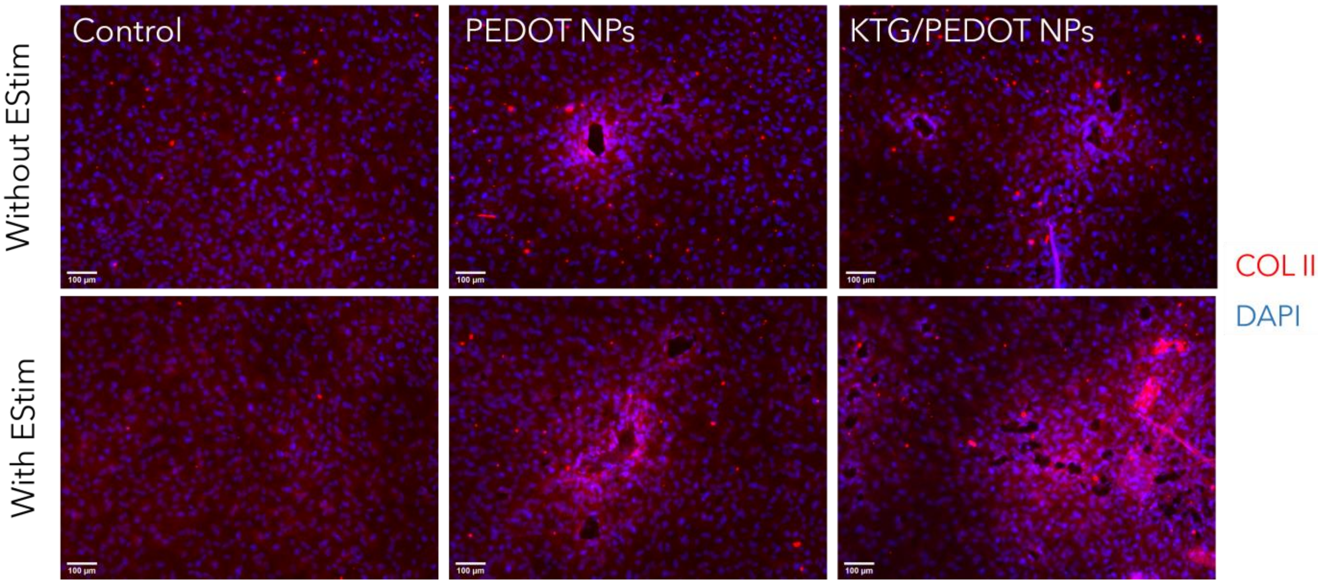

Figure 25 - Immunofluorescence analysis of hBMSCs cultured with PEDOT or KTG/PEDOT NPs under chondrogenic differentiation conditions for 21 days with and without electrical stimulation. Expression of collagen type II (COL II, red) and cell nuclei counterstained with DAPI (blue). Scale bar: 100 µm.

Following the 21 days of chondrogenic differentiation the gene expression levels of chondrogenic markers and other relevant genes such as *COL II*, *SOX9*, *COL I*, *COL X* and *MMP-13* were evaluated by quantitative reverse transcription-polymerase chain reaction (qRT-PCR) analysis (Figure 26). As *COL I* is major osteogenic phenotype marker[203], analysis of the expression levels of *COL I* can provide further insight on the differentiation fate of hBMSCs. *COL X* and *MMP-13* are markers of chondrocyte hypertrophy, that are usually overexpressed in diseased cartilage like in case of OA. As it can be seen, all the conditions exhibited a significant upregulation of both *SOX9* and *COL II* when compared to the control (hBMSCs at Day 0), confirming the cell's chondrogenic differentiation. However, no significant differences in the expression levels are observed between the different conditions, either with or without electrical stimulation. There was no significant upregulation of the *COL I* expression, indicating that there was a chondrogenic commitment of hBMSCs. Additionally, *MMP-13* and *COL X* expression levels were downregulated in all conditions, evidencing the lack of tissue hypertrophy. Overall, these results highlight the achieved chondrogenic differentiation of hBMSCs without hypertrophy, however, the lack of differences between conditions, especially for KTG/PEDOT NPs, was unexpected, as previous results highlighted improved GAG production with the release of KTG.

Overall, the use of electrical stimulation to trigger the release of KTG from KTG/PEDOT NPs appears to be a promising way to deliver this drug and promote the chondrogenic differentiation of hBMSCs, as higher levels of GAGs were detected, and no significant cytotoxicity was observed. However, the assays need to be repeated in order to draw conclusive results (and achieve statistical significance) as the gene expression analysis did not fully corroborate an increased chondrogenic differentiation in the presence of electrical stimulation.

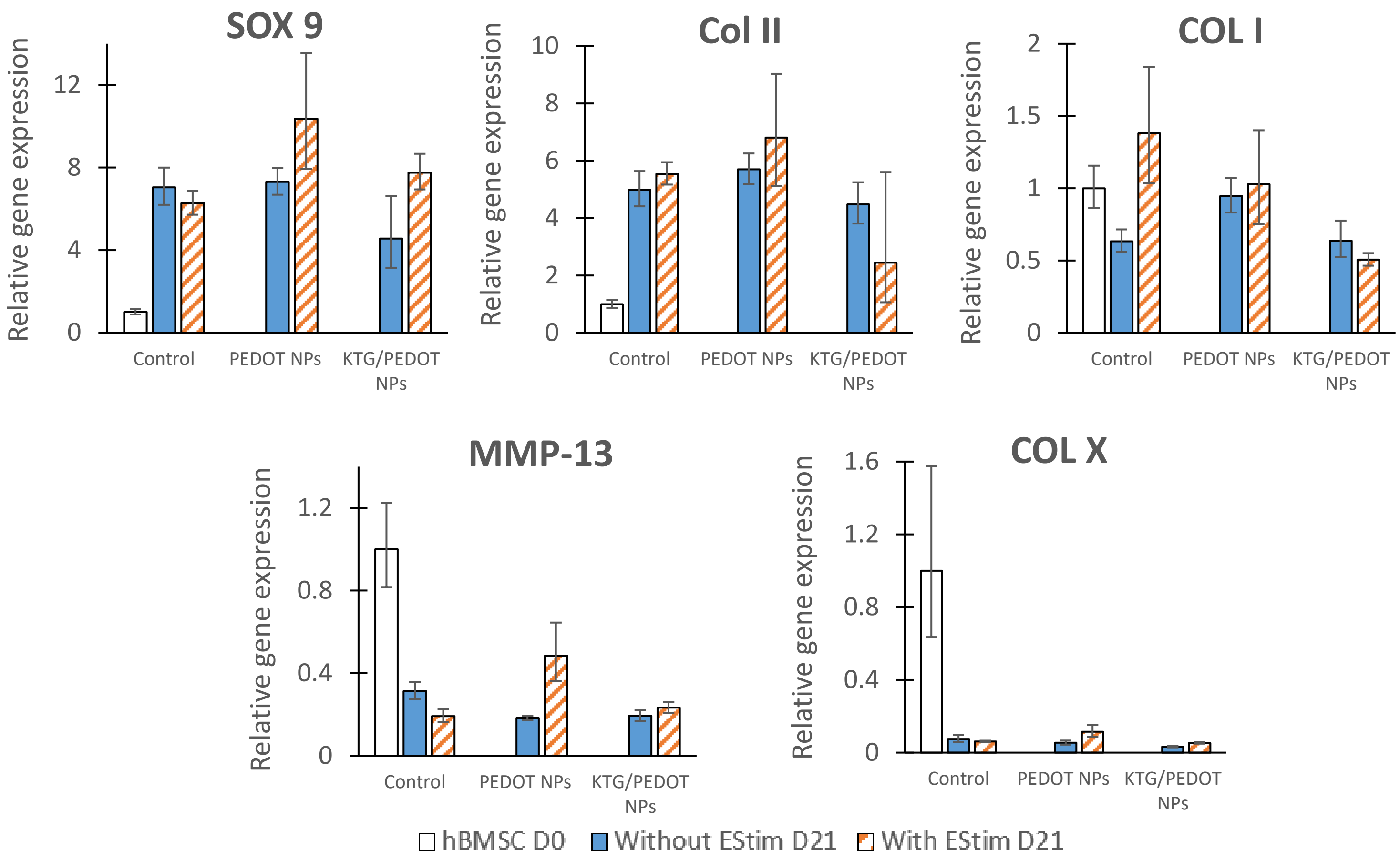

Figure 26- qRT-PCR analysis of hBMSCs after 21 days of chondrogenic differentiation in incomplete chondrogenic media with or without PEDOT or KTG/PEDOT NPs and with or without exposure to electrical stimulation. Gene expression of *SOX9*, *COL II*, *COL I*, *MMP-13* and *COL X* was normalized to the endogenous gene *GAPDH* and then calculated as a fold-change relative to the baseline expression of target gene measure in Day 0 experimental group (undifferentiated cells before seeding) (3 technical replicates from a single biological replicate (1 donor)).

4.3.7 Effects of HA-CS-KTG/PEDOT NPs hydrogel in the chondrogenic differentiation of encapsulated hBMSCs with electrical stimulation

After characterization of the various elements of the system, optimization of drug release upon electrical stimulation conditions and confirmation of the biocompatibility of the different conditions, the entire system was employed in order to assess the effects on the chondrogenic differentiation of encapsulated hBMSCs. As such, three types of hydrogels were fabricated; HA-CS, HA-CS-PEDOT NPs and HA-CS-KTG/PEDOT NPs, and hBMSCs were added before introducing the cross-linker in order to embed them in the scaffolds. As previously, a 21-day differentiation protocol was followed, where a 12-well plate with hydrogels of each type in incomplete chondrogenic media was electrically stimulated every time fresh media was added, while another plate in identical conditions did not receive electrical stimulation. The metabolic activity of the seeded cells was monitored on days 3, 7, 14 and 21. At day 3, it can be observed a notable difference in metabolic activity, even across the same gel types, indicating different cell seeding densities. This occurred due to the method used for the preparation of the hydrogels. Instead of individually preparing the triplicates, each hydrogel formulation was prepared in a single eppendorf, and the cells where homogenized in this mixture. After adding the cross-linker post cell-homogenization, some time had to be waited before pipetting the hydrogels to the wells. When the cross-linker was added (after cells were homogenized in the stock gel solution in the time it took for gelation to start), some cells had already started depositing when the gel was transferred to the wells, creating heterogeneities between samples. However, with this consideration, it can be seen that cells exhibited normal proliferation across all conditions, with higher metabolic activities at day 21 when compared to day 3. The fold increase (in metabolic activity) between day 21 and 3 was also determined (Figure 27). Interestingly, the fold increases obtained for HA-CS-PEDOT and HA-CS-KTG/PEDOT NPs were significantly higher than the HA-CS hydrogels, both with and without electrical stimulation, meaning that hBMSCs exhibited higher proliferation rates in the scaffolds formulated with NPs. This difference is likely caused by changes in the hydrogel's physical properties introduced by the NPs. As previously discussed, the introduction of nanoparticles to the formulations likely caused denser hydrogel cross-linking, which in turn generates stiffer scaffolds. Hydrogels stiffness plays a key role in cell-matrix interactions and cell behavior[204]. In fact, MSCs have demonstrated increased proliferative potential when cultured on stiff hydrogels compared with softer hydrogels[205], which corroborates the obtained results. The dependence of hBMSC proliferation on the mechanical properties of the scaffold is something that can be explored in future assays by modulating the concentration of NPs in the hydrogel formulation. Besides the differences in hBMSC proliferation observed between plain and NP embedded hydrogels, interesting results can also be observed between samples with or without electrical stimulation. In the case of HA-CS and HA-CS-PEDOT NPs hydrogels, no significant changes can be observed between stimulated and non-stimulated samples. However, in the case of HA-CS-KTG/PEDOT NPs hydrogels, samples that were electrically stimulated exhibited a significantly higher fold increase when compared to non-stimulated samples. This indicates that electrical stimulation triggered a response in these hydrogels that led to an increase in the proliferation rate of hBMCSs. Such response might be the release of KTG from the gel-embedded NPs, triggered by the stimulation. KTG has been seen to increase the metabolic activity of chondrocytes and adipose-derived stem cells elsewhere, although the mechanism that led to this increase remained unclear[206,207]. However, a possible explanation could be that KTG activates RUNX1, a transcription factor that plays important role in chondrocyte proliferation[208]. The similar fold increase observed between non-stimulated HA-CS-KTG/PEDOT and HA-CS-PEDOT NPs hydrogels further corroborates the involvement of KTG release in the increase of hBMSC proliferation rate. As It was previously seen, the passive release of KTG from KTG/PEDOT NPs is almost null, meaning that in the absence of electrical stimulation to trigger its release, similar results should be expected between drug-loaded and unloaded PEDOT NPs.

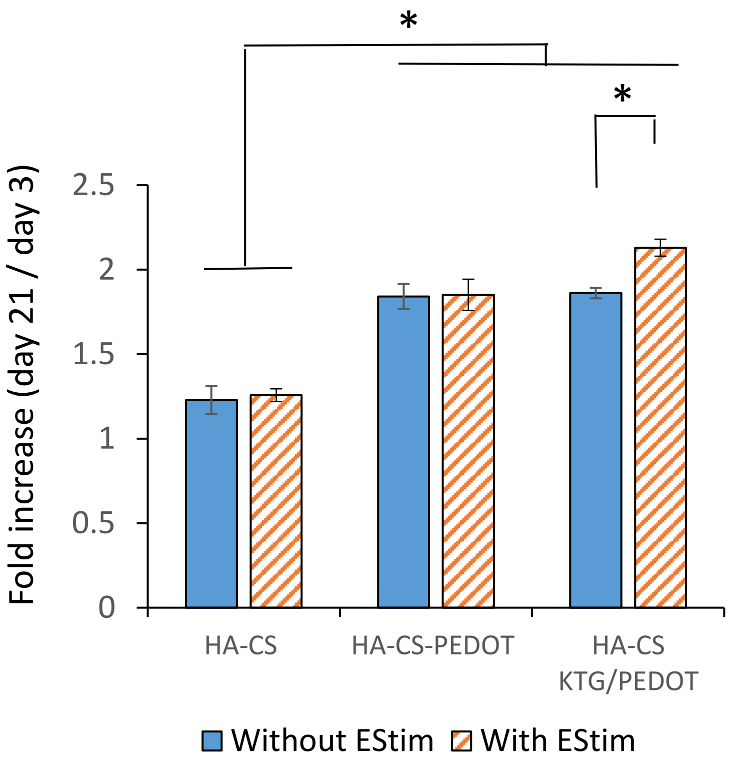

Figure 27 - Fold increase after 21 days of culture in relation to day 3. Non-stimulated hBMSCs cultured in standard expansion media without NPs were used as controls (n=3).

Following the 21 days of chondrogenic differentiation, a live/dead assay was performed in order to assess the biocompatibility of the entire system (Figure 28). Interestingly, almost no dead cells were found in any of the conditions and a high number of live cells stained with calcein can be clearly seen in all the conditions. In this case, the hBMSCs do not exhibit their usual morphology since they are not attached to the bottom of the well, but instead encapsulated within the hydrogel scaffold. Overall, this assay demonstrates the biological viability of the system. The excellent viability of the cells encapsulated in this hydrogel system was expected, since the hydrogel is mainly composed by HA and CS, which are natural polymers with intrinsic biocompatibility. Furthermore, the utilized NPs were composed by PEDOT, which is a synthetic polymer with proven good biocompatibility[209].

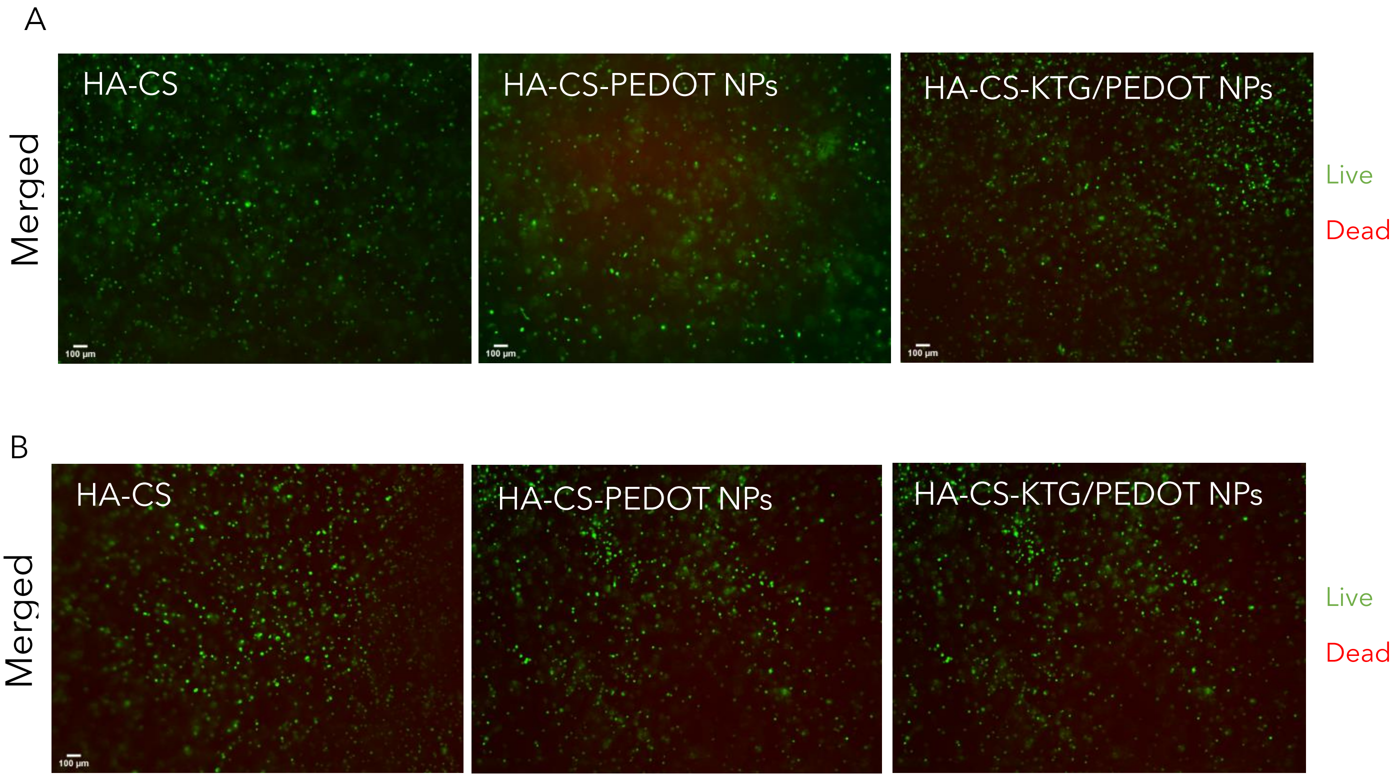

Figure 28 – Live/Dead assay of hBMSCs encapsulated in HA-CS, HA-CS-PEDOT NPs and HA-CS-KTG/PEDOT NPs hydrogels without (A) and with (B) electrical stimulation. Live cells were stained in green with calcein and dead cells (red) with ethidium bromide. Scale bar: 100 µm.

As GAGs production is characteristic of MSCs undergoing chondrogenic differentiation[210], a GAG quantification assay was performed after 21 days in order to measure the amount of sulfated GAGs in each condition (Figure 29). For this, hydrogels with encapsulated cells were digested using N-acetyl cysteine and centrifuged, with the pellet consisting of digested hydrogel and cells used for this assay. Analysis of the results does not show a concrete correlation between the different conditions and the amount of GAGs produced. Conditions with electrical stimulation showed an increase in GAGs production for the HA-CS-KTG/PEDOT and HA-CS hydrogel, when compared to the same gel without stimulation, but in the case of HA-CS-PEDOT, the contrary was verified. In conditions that were electrically stimulated, HA-CS-KTG/PEDOT showed the least amount of GAGs production, however, in non-stimulated conditions, HA-CS-PEDOT had the least amount. These somewhat erratic results make conclusions hard to be drawn, as there is no apparent correlation between the various system's response to electrical stimulation and GAGs production. However, these results can very likely be explained by the presence of CS in the hydrogel formulations. The detection of GAGs is achieved through the induction of metachromasia of DMMB by sulfated GAGs. However, unliked HA, CS is a sulfated GAG, which can also induce metachromasia of DMMB. As such, the measured absorbance is a contribution of not only the GAGs produced by the cells, but also from the CS present in the scaffolds.

In the 21 days differentiation assay previously described, a HA-CS hydrogel with no seeded cells was also present as a control. After performing the GAGs quantification assay with this hydrogel, it was found that the absorption levels were almost entirely a contribution of the CS present in the hydrogel. The various triplicates of each condition were seen to have some differences in the amount of hydrogel, which would lead to vast differences in the GAG measurements across conditions, masking the GAG amount contribution of embedded cells. Thus, in future assays, a control hydrogel without embedded cells for each condition should be prepared with an effort to achieve a close amount of hydrogel across the conditions.

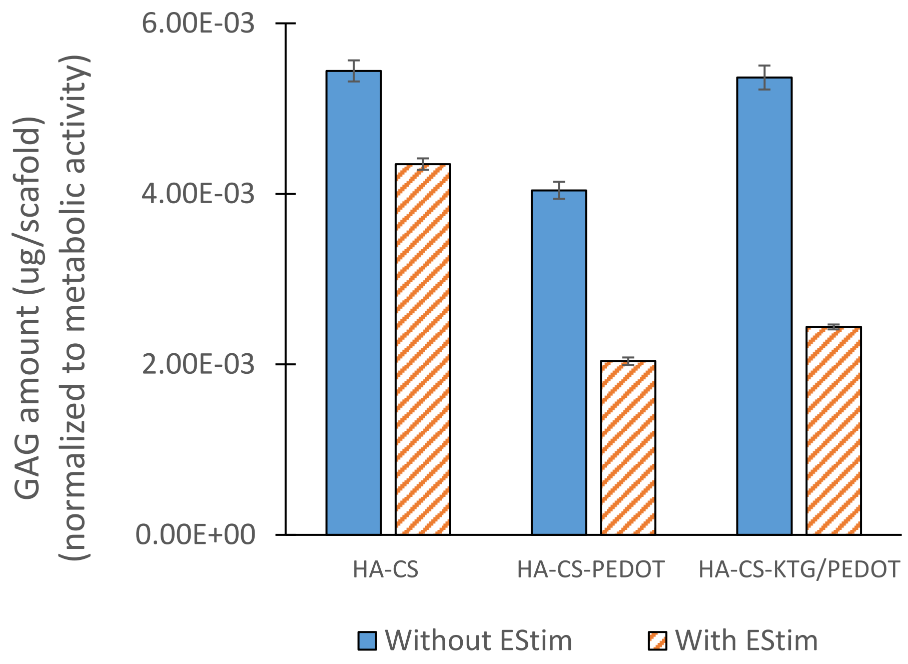

Figure 29 – GAG levels measurement through DMMB colorimetric assay. (n=3 technical replicates from a single biological replicate (1 donor)).

After the 21 days of chondrogenic differentiation, the expression levels of the genes previously analyzed (*COL II*, *SOX9*, *COL I*, *COL X* and *MMP-13*) were quantified (Figure 30). *SOX9* was upregulated in all conditions, but without relevant differences between samples that were electrically stimulated or non-stimulated. However, the expression of *SOX9* was higher across all conditions in hydrogel-seeded hBMSCs than the same cells cultured without the scaffolds, indicating a positive effect on chondrogenic differentiation. In terms of *COL II*, cells encapsulated in hydrogels with NPs exhibited a higher expression than cells cultured in HA-CS hydrogels, but there was again no difference between stimulated and non-stimulated conditions. The severe downregulation of *COL I* in all conditions indicates that the differentiation of hBMSCs was towards chondrogenic lineage. Furthermore, there was again no significant upregulation of either *MMP-13* or *COL X*, suggesting that cells in the final constructs were not hypertrophic. Due to previous results, it was expected that hydrogels with PEDOT nanoparticles would have the same results as non-stimulated hydrogels with KTG/PEDOT NPs, as the drug would notbe released, and that electrically stimulated HA-CS-KTG/PEDOT NPs would achieve enhanced chondrogenesis. This was not observed, however, this assay should be repeated in the future in order to obtain more conclusive results.

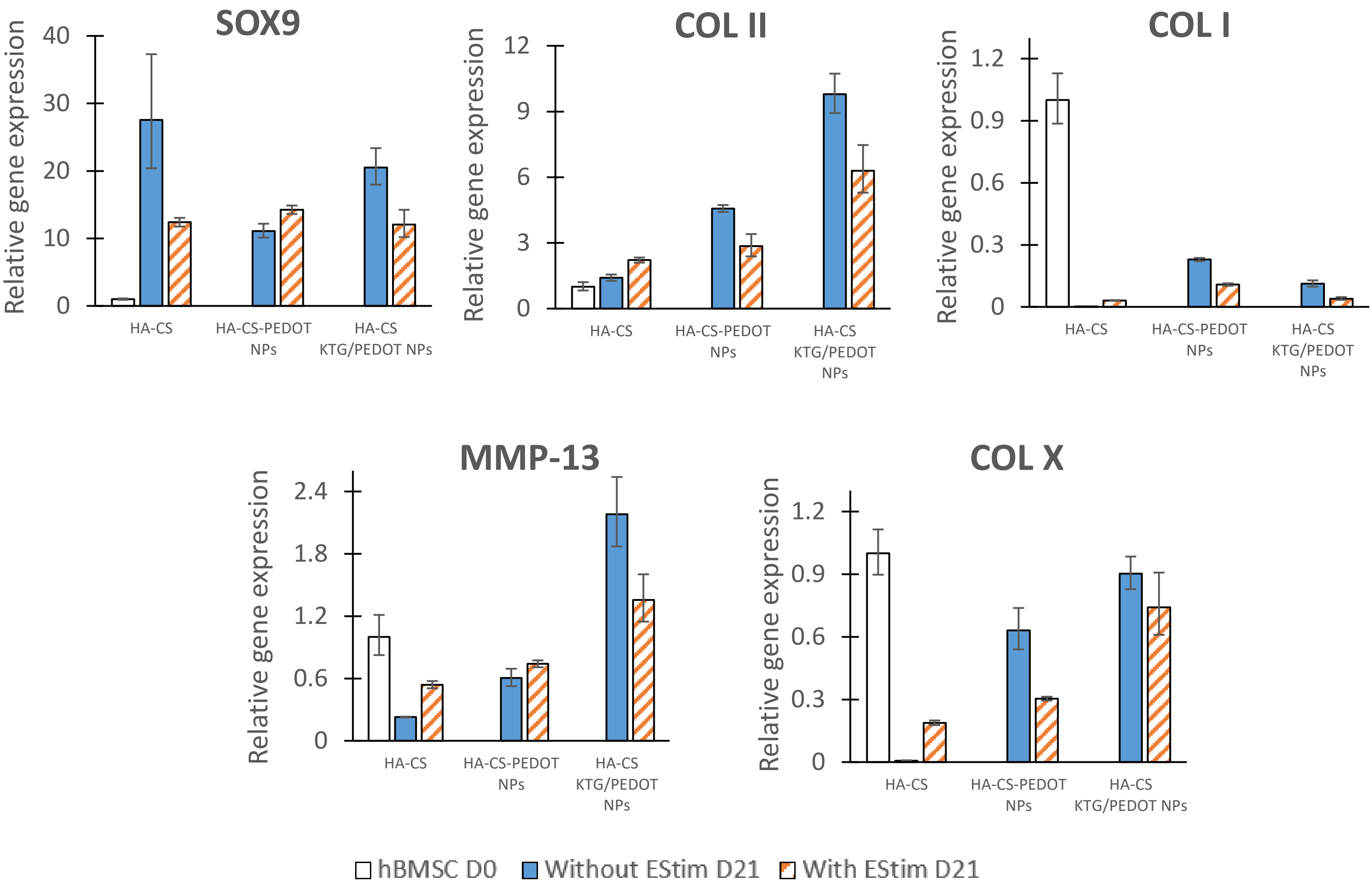

Figure 30 - qRT-PCR analysis of hBMSCs encapsulated in HA-CS, HA-CS-PEDOT NPs and HA-CS-KTG/PEDOT NPs after 21 days of chondrogenic differentiation in incomplete chondrogenic media with and without electrical stimulation. Gene expression levels of *SOX9*, *COL II*, *COL I*, *MMP-13* and *COL X* were normalized to the endogenous gene *GAPDH* and then calculated as a fold-change relative to the baseline expression of target gene measure in Day 0 experimental group (undifferentiated cells before seeding) (3 technical replicates from a single biological replicate (1 donor)).

Overall, introducing NP to the hydrogels formulation was seen to effectively increase the proliferation of seeded hBMSCs, likely due to higher hydrogel stiffness when compared to HA-CS hydrogels. Electrically stimulating cells encapsulated in hydrogels containing KTG/PEDOT NPs also showed enhanced proliferation, possibly due to the release of KTG. However, the effectiveness of the system in promoting the chondrogenic differentiation of seeded cells was inconclusive, and further assays regarding gene expression should be conducted.

5. Conclusions

Articular cartilage is a connective tissue paramount for healthy articulation and motion. However, due to its avascular nature, it has very limited self-repair capabilities upon lesions or degeneration. This problem is further exacerbated by the prevalence of osteoarthritis, which, due to risk factors like obesity and ageing, is expected to see a considerably rise in its incidence in the future. The current treatment options for this condition mainly focus on pain relief rather than cartilage regeneration, failing to address the core problem.

This MSs thesis focused on developing a novel system for cartilage regeneration by employing the principles of CTE, aiming to construct biomimetic scaffolds that could act as substitutes for native cartilage and promote its regeneration. As such, hydrogels were designed to serve both as scaffolds for hBMSCs and as a drug delivery system that allowed the controlled delivery of KTG through electrical stimulation, promoting the chondrogenesis of seeded cells. In this work, KTG was successfully loaded in PEDOT NPs with a high efficiency, and its encapsulation was confirmed through various assays. Through cyclic voltammetry, the produced NPs were seen to be electroactive, which allowed for a controlled release of encapsulated KTG through electrical stimulation. As chondrogenic differentiation is a 21-day process, the drug delivery system presented in this work may be optimal for effectively promoting differentiation, allowing a stimuli-dependent delivery of controllable doses along the entire differentiation process. Furthermore, the produced NPs and stimulation protocol used in this work exhibited excellent biocompatibility. However, further assays regarding KTG release triggered by electrical stimulation need to be conducted, with different stimulation conditions being employed and a higher number of replicates used.

The addition of NPs to HA-CS hydrogels significantly lowered the swelling ratio of the scaffolds without compromising their water content, which would allow them to retain their mechanical strength in an *in vivo* environment. Additionally, this addition also enhanced the conductivity and mechanical strength of the scaffolds. The results obtained highlight the customization potential of this hydrogel, were adjusting NP concentration allows the modulation of crucial properties required to create a scaffold that mimics native cartilage. Furthermore, as the addition of NPs prolonged the gelation time of the hydrogels, these could potentially be utilized as injectable hydrogels, which would further aid their clinical translation.

hBMSCs cultured with KTG/PEDOT NPs exhibited higher levels of GAG production when electrically stimulated, pointing to an effective release of the drug that promoted the chondrogenic differentiation of the cells. Gene expression analysis also confirmed the differentiation of the seeded cells towards hyaline chondrogenic outcomes, highlighted by the upregulation of *SOX 9* and *COL II* and downregulation of *COL I*, *COL X* and *MMP-13*. In hydrogels fabricated with NPs, seeded hBMSCs exhibited enhanced proliferation, which was likely caused by the increased stiffness of the scaffold. Interestingly, cells encapsulated in HA-CS-KTG/PEDOT NPs hydrogels that were electrically stimulated showed increased proliferation, suggesting the release of KTG from the nanoparticles. Despite the promising results regarding the effectiveness of the system in promoting the proliferation and chondrogenic differentiation of seeded cells, further assays are required in order to draw definitive conclusions, as gene expression analysis did not corroborate the release of KTG in electrically stimulated conditions.

6. Future perspectives

The development of a CTE inspired system capable of mimicking the properties of native cartilage and allow controlled drug delivery, is a very promising approach to target cartilage regeneration. If correctly optimized, this system has the potential for an effective clinical translation, where the NPs embedded hydrogels could be injected into damaged cartilage sites of patients, and already existing devices could be used to electrically stimulate the tissue, triggering the KTG release and promoting regeneration. However, there is still a need for further investigation and optimization in order to make this a reality.

In the future, some of the assays performed for this work need to be re-conducted, in order to gather more robust results. The KTG release assays should be re-done in triplicates, and more electrical stimulation conditions studied, possibly by changing stimulation times and frequencies. KTG release assays should also be performed with NP embedded hydrogels, as the conductivity of the hydrogel can influence the effectiveness of electrical stimulation on drug release. The quantification of GAGs and gene expression analysis also require further analysis to acquire more robust results.

After confirming the results obtained in this work with future assays, the hydrogels and stimulation protocol need to be optimized in order to not only construct a native cartilage mimetic scaffold, but to maximize tissue regeneration potential through cell proliferation and differentiation. In order to achieve this, the hydrogel's composition should be adjusted, by changing crosslinker and nanoparticle concentrations, with posterior rheological characterizations. Furthermore, as the prolonged presence of a biocompatible hydrogel can hinder the growth of new tissue, being a key parameter for an effective clinical translation, the biodegradability of the hydrogels needs to be improved possibly by introducing biodegradable materials to their formulation. In terms of electrical stimulation, a deeper dive in the molecular mechanisms behind the chondrogenic inducing abilities of KTG should be taken, as drug delivery timings could improve the chondrogenic differentiation of MSCs.

The introduction of the designed system in a multilayered scaffold would also be an interesting option, as it would be more closely mimic the different zones of articular cartilage. Finally, after more robust results are obtained and the designed system further optimized, studying the system potential *in vivo* would be invaluable to assess its potential for clinical translation.

7. Bibliography

1. Woo, S. L. & Buckwalter, J. A. Injury and repair of the musculoskeletal soft tissues. Savannah, Georgia, June 18–20, 1987. *Journal of Orthopaedic Research* **6**, 907–931 (1988).
2. Eyre, D. R. & Wu, J. J. Collagen structure and cartilage matrix integrity. *J Rheumatol Suppl* **43**, 82–85 (1995).
3. Mow, V. C., Ratcliffe, A. & Robin Poole, A. Cartilage and diarthrodial joints as paradigms for hierarchical materials and structures. *Biomaterials* **13**, 67–97 (1992).
4. Roughley, P. J. & Lee, E. R. Cartilage proteoglycans: Structure and potential functions. *Microsc Res Tech* **28**, 385–397 (1994).
5. Buckwalter, J. A. M. M. V. C. P. R. A. PhD. Restoration of Injured or Degenerated Articular Cartilage. *JAAOS - Journal of the American Academy of Orthopaedic Surgeons* **2**, 192–201 (1994).
6. Sophia Fox, A. J., Bedi, A. & Rodeo, S. A. The Basic Science of Articular Cartilage: Structure, Composition, and Function. *Sports Health* **1**, 461 (2009).
7. Mow, V. C., Holmes, M. H. & Ael Ln, W. M. FLUID TRANSPORT AND MECHANICAL PROPERTIES OF ARTICULAR CARTILAGE: A REVIEW. *J Biomech* **17**, 377–94 (1984).
8. Sophia Fox, A. J., Bedi, A. & Rodeo, S. A. The Basic Science of Articular Cartilage: Structure, Composition, and Function. *Sports Health* **1**, 461 (2009).
9. Ulrich-Vinther, M., Maloney, M. D., Schwarz, E. M., Rosier, R. & O'keefe, R. J. Articular Cartilage Biology. *Orthopaedic Research Society Special Article* **11**, 421 (2003).
10. Gorbachova, T., Melenevsky, Y., Cohen, M. & Cerniglia, B. W. Osteochondral lesions of the knee: Differentiating the most common entities at MRI. *Radiographics* **38**, 1478–1495 (2018).
11. Steinwachs, M. R., Engebretsen, L. & Brophy, R. H. Scientific Evidence Base for Cartilage Injury and Repair in the Athlete. *Cartilage* **3**, 11S (2012).
12. Goldring, S. R., Goldring, M. B. & Goldring, S. R. Clinical aspects, pathology and pathophysiology of osteoarthritis. *J Musculoskelet Neuronal Interact* **6**, 376–378 (2006).
13. Felson, D. T. Clinical practice. Osteoarthritis of the knee. *N Engl J Med* **354**, 841–8 (2006).
14. Kapoor, M., Martel-Pelletier, J., Lajeunesse, D., Pelletier, J. P. & Fahmi, H. Role of proinflammatory cytokines in the pathophysiology of osteoarthritis. *Nat Rev Rheumatol* **7**, 33–42 (2011).
15. Chadjichristos, C. *et al.* Sp1 and Sp3 transcription factors mediate interleukin-1 beta down-regulation of human type II collagen gene expression in articular chondrocytes. *J Biol Chem* **278**, 39762–39772 (2003).
16. Séguin, C. A. & Bernier, S. M. TNFalpha suppresses link protein and type II collagen expression in chondrocytes: Role of MEK1/2 and NF-kappaB signaling pathways. *J Cell Physiol* **197**, 356–369 (2003).

17. Tetlow, L. C., Adlam, D. J. & Woolley, D. E. Matrix Metalloproteinase and Proinflammatory Cytokine Production by Chondrocytes of Human Osteoarthritic Cartilage Associations With Degenerative Changes. *Arthritis Rheum* **44**, 585–594 (2001).

18. Lee, A. S. *et al.* A current review of molecular mechanisms regarding osteoarthritis and pain. doi:10.1016/j.gene.2013.05.069.

19. Mengshol, J. A. , V. M. P. , C. C. I. , B. A. , & B. C. E. Interleukin-1 induction of collagenase 3 (matrix metalloproteinase 13) gene expression in chondrocytes requires p38, c-jun N-terminal kinase, and nuclear factor κB: Differential regulation of collagenase 1 and collagenase 3. *Arthritis Rheum* **43**, 801–811 (2000).

20. Wojdasiewicz, P., Poniatowski, Ł. A. & Szukiewicz, D. The role of inflammatory and anti-inflammatory cytokines in the pathogenesis of osteoarthritis. *Mediators Inflamm* **2014**, (2014).

21. Derry, S. *et al.* Osteoarthritis. *Cochrane Database of Systematic Reviews* **2017**, (2022).

22. Zhang, Y. & Jordan, J. M. Epidemiology of Osteoarthritis. *Clin Geriatr Med* **26**, 355 (2010).

23. Plotnikoff, R. *et al.* Osteoarthritis prevalence and modifiable factors: A population study Chronic Disease epidemiology. *BMC Public Health* **15**, 1–10 (2015).

24. Gu, Y.-Y. *et al.* Research progress on osteoarthritis treatment mechanisms. *Biomedicine et Pharmacotherapy* **93**, 1246–1252 (2017).

25. Litwic, A., Edwards, M. H., Dennison, E. M. & Cooper, C. Epidemiology and burden of osteoarthritis. *Br Med Bull* **105**, 185–199 (2013).

26. Lawrence, R. C. *et al.* Estimates of the prevalence of arthritis and other rheumatic conditions in the United States: Part II. *Arthritis Rheum* **58**, 26–35 (2008).

27. Turkiewicz Y Z *, A. *et al.* Current and future impact of osteoarthritis on health care: a population-based study with projections to year 2032. *Osteoarthritis Cartilage* **22**, 1826–1832 (2014).

28. Kotlarz, H., Gunnarsson, C. L., Fang, H. & Rizzo, J. A. Insurer and out-of-pocket costs of osteoarthritis in the US: evidence from national survey data. *Arthritis Rheum* **60**, 3546–3553 (2009).

29. Zhang, W., Ouyang, H., Dass, C. R. & Xu, J. Current research on pharmacologic and regenerative therapies for osteoarthritis. *Bone Research 2016 4:1* **4**, 1–14 (2016).

30. Bentley, G. *et al.* Minimum ten-year results of a prospective randomised study of autologous chondrocyte implantation versus mosaicplasty for symptomatic articular cartilage lesions of the knee. *J Bone Joint Surg Br* **94**, 504–509 (2012).

31. Schuette, H. B., Kraeutler, M. J. & McCarty, E. C. Matrix-Assisted Autologous Chondrocyte Transplantation in the Knee: A Systematic Review of Mid- to Long-Term Clinical Outcomes. *Orthop J Sports Med* **5**, (2017).

32. Marcacci Elizaveta Kon, M. *et al.* Knee: Systematic Clinical Data Review and Study Quality Analysis Matrix-Assisted Autologous Chondrocyte Transplantation for the Repair of Cartilage Defects of the Matrix-Assisted Autologous Chondrocyte Transplantation for the Repair of

Cartilage Defects of the Knee Systematic Clinical Data Review and Study Quality Analysis. (2009) doi:10.1177/0363546509351649.

33. Andriolo, L., Merli, G., Filardo, G., Marcacci, M. & Kon, E. Failure of Autologous Chondrocyte Implantation. *Sports Med Arthrosc Rev* **25**, 10–18 (2017).

34. Daher, R. J., Chahine, N. O., Greenberg, A. S., Sgaglione, N. A. & Grande, D. A. New methods to diagnose and treat cartilage degeneration. *Nature Reviews Rheumatology 2009 5:11* **5**, 599–607 (2009).

35. Tuli, R., Li, W. J. & Tuan, R. S. Current state of cartilage tissue engineering. *Arthritis Res Ther* **5**, 235–238 (2003).

36. Keeney, M., Lai, J. H. & Yang, F. Recent progress in cartilage tissue engineering. *Curr Opin Biotechnol* **22**, 734–740 (2011).

37. Fox, A. J. S., Bedi, A. & Rodeo, S. A. The Basic Science of Articular Cartilage: Structure, Composition, and Function. (2009) doi:10.1177/1941738109350438.

38. Huey, D. J., Hu, J. C. & Athanasiou, K. A. Unlike Bone, Cartilage Regeneration Remains Elusive. *Science* **338**, 917 (2012).

39. Bružauskaitė, I., Bironaitė, D., Bagdonas, E. & Bernotienė, E. Scaffolds and cells for tissue regeneration: different scaffold pore sizes-different cell effects. *Cytotechnology* **68**, 355–369 (2016).

40. Demoor, M. *et al.* Cartilage tissue engineering: molecular control of chondrocyte differentiation for proper cartilage matrix reconstruction. *Biochim Biophys Acta* **1840**, 2414–2440 (2014).

41. Wichterle, O. & Lím, D. Hydrophilic Gels for Biological Use. *Nature 1960 185:4706* **185**, 117–118 (1960).

42. Gong, J. P. Friction and lubrication of hydrogels-its richness and complexity. *Soft Matter* **2**, 544–552 (2006).

43. Melrose, J., Chuang, C. & Whitelock, J. Tissue engineering of cartilages using biomatrices. *Journal of Chemical Technology & Biotechnology* **83**, 444–463 (2008).

44. Chuang, E. Y., Chiang, C. W., Wong, P. C. & Chen, C. H. Hydrogels for the Application of Articular Cartilage Tissue Engineering: A Review of Hydrogels. *Advances in Materials Science and Engineering* **2018**, (2018).

45. Spiller, K. L., Maher, S. A. & Lowman, A. M. Hydrogels for the Repair of Articular Cartilage Defects. doi:10.1089/ten.teb.2011.0077.

46. Shen, Z. sen *et al.* Tough biodegradable chitosan–gelatin hydrogels via in situ precipitation for potential cartilage tissue engineering. *RSC Adv* **5**, 55640–55647 (2015).

47. Sim, H. J., Thambi, T. & Lee, D. S. Heparin-based temperature-sensitive injectable hydrogels for protein delivery. *J Mater Chem B* **3**, 8892–8901 (2015).

48. Bidarra, S. J., Barrias, C. C. & Granja, P. L. Injectable alginate hydrogels for cell delivery in tissue engineering. *Acta Biomater* **10**, 1646–1662 (2014).

49. Saraf, S., Alexander, A., Ajazuddin, Khan, J. & Saraf, S. Poly(ethylene glycol)–poly(lactic-co-glycolic acid) based thermosensitive injectable hydrogels for biomedical applications. *Journal of Controlled Release* **172**, 715–729 (2013).

50. Ossipov, D. A., Piskounova, S. & Hilborn, J. Poly(vinyl alcohol) Cross-Linkers for in Vivo Injectable Hydrogels. *Macromolecules* **41**, 3971–3982 (2008).

51. Wang, F. *et al.* Injectable, rapid gelling and highly flexible hydrogel composites as growth factor and cell carriers. *Acta Biomater* **6**, 1978–1991 (2010).

52. Dorsey, S. M. *et al.* MRI evaluation of injectable hyaluronic acid-based hydrogel therapy to limit ventricular remodeling after myocardial infarction. *Biomaterials* **69**, 65–75 (2015).

53. Jin, R. *et al.* Injectable chitosan-based hydrogels for cartilage tissue engineering. *Biomaterials* **30**, 2544–2551 (2009).

54. Place, E. S., George, J. H., Williams, C. K. & Stevens, M. M. Synthetic polymer scaffolds for tissue engineering. *Chem Soc Rev* **38**, 1139–1151 (2009).

55. Zhao, W., Jin, X., Cong, Y., Liu, Y. & Fu, J. Degradable natural polymer hydrogels for articular cartilage tissue engineering. *Journal of Chemical Technology and Biotechnology* **88**, 327–339 (2013).

56. Radulescu, D. M., Neacsu, I. A., Grumezescu, A. M. & Andronescu, E. New Insights of Scaffolds Based on Hydrogels in Tissue Engineering. *Polymers 2022, Vol. 14, Page 799* **14**, 799 (2022).

57. Miguel, F., Barbosa, F., Ferreira, F. C. & Silva, J. C. Electrically Conductive Hydrogels for Articular Cartilage Tissue Engineering. *Gels* **8**, 710 (2022).

58. Jin, R. *et al.* Chondrogenesis in injectable enzymatically crosslinked heparin/dextran hydrogels. *Journal of Controlled Release* **152**, 186–195 (2011).

59. Funayama, A. *et al.* Repair of full-thickness articular cartilage defects using injectable type II collagen gel embedded with cultured chondrocytes in a rabbit model. *J Orthop Sci* **13**, 225–232 (2008).

60. Gu, L. *et al.* Preparation and characterization of methacrylated gelatin/bacterial cellulose composite hydrogels for cartilage tissue engineering. *Regen Biomater* **7**, 195–202 (2020).

61. Skaalure, S. C., Chu, S. & Bryant, S. J. An Enzyme-Sensitive PEG Hydrogel Based on Aggrecan Catabolism for Cartilage Tissue Engineering. *Adv Healthc Mater* **4**, 420–431 (2015).

62. Li, X. *et al.* A chondroitin sulfate based injectable hydrogel for delivery of stem cells in cartilage regeneration. *Biomater Sci* **9**, 4139–4148 (2021).

63. Wang, G. *et al.* A Hyaluronic Acid Based Injectable Hydrogel Formed via Photo-Crosslinking Reaction and Thermal-Induced Diels-Alder Reaction for Cartilage Tissue Engineering. *Polymers (Basel)* **10**, 949 (2018).

64. Mahmoudifar, N. & Doran, P. M. Chondrogenesis and cartilage tissue engineering: The longer road to technology development. *Trends Biotechnol* **30**, 166–176 (2012).

65. You, F., Eames, B. F. & Chen, X. Application of Extrusion-Based Hydrogel Bioprinting for Cartilage Tissue Engineering. *Int J Mol Sci* **18**, 1597 (2017).

66. Oldershaw, R. A. *et al.* Directed differentiation of human embryonic stem cells toward chondrocytes. *Nat Biotechnol* **28**, 1187–1194 (2010).

67. Nakagawa, T., Lee, S. Y. & Reddi, A. H. Induction of chondrogenesis from human embryonic stem cells without embryoid body formation by bone morphogenetic protein 7 and transforming growth factor beta1. *Arthritis Rheum* **60**, 3686–3692 (2009).

68. Koyama, N. *et al.* Human induced pluripotent stem cells differentiated into chondrogenic lineage via generation of mesenchymal progenitor cells. *Stem Cells Dev* **22**, 102–113 (2013).

69. Tsumaki, N., Okada, M. & Yamashita, A. iPS cell technologies and cartilage regeneration. *Bone* **70**, 48–54 (2015).

70. Colombini, A. *et al.* Mesenchymal stem cells in the treatment of articular cartilage degeneration: New biological insights for an old-timer cell. *Cytotherapy* **21**, 1179–1197 (2019).

71. Le, H. *et al.* Mesenchymal stem cells for cartilage regeneration. *J Tissue Eng* **11**, 469–488 (2020).

72. Ringe, J., Burmester, G. R. & Sittinger, M. Regenerative medicine in rheumatic disease-progress in tissue engineering. *Nat Rev Rheumatol* **8**, 493–498 (2012).

73. Farooqi, A. R., Bader, R. & van Rienen, U. Numerical Study on Electromechanics in Cartilage Tissue with Respect to Its Electrical Properties. *Tissue Eng Part B Rev* **25**, 152–166 (2019).

74. Brady, M. A., Waldman, S. D. & Ethier, C. R. The Application of Multiple Biophysical Cues to Engineer Functional Neocartilage for Treatment of Osteoarthritis. Part I: Cellular Response. *https://home.liebertpub.com/teb* **21**, 1–19 (2014).

75. Jahr, H., Matta, C. & Mobasheri, A. Physicochemical and Biomechanical Stimuli in Cell-Based Articular Cartilage Repair. *Curr Rheumatol Rep* **17**, 22 (2015).

76. Myers, E. R., Lai, W. M. & Mow, V. C. A continuum theory and an experiment for the ion-induced swelling behavior of articular cartilage. *J Biomech Eng* **106**, 151–158 (1984).

77. Chen, A. C., Bae, W. C., Schinagl, R. M. & Sah, R. L. Depth- and strain-dependent mechanical and electromechanical properties of full-thickness bovine articular cartilage in confined compression. *J Biomech* **34**, 1–12 (2001).

78. Mow, V. C. & Guo, X. E. Mechano-Electrochemical Properties Of Articular Cartilage: Their Inhomogeneities and Anisotropies. *Annu Rev Biomed Eng* **4**, 175–209 (2003).

79. Mlynárik, V. & Trattnig, S. Physicochemical properties of normal articular cartilage and its MR appearance. *Invest Radiol* **35**, 589–594 (2000).

80. Sun, D. D., Guo, X. E., Likhitpanichkul, M., Lai, W. M. & Mow, V. C. The influence of the fixed negative charges on mechanical and electrical behaviors of articular cartilage under unconfined compression. *J Biomech Eng* **126**, 6–16 (2004).

81. Xu, J., Wang, W., Clark, C. C. & Brighton, C. T. Signal transduction in electrically stimulated articular chondrocytes involves translocation of extracellular calcium through voltage-gated channels. *Osteoarthritis Cartilage* **17**, 397–405 (2009).

82. Xu, J., Wang, W., Clark, C. C. & Brighton, C. T. Signal transduction in electrically stimulated articular chondrocytes involves translocation of extracellular calcium through voltage-gated channels. *Osteoarthritis Cartilage* **17**, 397–405 (2009).

83. Matta, C., Zákány, R. & Mobasheri, A. Voltage-dependent calcium channels in chondrocytes: roles in health and disease. *Curr Rheumatol Rep* **17**, 43 (2015).

84. Zuzzi, D. C. *et al.* Evaluation of the effects of electrical stimulation on cartilage repair in adult male rats. *Tissue Cell* **45**, 275–281 (2013).

85. Krueger, S. *et al.* Re-Differentiation Capacity of Human Chondrocytes in Vitro Following Electrical Stimulation with Capacitively Coupled Fields. *J Clin Med* **8**, 1771 (2019).

86. Deng, Z. H., Li, Y. S., Gao, X., Lei, G. H. & Huard, J. Bone morphogenetic proteins for articular cartilage regeneration. *Osteoarthritis Cartilage* **26**, 1153–1161 (2018).

87. Aaron, R. K., Wang, S. & Ciombor, D. M. Upregulation of basal TGFP, levels by EMF coincident with chondrogenesis-implications for skeletal repair and tissue engineering. *Journal of Orthopaedic ELSEVIER Journal of Orthopaedic Research* **20**, 233–240 (2002).

88. Ciombor, D. M., Lester, G., Aaron, R. K., Neame ', P. & Caterson, B. Journal of Orthopaedic Research Low frequency EMF regulates chondrocyte differentiation and expression of matrix proteins. *Journal of Orthopaedic Research* **20**, 40–50 (2002).

89. Car, B., Brighton, T., Wang, W. & Clark, C. C. The Effect of Electrical Eields on Gene and Protein Expression in Human Osteoarthritic Cartilage Expiants. *J Bone Joint Surg Am* **90**, 833–848 (2008).

90. Luisa Hernández-Bule, M., Luis, C., María, P., Trillo, Á. & Úbeda, A. Hernández-Bule et al.: Electric Stimulation of Stem Cell Proliferation Electric Stimulation at 448 kHz Promotes Proliferation of Human Mesenchymal Stem Cells. *Cell Physiol Biochem* **34**, 1741–1755 (2014).

91. Hardy, J. G. *et al.* Electrical stimulation of human mesenchymal stem cells on biomineralized conducting polymers enhances their differentiation towards osteogenic outcomes. *J Mater Chem B* **3**, 8059–8064 (2015).

92. Kwon, H. J., Lee, G. S. & Chun, H. Electrical stimulation drives chondrogenesis of mesenchymal stem cells in the absence of exogenous growth factors. *Sci Rep* **6**, 1–13 (2016).

93. Vaca-González, J. J. *et al.* Effect of electrical stimulation on chondrogenic differentiation of mesenchymal stem cells cultured in hyaluronic acid – Gelatin injectable hydrogels. *Bioelectrochemistry* **134**, (2020).

94. Zhao, X. *et al.* Thermoswitchable Electronic Properties of a Gold Nanoparticle/Hydrogel Composite. *Macromol Rapid Commun* **26**, 1784–1787 (2005).

95. Kumar, A., Behl, T. & Chadha, S. Synthesis of physically crosslinked PVA/Chitosan loaded silver nanoparticles hydrogels with tunable mechanical properties and antibacterial effects. *Int J Biol Macromol* **149**, 1262–1274 (2020).

96. Fan, Z. *et al.* A Novel Wound Dressing Based on Ag/Graphene Polymer Hydrogel: Effectively Kill Bacteria and Accelerate Wound Healing. *Adv Funct Mater* **24**, 3933–3943 (2014).

97. Nambiar, S. & Yeow, J. T. W. Conductive polymer-based sensors for biomedical applications. *Biosens Bioelectron* **26**, 1825–1832 (2011).

98. Bhat, M. A., Rather, R. A. & Shalla, A. H. PEDOT and PEDOT:PSS conducting polymeric hydrogels: A report on their emerging applications. *Synth Met* **273**, 116709 (2021).

99. Balint, R., Cassidy, N. J. & Cartmell, S. H. Conductive polymers: Towards a smart biomaterial for tissue engineering. *Acta Biomater* **10**, 2341–2353 (2014).

100. Gueye, M. N. *et al.* Structure and Dopant Engineering in PEDOT Thin Films: Practical Tools for a Dramatic Conductivity Enhancement. *Chemistry of Materials* **28**, 3462–3468 (2016).

101. Ravichandran, R., Sundarrajan, S., Venugopal, J. R., Mukherjee, S. & Ramakrishna, S. Applications of conducting polymers and their issues in biomedical engineering. *J R Soc Interface* **7**, 559–579 (2010).

102. Gilmore, K. *et al.* Skeletal muscle cell proliferation and differentiation on polypyrrole substrates doped with extracellular matrix components. *Elsevier* **30**, 5292–5304 (2009).

103. Fang, Y. *et al.* PEDOT: PSS-Based Microfluidic-Spun Microfibers for Tunable Release of Acetaminophen via Electrical Stimulation. *Adv Mater Technol* **7**, 2200103 (2022).

104. Lee, K., Lee, H., Bae, K. H. & Park, T. G. Heparin immobilized gold nanoparticles for targeted detection and apoptotic death of metastatic cancer cells. *Biomaterials* **31**, 6530–6536 (2010).

105. Bharti, A., Singh, S., Meena, V. K. & Goyal, N. Structural Characterization of Silver-Hydroxyapatite Nanocomposite: A Bone Repair Biomaterial. *Mater Today Proc* **3**, 2113–2120 (2016).

106. Yang, H. *et al.* One-pot synthesis of amphiphilic superparamagnetic FePt nanoparticles and magnetic resonance imaging in vitro. *J Magn Magn Mater* **322**, 973–977 (2010).

107. Comba, F. N., Romero, M. R., Garay, F. S. & Baruzzi, A. M. Mucin and carbon nanotube-based biosensor for detection of glucose in human plasma. *Anal Biochem* **550**, 34–40 (2018).

108. Xia, B. *et al.* Photothermal and biodegradable polyaniline/porous silicon hybrid nanocomposites as drug carriers for combined chemo-photothermal therapy of cancer. *Acta Biomater* **51**, 197–208 (2017).

109. Abidian, M. R., Kim, D. H. & Martin, D. C. Conducting-Polymer Nanotubes for Controlled Drug Release. *Adv Mater* **18**, 405 (2006).

110. Chan, E. W. C. *et al.* Electrospun Polythiophene Phenylenes for Tissue Engineering. *Biomacromolecules* **19**, 1456–1468 (2018).

111. Distler, T. *et al.* Electrically Conductive and 3D-Printable Oxidized Alginate-Gelatin Polypyrrole:PSS Hydrogels for Tissue Engineering. *Adv Healthc Mater* **10**, 2001876 (2021).

112. Zhang, S. *et al.* Bioinspired Conductive Hydrogel with Ultrahigh Toughness and Stable Antiswelling Properties for Articular Cartilage Replacement. *ACS Mater Lett* **3**, 807–814 (2021).

113. Shen, H. *et al.* Chondroinductive factor-free chondrogenic differentiation of human mesenchymal stem cells in graphene oxide-incorporated hydrogels. *J Mater Chem B* **6**, 908–917 (2018).

114. Distler, T. *et al.* Electrically Conductive and 3D-Printable Oxidized Alginate-Gelatin Polypyrrole:PSS Hydrogels for Tissue Engineering. *Adv Healthc Mater* **10**, 2001876 (2021).

115. Augustyniak, E., Trzeciak, T., Richter, M., Kaczmarczyk, J. & Suchorska, W. The role of growth factors in stem cell-directed chondrogenesis: a real hope for damaged cartilage regeneration. *Int Orthop* **39**, 995–1003 (2015).

116. Ohba, S., Hojo, H. & Chung, U. il. Bioactive factors for tissue regeneration: state of the art. *Muscles Ligaments Tendons J* **2**, 193 (2012).

117. Mehlhorn, A. T. *et al.* Mesenchymal Stem Cells Maintain TGF-β-Mediated Chondrogenic Phenotype in Alginate Bead Culture. *https://home.liebertpub.com/ten* **12**, 1393–1403 (2006).

118. Choi, S. J. *et al.* Combination of ascorbate and growth factor (TGF beta-3) in thermo-reversible hydrogel constructs embedded with rabbit chondrocytes for neocartilage formation. *J Biomed Mater Res A* **83**, 897–905 (2007).

119. Longobardi, L. *et al.* Effect of IGF-I in the Chondrogenesis of Bone Marrow Mesenchymal Stem Cells in the Presence or Absence of TGF-β Signaling. *Journal of Bone and Mineral Research* **21**, 626–636 (2006).

120. Stowers, R. S., Drinnan, C. T., Chung, E. & Suggs, L. J. Mesenchymal stem cell response to TGF-β1 in both 2D and 3D environments. *Biomater Sci* **1**, 860–869 (2013).

121. Elford, P. R. *et al.* Induction of swelling, synovial hyperplasia and cartilage proteoglycan loss upon intra-articular injection of transforming growth factor beta-2 in the rabbit. *Cytokine* **4**, 232–238 (1992).

122. van der Kraan, P. M. & van den Berg, W. B. Osteophytes: relevance and biology. *Osteoarthritis Cartilage* **15**, 237–244 (2007).

123. Lo, K. W. H., Ashe, K. M., Kan, H. M. & Laurencin, C. T. The role of small molecules in musculoskeletal regeneration. *Regenerative Med* **7**, 535 (2012).

124. Wang, Y. *et al.* Small molecules and their controlled release that induce the osteogenic/chondrogenic commitment of stem cells. *Biotechnol Adv* **33**, 1626–1640 (2015).

125. Johnson, K. *et al.* A stem cell-based approach to cartilage repair. *Science* **336**, 717–721 (2012).

126. Zhang, J. & Wang, J. H. C. Kartogenin induces cartilage-like tissue formation in tendon-bone junction. *Bone Res* **2**, 14008 (2014).

127. Silva, J. C. *et al.* Kartogenin-loaded coaxial PGS/PCL aligned nanofibers for cartilage tissue engineering. *Materials Science and Engineering: C* **107**, 110291 (2020).

128. Cai, G. *et al.* Recent advances in kartogenin for cartilage regeneration. *J Drug Target* **27**, 28–32 (2018).

129. Xu, X. *et al.* Exosome-mediated delivery of kartogenin for chondrogenesis of synovial fluid-derived mesenchymal stem cells and cartilage regeneration. *Biomaterials* **269**, 120539 (2021).

130. Wilczewska, A. Z., Niemirowicz, K., Markiewicz, K. H. & Car, H. Nanoparticles as drug delivery systems. *Pharmacological Reports* **64**, 1020–1037 (2012).

131. Nevozhay, D. , K. U. , B. R. , & B. J. Current status of research on conjugates and related drug delivery systems in the treatment of cancer and other diseases. *Postepy Hig Med Dosw* **61**, 350–360 (2007).

132. Almeida, B., Wang, Y. & Shukla, A. Effects of Nanoparticle Properties on Kartogenin Delivery and Interactions with Mesenchymal Stem Cells. *Ann Biomed Eng* **48**, 2090–2102 (2020).

133. Woeppel, K. M., Zheng, X. S., Schulte, Z. M., Rosi, N. L. & Cui, X. T. Nanoparticle Doped PEDOT for Enhanced Electrode Coatings and Drug Delivery. *Adv Healthc Mater* **8**, 1900622 (2019).

134. Kang, M. L., Ko, J. Y., Kim, J. E. & Im, G. il. Intra-articular delivery of kartogenin-conjugated chitosan nano/microparticles for cartilage regeneration. *Biomaterials* **35**, 9984–9994 (2014).

135. Shi, D. *et al.* Photo-cross-linked scaffold with kartogenin-encapsulated nanoparticles for cartilage regeneration. *ACS Nano* **10**, 1292–1299 (2016).

136. Fan, W. *et al.* Intra-articular injection of kartogenin-conjugated polyurethane nanoparticles attenuates the progression of osteoarthritis. *https://doi.org/10.1080/10717544.2018.1461279* **25**, 1004–1012 (2018).

137. Xu, J. *et al.* Nanocarrier-Mediated Codelivery of Small Molecular Drugs and siRNA to Enhance Chondrogenic Differentiation and Suppress Hypertrophy of Human Mesenchymal Stem Cells. *Adv Funct Mater* **26**, 2463–2472 (2016).

138. Li, J. *et al.* Near-infrared light-triggered release of small molecules for controlled differentiation and long-term tracking of stem cells in vivo using upconversion nanoparticles. *Biomaterials* **110**, 1–10 (2016).

139. Kang, H. *et al.* Remote Control of Intracellular Calcium Using Upconversion Nanotransducers Regulates Stem Cell Differentiation In Vivo. *Adv Funct Mater* **28**, 1802642 (2018).

140. Bocca, B., Sabbioni, E., Mičetić, I., … A. A.-J. of A. & 2017, undefined. Size and metal composition characterization of nano- and microparticles in tattoo inks by a combination of analytical techniques. *J. Anal. At. Spectrom* **32**, 616–628 (2017).

141. Crouzier, L. *et al.* Influence of electron landing energy on the measurement of the dimensional properties of nanoparticle populations imaged by SEM. *Ultramicroscopy* **226**, 113300 (2021).

142. Wilson, B. K. & Prud'homme, R. K. Nanoparticle size distribution quantification from transmission electron microscopy (TEM) of ruthenium tetroxide stained polymeric nanoparticles. *J Colloid Interface Sci* **604**, 208–220 (2021).

143. Stavis, S. M., Fagan, J. A., Stopa, M. & Liddle, J. A. Nanoparticle Manufacturing-Heterogeneity through Processes to Products. *ACS Appl Nano Mater* **1**, 4358–4385 (2018).

144. Boyd, R. D., Pichaimuthu, S. K. & Cuenat, A. New approach to inter-technique comparisons for nanoparticle size measurements; using atomic force microscopy, nanoparticle tracking analysis and dynamic light scattering. *Colloids Surf A Physicochem Eng Asp* **387**, 35–42 (2011).

145. Geiser, M. *et al.* Ultrafine Particles Cross Cellular Membranes by Nonphagocytic Mechanisms in Lungs and in Cultured Cells. *Environ Health Perspect* **113**, 1555 (2005).

146. Chithrani, B. D. & Chan, W. C. W. Elucidating the mechanism of cellular uptake and removal of protein-coated gold nanoparticles of different sizes and shapes. *Nano Lett* **7**, 1542–1550 (2007).

147. Jin, H., Heller, D. A., Sharma, R. & Strano, M. S. Size-dependent cellular uptake and expulsion of single-walled carbon nanotubes: single particle tracking and a generic uptake model for nanoparticles. *ACS Nano* **3**, 149–158 (2009).

148. Marano, F., Hussain, S., Rodrigues-Lima, F., Baeza-Squiban, A. & Boland, S. Nanoparticles: molecular targets and cell signalling. *Arch Toxicol* **85**, 733–741 (2011).

149. Goodman, C. M., McCusker, C. D., Yilmaz, T. & Rotello, V. M. Toxicity of gold nanoparticles functionalized with cationic and anionic side chains. *Bioconjug Chem* **15**, 897–900 (2004).

150. Dawson, K. A., Salvati, A. & Lynch, I. Nanotoxicology: nanoparticles reconstruct lipids. *Nat Nanotechnol* **4**, 84–85 (2009).

151. Johnson, K. *et al.* A stem cell-based approach to cartilage repair. *Science* **336**, 717–721 (2012).

152. Dietrich, M., Heinze, J., Heywang, G. & Jonas, F. Electrochemical and spectroscopic characterization of polyalkylenedioxythiophenes. *Journal of Electroanalytical Chemistry* **369**, 87–92 (1994).

153. M. Marzocchi. Conducting Polymers as Novel Tools for Biosensing and Tissue Engineering. *Materials Science* (2016).

154. Cyclic Voltammetry 3/4- What Information Can a CV Provide? - PalmSens. https://www.palmsens.com/knowledgebase-article/cyclic-voltammetry-what-information-can-a-cv-provide/.

155. Elgrishi, N. *et al.* A Practical Beginner's Guide to Cyclic Voltammetry. *J Chem Educ* **95**, 197–206 (2018).

156. Liu, Y., Yang, G., Jin, S., Xu, L. & Zhao, C. X. Development of High-Drug-Loading Nanoparticles. *Chempluschem* **85**, 2143–2157 (2020).

157. Cai, K. *et al.* Dimeric Drug Polymeric Nanoparticles with Exceptionally High Drug Loading and Quantitative Loading Efficiency. *J Am Chem Soc* **137**, 3458–3461 (2015).

158. Almeida, B., Wang, Y. & Shukla, A. Effects of Nanoparticle Properties on Kartogenin Delivery and Interactions with Mesenchymal Stem Cells. *Ann Biomed Eng* **48**, 2090–2102 (2020).

159. Svirskis, D., Travas-Sejdic, J., Rodgers, A. & Garg, S. Electrochemically controlled drug delivery based on intrinsically conducting polymers. *J Control Release* **146**, 6–15 (2010).

160. Tao, X. *et al.* Effects of Particle Hydrophobicity, Surface Charge, Media pH Value and Complexation with Human Serum Albumin on Drug Release Behavior of Mitoxantrone-Loaded Pullulan Nanoparticles. *Nanomaterials* **6**, 2 (2016).

161. Rohman, A. *et al.* Comprehensive Review on Application of FTIR Spectroscopy Coupled with Chemometrics for Authentication Analysis of Fats and Oils in the Food Products. *Molecules* **25**, 5485 (2020).

162. Yahyaei, B. one step conjugation of some chemotherapeutic drugs to the biologically produced gold nanoparticles and assessment of their anticancer effects. *Sci Rep* **9**, 10242 (2019).

163. Meneses, J., Fernandes, S., Alves, N., Pascoal-Faria, P. & Miranda, P. C. How to correctly estimate the electric field in capacitively coupled systems for tissue engineering: a comparative study. *Sci Rep* **12**, 11049 (2022).

164. Slobodyan, O. *et al.* Analysis of the dependence of critical electric field on semiconductor bandgap. *J Mater Res* **37**, 849–865 (2022).

165. Miller, L. L., Zhou, X. Q., Miller, L. L. & Zhou, X. Q. Poly(N-methylpyrrolylium) poly(styrenesulfonate) - a conductive, electrically switchable cation exchanger that cathodically binds and anodically releases dopamine. *MaMol* **20**, 1594–1597 (1987).

166. Bidan, G., Lopez, C., Mendes-Viegas, F., Vieil, E. & Gadelle, A. Incorporation of sulphonated cyclodextrins into polypyrrole: an approach for the electro-controlled delivering of neutral drugs. *Biosens Bioelectron* **10**, 219–229 (1995).

167. Gandhi, M., Murray, P., Spinks, G., metals, G. W.-S. & 1995, undefined. Mechanism of electromechanical actuation in polypyrrole. *Synth Met* **73**, 247–256 (1995).

168. Jarai, B. M. & Fromen, C. A. Nanoparticle Internalization Promotes the Survival of Primary Macrophages. *Adv Nanobiomed Res* **2**, 2100127 (2022).

169. He, H. *et al.* Biocompatible Conductive Polymers with High Conductivity and High Stretchability. *ACS Appl Mater Interfaces* **11**, 26185–26193 (2019).

170. Lu, Y., Liu, R., Hang, X. C. & Young, D. J. Biocompatible, flexible and conductive polymers prepared by biomass-derived ionic liquid treatment. *Polym Chem* **12**, 2115–2121 (2021).

171. TWEEN 20 Sigma-Aldrich CAS No.9005-64-5. https://www.sigmaaldrich.com/PT/en/product/sial/p1379.

172. Gun'ko, V. M., Savina, I. N. & Mikhalovsky, S. v. Properties of Water Bound in Hydrogels. *Gels* **3**, 37 (2017).

173. Kamata, H., Akagi, Y., Kayasuga-Kariya, Y., Chung, U. il & Sakai, T. 'Nonswellable' hydrogel without mechanical hysteresis. *Science (1979)* **343**, 873–875 (2014).

174. Yacob, N. & Hashim, K. Morphological effect on swelling behaviour of hydrogel. **1584**, 153 (2014).

175. Mulhbacher, J., Ispas-Szabo, P. & Mateescu, M. A. Cross-linked high amylose starch derivatives for drug release: II. Swelling properties and mechanistic study. *Int J Pharm* **278**, 231–238 (2004).

176. Lee, W. F. & Tsao, K. T. Effect of silver nanoparticles content on the various properties of nanocomposite hydrogels by in situ polymerization. *J Mater Sci* **45**, 89–97 (2010).

177. Paydayesh, A., Heleil, L. & Dadkhah, A. S. Preparation and application of poly (hydroxyl ethyl methacrylate) nanocomposite hydrogels containing iron oxide nanoparticles as wound dressing. *Original Research Article Polymers and Polymer Composites* **30**, 1–10 (2019).

178. Mulder, M., Crosier, J. & Dunn, R. Cauda equina compression by hydrogel dural sealant after a laminotomy and discectomy: case report. *Spine (Phila Pa 1976)* **34**, 144–148 (2009).

179. Zhan, Y., Fu, W., Xing, Y., Ma, X. & Chen, C. Advances in versatile anti-swelling polymer hydrogels. *Materials Science and Engineering: C* **127**, 112208 (2021).

180. Wilson, D. I. What is rheology? *Eye 2018 32:2* **32**, 179–183 (2017).

181. Mills, N., Jenkins, M. & Kukureka, S. Viscoelastic behaviour. *Plastics* 111–125 (2020) doi:10.1016/B978-0-08-102499-7.00007-2.

182. Sun Han Chang, R., Lee, J. C. W., Pedron, S., Harley, B. A. C. & Rogers, S. A. Rheological Analysis of the Gelation Kinetics of an Enzyme Cross-linked PEG Hydrogel. *Biomacromolecules* **20**, 2198–2206 (2019).

183. Huynh, C. T., Liu, F., Cheng, Y., Coughlin, K. A. & Alsberg, E. Thiol-Epoxy 'click' Chemistry to Engineer Cytocompatible PEG-Based Hydrogel for siRNA-Mediated Osteogenesis of hMSCs. *ACS Appl Mater Interfaces* **10**, 25936–25942 (2018).

184. Mihajlovic, M. *et al.* Viscoelastic Chondroitin Sulfate and Hyaluronic Acid Double-Network Hydrogels with Reversible Cross-Links. *Biomacromolecules* **23**, 1350–1365 (2022).

185. Parhi, R. Cross-Linked Hydrogel for Pharmaceutical Applications: A Review. *Adv Pharm Bull* **7**, 515 (2017).

186. Roylance, D. STRESS-STRAIN CURVES. (2001).

187. Barbucci, R., Rappuoli, R., Borzacchiello, A. & Ambrosio, L. Synthesis, chemical and rheological characterization of new hyaluronic acid-based hydrogels. *J Biomater Sci Polym Ed* **11**, 383–399 (2000).

188. Grosskopf, A. K., Saouaf, O. A., Lopez Hernandez, H. & Appel, E. A. Gelation and yielding behavior of polymer–nanoparticle hydrogels. *Journal of Polymer Science* **59**, 2854–2866 (2021).

189. Zaragoza, J. & Asuri, P. Exploring the Effects of Nanoparticle Incorporation on the Mechanical Properties of Hydrogels. *Proc West Mark Ed Assoc Conf* **3**, 2 (2018).

190. Chippada, U., Yurke, B. & Langrana, N. A. Simultaneous determination of Young's modulus, shear modulus, and Poisson's ratio of soft hydrogels. *J Mater Res* **25**, 545–555 (2010).

191. Hafezi, M., Khorasani, S. N., Zare, M., Neisiany, R. E. & Davoodi, P. Advanced Hydrogels for Cartilage Tissue Engineering: Recent Progress and Future Directions. *Polymers (Basel)* **13**, 4199 (2021).

192. Camci-Unal, G., Cuttica, D., Annabi, N., Demarchi, D. & Khademhosseini, A. Synthesis and characterization of hybrid hyaluronic acid-gelatin hydrogels. *Biomacromolecules* **14**, 1085–1092 (2013).

193. Lee, H. Y., Hwang, C. H., Kim, H. E. & Jeong, S. H. Enhancement of bio-stability and mechanical properties of hyaluronic acid hydrogels by tannic acid treatment. *Carbohydr Polym* **186**, 290–298 (2018).

194. Wan, T. *et al.* Multiple Crosslinking Hyaluronic Acid Hydrogels with Improved Strength and 3D Printability. *ACS Appl Bio Mater* **5**, 334–343 (2022).

195. Yang, J., Choe, G., Yang, S., Jo, H. & Young Lee, J. Polypyrrole-incorporated conductive hyaluronic acid hydrogels. *Biomater Res* **20**, 31 (2016).

196. Spencer, A. R. *et al.* Electroconductive Gelatin Methacryloyl-PEDOT:PSS Composite Hydrogels: Design, Synthesis, and Properties. *ACS Biomater Sci Eng* **4**, 1558–1567 (2018).

197. Mihic, A. *et al.* A conductive polymer hydrogel supports cell electrical signaling and improves cardiac function after implantation into myocardial infarct. *Circulation* **132**, 772–784 (2015).

198. Pinelli, F., Magagnin, L. & Rossi, F. Can nanostructures improve hydrogel-based biosensors performance? *Nanomedicine* **16**, 681–683 (2021).

199. Phuchaduek, W., Jamnongkan, T., Rattanasak, U., Boonsang, S. & Kaewpirom, S. Improvement in physical and electrical properties of poly(vinyl alcohol) hydrogel conductive polymer composites. *J Appl Polym Sci* **132**, 42234 (2015).

200. Hernández-Bule, M. L., Paíno, C. L., Trillo, M. Á. & Úbeda, A. Electric Stimulation at 448 kHz Promotes Proliferation of Human Mesenchymal Stem Cells. *Cellular Physiology and Biochemistry* **34**, 1741–1755 (2014).

201. Kanawa, M. *et al.* Genetic markers can predict chondrogenic differentiation potential in bone marrow-derived mesenchymal stromal cells. *Stem Cells Int* **3**, (2018).

202. Mardani, M. *et al.* Comparison between Chondrogenic Markers of Differentiated Chondrocytes from Adipose Derived Stem Cells and Articular Chondrocytes In Vitro. *Iran J Basic Med Sci* **16**, 763 (2013).

203. Choi, J. W. *et al.* Rapid Induction of Osteogenic Markers in Mesenchymal Stem Cells by Adipose-Derived Stromal Vascular Fraction Cells. *Cellular Physiology and Biochemistry* **44**, 53–65 (2017).

204. Ahearne, M. Introduction to cell–hydrogel mechanosensing. *Interface Focus* **4**, 20130038 (2014).

205. Marklein, R. A. & Burdick, J. A. Spatially controlled hydrogel mechanics to modulate stem cell interactions. *Soft Matter* **6**, 136–143 (2009).

206. Baharlou Houreh, A., Masaeli, E. & Nasr-Esfahani, M. H. Chitosan/polycaprolactone multilayer hydrogel: A sustained Kartogenin delivery model for cartilage regeneration. *Int J Biol Macromol* **177**, 589–600 (2021).

207. Zhu, Y. *et al.* Development of kartogenin-conjugated chitosan–hyaluronic acid hydrogel for nucleus pulposus regeneration. *Biomater Sci* **5**, 784–791 (2017).

208. Wang, Y. J. *et al.* Runx1/AML1/Cbfa2 mediates onset of mesenchymal cell differentiation toward chondrogenesis. *Journal of Bone and Mineral Research* **20**, 1624–1636 (2005).

209. Winters, C., Zamboni, F., Beaucamp, A., Culebras, M. & Collins, M. N. Synthesis of conductive polymeric nanoparticles with hyaluronic acid based bioactive stabilizers for biomedical applications. *Mater Today Chem* **25**, 100969 (2022).

210. Kim, Y. il *et al.* Overexpression of TGF-β1 enhances chondrogenic differentiation and proliferation of human synovium-derived stem cells. *Biochem Biophys Res Commun* **450**, 1593–1599 (2014).

8. Supplementary material

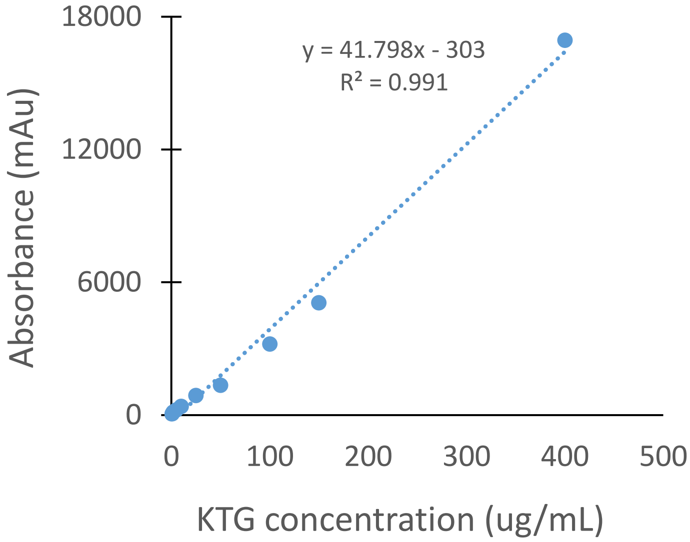

Figure S1 – KTG concentration calibration curve used to calculate LE.

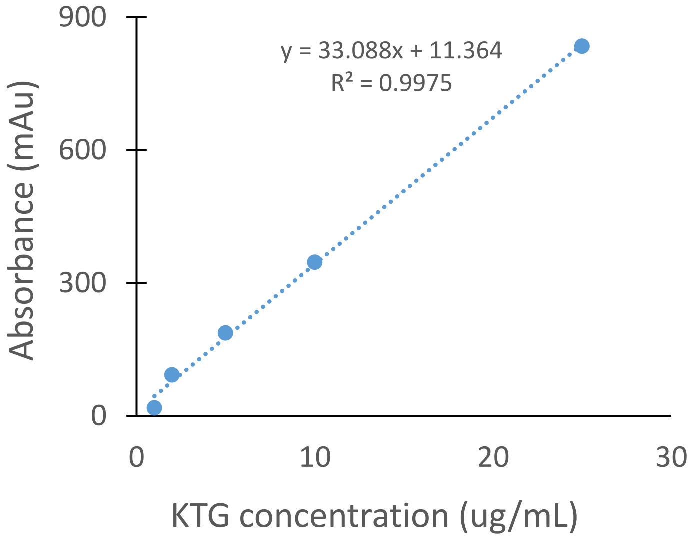

Figure S2 - KTG concentration calibration curve used to calculate KTG release.

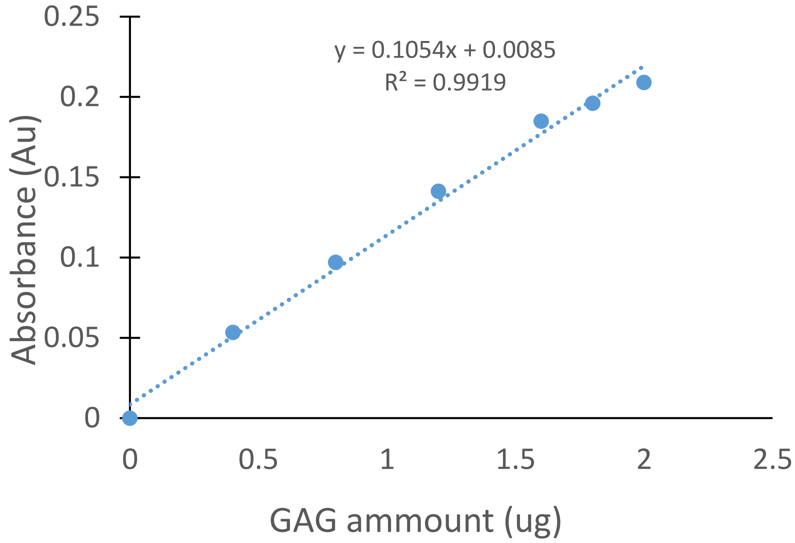

Figure S3 – Sulfated GAGs calibration curve.

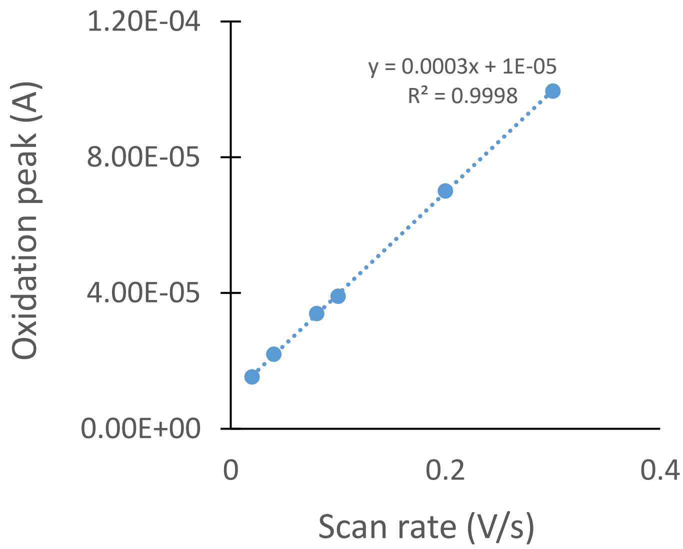

Figure S4 – Peak conductivity of KTG at 0.6 V plotted against the various scan rates.

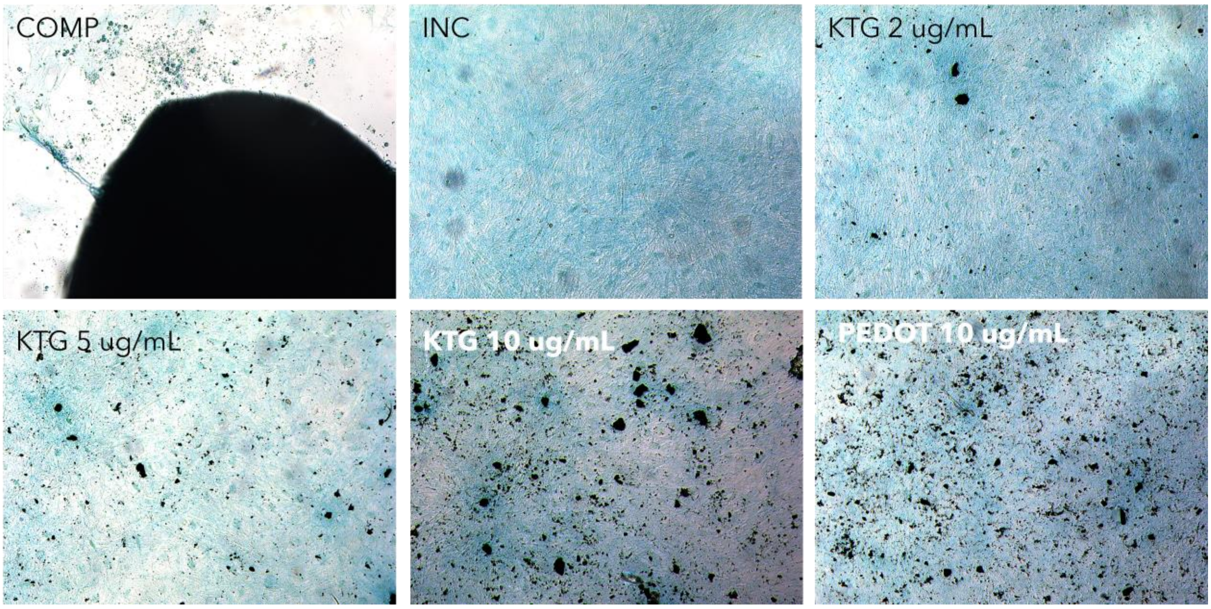

Figure S5 – Alcian blue staining of hBMSCs cultured in complete and incomplete chondrogenic media supplemented with different concentrations of KTG/PEDOT or PEDOT NPs.